STRING STABILITY ANALYSIS OF COOPERATIVE ADAPTIVE CRUISE CONTROL (CACC) WITH ACTUATOR SATURATION

HİLAL BİNGÖL

MAY 2017

STRING STABILITY ANALYSIS OF COOPERATIVE ADAPTIVE CRUISE

CONTROL (CACC) WITH ACTUATOR SATURATION

A THESIS SUBMITTED TO

THE GRADUATE SCHOOL OF NATURAL AND APPLIED SCIENCES

OF

ÇANKAYA UNIVERSITY

BY

HİLAL BİNGÖL

IN PARTIAL FULFILLMENT OF THE REQUIREMENTS

FOR

THE DEGREE OF MASTER OF SCIENCE

IN

ELECTRONIC AND COMMUNICATION ENGINEERING

MAY 2017

Title of the Thesis: **String Stability Analysis of Cooperative Adaptive Cruise Control (CACC) With Actuator Saturation.**
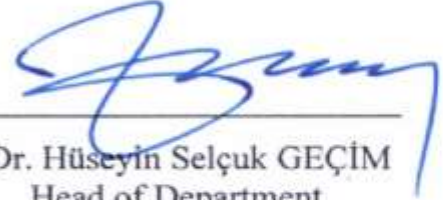
Submitted by **Hilal BİNGÖL**

Approval of the Graduate School of Natural and Applied Sciences, Çankaya University.

Prof. Dr. Can ÇOĞUN
Director

I certify that this thesis satisfies all the requirements as a thesis for the degree of Master of Science.

Prof. Dr. Hüseyin Selçuk GEÇİM
Head of Department

This is to certify that we have read this thesis and that in our opinion it is fully adequate, in scope and quality, as a thesis for the degree of Master of Science.

Assoc. Prof. Dr. Klaus Werner SCHMIDT
Supervisor

Examination Date: 29.05.2017

Examining Committee Members

Assoc. Prof. Dr. Orhan GAZİ	(Çankaya Univ.)	
Assoc. Prof. Dr. Klaus Werner SCHMIDT	(Çankaya Univ.)	
Assist. Prof. Dr. Emre ÖZKAN	(Middle East Technical Univ.)	

STATEMENT OF NON-PLAGIARISM PAGE

I hereby declare that all information in this document has been obtained and presented in accordance with academic rules and ethical conduct. I also declare that, as required by these rules and conduct, I have fully cited and referenced all material and results that are not original to this work.

Name, Last Name : Hilal, BİNGÖL

Signature :

Date : 29.05.2017

ABSTRACT

STRING STABILITY ANALYSIS OF COOPERATIVE ADAPTIVE CRUISE CONTROL (CACC) WITH ACTUATOR SATURATION

BİNGÖL, Hilal.

M.S.c., Department of Electronic and Communication Engineering

Supervisor: Assoc. Prof. Dr. Klaus Werner SCHMIDT

May 2017, 126 pages

Intelligent transportation systems aim at improving the efficiency and safety of transportation. In dense traffic, vehicles are aggregated to vehicle strings that travel on the same lane, whereby it is desired to maintain a small but safe distance between the vehicles. In the literature, this task is captured by the notion of string stability: fluctuations that are introduced by maneuvers of the leader vehicle should be attenuated by the follower vehicles.

The literature provides various methods for achieving string stability under the assumption that the vehicles are modeled as linear systems. In this thesis, we study the case where vehicles are modeled as nonlinear systems and hence face actuation constraints as well as state constraints. Different methods are employed. First, a reachability analysis based on the level-set method determines the states that are reachable under limitations on the engine force of vehicles. It turns out in the thesis

that, although the reachability analysis is the proper method to analytically address the problem of saturation, it is computationally not feasible due to the large state space of the vehicle model.

As a remedy, a further analysis of the model is carried out for the special case of maneuvers. Based on the realistic assumption that the impulse response of the vehicle following model is positive, several sufficient conditions for the input signal of the leader vehicle are derived in order to preserve string stability under actuator saturation. The first set of condition is concerned with the computation of maximum/minimum input signal that generated based on optimal control solution. These maximum/minimum input signals depend on the initial velocity of the vehicle string. The second set of conditions allows computing suitable input signals of the leader vehicle analytically and is hence highly beneficial in practice. The obtained results are illustrated by extensive simulation experiments.

ÖZ

AKTÜATOR SATÜRASYONU ALTINDA DİZİ KARARLI KOOPERATİF OTOMATİK SEYİR KONTROLÜ

BİNGÖL, Hilal

Yüksek Lisans, Elektronik ve Haberleşme Mühendisliği Anabilim Dalı

Tez Yöneticisi: Doç Dr. Klaus Werner SCHMIDT

Mayıs 2017, 126 sayfa

Akıllı Ulaşım Sistemleri, akıllı ve güvenli ulaşımın geliştirilmesini amaçlamaktadır. Yoğun trafikte, aynı kulvarda seyahat eden araç dizileri oluşturularak küçük fakat güvenli mesafede araçları arası mesafeyi koruyarak ilerler. Literatürde, bu konu dizi kararlılığı olarak adlandırılır ve bu durumda lider aracın manevraları sonucunda meydana gelen dalgalanmalar takipçi araçlar tarafından sönümlenir.

Literatürde, araçların doğrusal sistemler ile modellediğinde varsayılarak dizi kararlılığı konusunda birçok metot geliştirilmiştir. Bu tezde, araçlar doğrusal olmayan sistemler ile modellendiğinden eyleyici ve durum (states) kısıtlamaları ile karşılaşılır. Çalışmada farklı metotlar kullanılmıştır. İlk olarak, seviye - set yöntemi (level – set method) kullanılarak durum belirlemeleri yapılır, bunun anlamı araçların motor gücü sınırlamaları altında erişilebilirlik durumlarının incelenmesidir. Tez çalışmasında, satürasyon sorunu için erişilebilirlik analizinin uygun analitik bir metot olmasına rağmen, araç modelinin daha fazla durumdan oluşmasından dolayı hesaplamanın mümkün olamayacağı görülmüştür.

Çözüm olarak, model için özel hız değişim manevra analizleri gerçekleştirilmiştir. Araç takip modelinin dürtü yanıtı pozitif varsayımına göre, dizi kararlılığını korumak için lider aracın giriş sinyali ile ilgili iki etkili durum irdelenmiştir. İlk durum grubuna göre optimum kontrol çözümü (optimal control solution) temel alınarak maksimum/minimum giriş sinyali üretilmiştir. Üretilen maksimum/minimum giriş sinyalleri araç dizisinin ilk hızıyla doğrudan bağlıdır. İkinci durum grubu ise lider aracın giriş sinyalini analitik olarak hesaplanmasına olanak sağlar ve pratikte çok faydalıdır. Elde edilen sonuçlar kapsamlı bir şekilde simülasyonlar ile gösterilmiştir.

Anahtar Kelimeler: Akıllı Ulaştırma Sistemleri, Kooperatif Otomatik Seyir Kontrolü, Doğrusal Olmayan Sistemler, Satürasyon.

ACKNOWLEDGEMENTS

I would like to express my deepest thanks and gratitude to Assoc. Prof. Dr. Klaus Werner SCHMIDT; for his guidance, encouragement, motivation and comprehensive advice during my thesis. It is a great honor to study under his supervision.

I thankful to my dearest family for the love and encourage. Especially, I am grateful to my mother for her love and understanding and for unconditionally supporting me every moment in my life.

I dedicate my thesis to my dear dad who died in 2007.

TABLE OF CONTENTS

LIST OF FIGURES

LIST OF TABLES

LIST OF ABBREVIATIONS

ITS	Intelligent Transportation Systems
CACC	Cooperative Adaptive Cruise Control
ACC	Adaptive Cruise Control
V2V	Vehicle to Vehicle
v_i	Velocity of Vehicle i
a_i	Acceleration of Vehicle i
u_i	Input Signal of Vehicle i
$\widehat{u_i}$	Controller Output of Vehicle i
η_i	Controller Vtate Vector of Vehicle i
c_i	Engine Input of Vehicle i
m_i	Mass of Vehicle i
r_i	Standstill Distance of Vehicle i
d_i	Actual Inter-Vehicle Distance of Vehicle i
$d_{r,i}$	Desired Inter-Vehicle Distance of Vehicle i
h	Time Headway
e_i	Spacing Error of Vehicle i
q_i	Rear Bumper Position of Vehicle i
L_i	Length of Vehicle i
θ	Communication Delay
ϕ	Possible Plant Delay
G(s)	Plant Trasnfer Function of Vehicle
Γ(s)	Closed Loop Transfer Function
Γ(t)	Inverse Laplace Transform of Γ(s)
K_{fb}	Feedback Controller
K_{ff}	Feedforward Controller

τ_i	Time Constant
σ_i	Specific Mass of the Air
A_i	Cross Sectional Area of Vehicle
$c_{d,i}$	Drag Coefficient of Vehicle
$d_{m,i}$	Mechanical Coefficient of Vehicle
μ	Peak Coefficient of Friction
W_i	Total Weight of Vehicle i

CHAPTER 1

INTRODUCTION

Remarkable advances in the automotive industry rapidly lead to increasing mobility in both private and commercial applications [1, 2, 3]. As a result of this mobility in the automotive industry, vehicles become a significant part of the society. This dependency unfortunately led to traffic congestion, accidental deaths, fuel consumption, environmental impacts such as air and noise pollution [4, 5].

Intelligent Transport Systems (ITS) have developed into a profitable solution for the improvement of the operational performance of traffic systems [3, 6] such as planning, construction design operations, safety and so on [6]. One of the proposed and simple solutions of ITS in dense traffic is to allow vehicles traveling as a group at a safe distance instead of driving independently. The method is initially adopted from Cruise Control (CC) which is set by the driver to preserve a desired velocity. Adaptive Cruise Control (ACC) is a slightly more advanced and safe version of the CC method, where vehicles evaluate the inter-vehicle spacing and velocity difference between vehicles based on a sensor measurement to detect preceding traffic [5, 6]. Then, the following vehicle also speeds up or slows down to preserve the desired distance to the leader vehicle.

Cooperative Adaptive Cruise Control (CACC) is an extended version of ACC and it enables automating the longitudinal vehicle motion [7, 8, 9, 10, 11]. Analogous to Adaptive Cruise Control (ACC) [12, 13, 14, 15]. CACC allows to travel at a desired vehicle speed and inter-vehicle spacing, hence maintaining a safe distance to predecessor vehicles based on the distance measurements (RADAR or LIDAR). Commonly, a velocity-dependent spacing policy with a constant headway time (time to reach the position of the predecessor vehicle) is chosen. CACC also uses state information of the predecessor vehicles such as acceleration or velocity that is provided via vehicle-to-vehicle (V2V) communication. Accordingly, CACC enables small inter-vehicle distances which is a prerequisite for high levels of traffic throughout [21, 4, 16, 15].

When using CACC in dense traffic, the essential condition of *string stability* has to be fulfilled: fluctuations in the motion of any vehicle have to be *attenuated* by the follower vehicles [23, 22]. The existing literature provides several control methods to achieve string stability by using CACC. [17] and [18] use H_∞-control and [24] proposes a model-predictive control strategy to achieve string stability. [19] focuses on the impact of communication delays on string stability.

It has to be noted that the fulfillment of string stability in the existing works is based on the assumption of a linear vehicle model. Differently, this thesis focuses on the usage of a nonlinear vehicle model, whose input signal is the potentially limited engine force. Applying feedback linearization, a linear model that is suitable for the CACC design is obtained as long as the engine force stays within its bounds. Nevertheless, nonlinear behavior is obtained if the engine force saturates, invalidating the results on string stability.

In this context, the thesis has three main contributions. In all cases, it is assumed that CACC is used and an appropriate controller design has been performed.

1. It is shown that the verification if string stability is violated due to saturation of the engine force can be formulated as a reach-ability analysis. Then, the level set method can be used as a computational tool. However, it turns out that the computational effort of the level set method grows exponentially with the size of the model to be analyzed. Hence, using the formulated reach-ability analysis is not practical.

2. The main contribution of the thesis is a detailed analysis of the engine force propagation along a vehicle string in the case of velocity change maneuvers. In particular, we derive different sufficient conditions for the input signal of the linear vehicle model such that the engine force of follower vehicles does not saturate. The first set of conditions determines a maximum/minimum input signal that can be obtained by optimal control for each possible initial velocity. It then holds that any input signal that stays below the minimum/above the maximum input signal avoids saturation of the engine force. The second set of conditions are based on the computation of an absolute maximum/minimum input signal value. Using this value, suitable input signals can be computed analytically independent of the initial velocity.

3. The obtained results are illustrated by extensive simulation experiments with different vehicle velocities, dynamic parameters and traction forces.

To the best of our knowledge, this is the first study on this topic. [25] studies the effect of acceleration limits on string stability using a linear vehicle model. In [26], non-linear model is studied and its input signal is limited by engine force. Papers points out that the engine force of the vehicles along vehicle string is not saturated as long as the engine force of the leader vehicle does not exceed its limit.

CHAPTER 2

BACKGROUND

This chapter gives background information about the main topic of the thesis: Vehicle following and cooperative adaptive cruise control (CACC). Section 2.1 provides detailed information regarding CACC. Vehicle following and string stability are introduced in Section 2.1.1 and 2.1.2, respectively. Finally, the CACC controller design and model for linear systems is pointed out in Section 2.2.

2.1 Cooperative Adaptive Cruise Control (CACC)

CACC is used to increase the traffic capacity by tight vehicle following. The properties of CACC can be categorized into two main parts. Basically, CACC enables maintaining a desired cruise speed in dense traffic similar to adaptive cruise control (ACC). Here, the range between leader vehicle and following vehicle(s) is sensed by sensor measurements (i.e., RADAR or LIDAR) [1, 9, 27]. In addition to this, CACC uses vehicle-to-vehicle (V2V) communication to obtain relevant signals such as velocity and acceleration from the leader vehicles. The CACC system properties are briefly explained in the next subsections.

2.1.1 Vehicle Following

One dimensional platooning, where vehicles follow each other as a string is the basic configuration of the CACC method. A group of vehicles in a platoon is denoted as a vehicle string with a small inter-vehicle spacing. An example of platoon configuration for three vehicles is depicted in Fig.1. The length, rear bumper position and velocity of vehicle i are represented by L_i, q_i, v_i, respectively. Here, d_i is the distance between
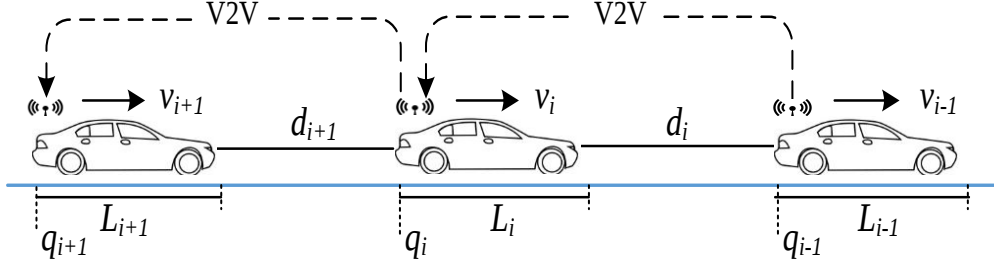
Figure 1: One dimensional vehicle string with CACC functionality.

vehicle $i-1$ and vehicle i, obtained from sensor measurements and computed as

$$d_i(t) = q_{i-1}(t) - q_i(t) - L_i. \tag{2.1}$$

In addition to this, the term spacing policy is used to represent the desired inter-vehicle distance in vehicle motion and it has a considerable effect on the driving behavior, string stability and traffic flow. The most popular spacing policies in the literature are the constant headway time policy and the constant gap spacing policy [28]. In this thesis, the constant headway time policy is preferred, since it is most frequently used in the recent literature. On account of this, the constant headway time policy is defined as follows

$$d_{i,r} = r_i + h v_i. \tag{2.2}$$

Here, $d_{i,r}$ is the desired inter-vehicle distance and r_i is the standstill distance. h denotes the desired headway time taken by each vehicle i to arrive at the current position of vehicle $i-1$. According to (2.1) and (2.2), the spacing error $e_i(t)$ is found as

$$
\begin{aligned}
e_i(t) &= d_i(t) - d_{i,r}(t) \\
&= (q_{i-1}(t) - q_i(t) - L_i) - (r_i + h v_i(t)).
\end{aligned} \tag{2.3}
$$

The important point to notice is that a small spacing error is one of the basic requirements for a stable behavior of vehicles in vehicle following.

2.1.2 String Stability

To enable comfortable and safe driving in one dimensional platoons as shown in Fig. 2, vehicles must ensure individual stability and also stability as a group when traveling in dense traffic [7]. In the literature this property is denoted as string stability [29, 30, 31, 33]. An extensive definition of this term is that automated vehicles in the string must avoid collisions, which is ensured if hte spacing error between two vehicles is attenuated through the platoon. Even, any acceleration or velocity signal disturbances of the leader vehicle must not be propagated by its follower vehicles through the platoon.
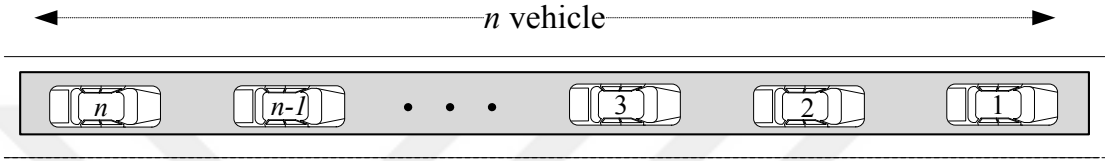
Figure 2: String with *n* vehicles.

In the literature, the string stability term is discussed extensively [17, 19, 20, 29, 30, 31, 32, 33]. In one of the studies, the difference between homogeneous and heterogeneous string stability is explained briefly [32]. In the case of homogeneous strings, vehicles in the platoon are assumed to have the same properties such as identical vehicle dynamics, spacing policy and longitudinal controller. On the other hand, it is highlighted that heterogeneous string stability represents the more realistic case where each vehicle has different vehicle dynamics in practice.

In [30], the mathematical preliminaries regarding string stability are explained clearly. For the case of a homogeneous platoon, the closed-loop transfer function is denoted as $\Gamma_i(s)$ as indicated in (2.4) and it is identical for all vehicles, i.e. $\Gamma_i(s) = \Gamma(s)$.

$$\Gamma_i(s) = \frac{Y_i(s)}{Y_{i-1}(s)}. \tag{2.4}$$

$y_i(t)$ is a relevant output signal of vehicle i and $Y_i(s)$ represents its Laplace transform. Also, the inverse Laplace transform of $\Gamma(s)$ is written as $\gamma(t)$. From this point, we bound the output signal as

$$||y_i||_\infty \leq ||\gamma||_1 \cdot ||y_i||_\infty. \tag{2.5}$$

where $||\bullet||_\infty$ expresses the L_∞ norm and $||\bullet||_1$ expresses the 1-norm, which is defined

as

$$||\gamma||_1 = \int_0^\infty |\gamma(t)| dt. \tag{2.6}$$

In order to attenuate signals along the string, that is, $||y_i||_\infty \leq ||y_{i-1}||_\infty$, it is desired that

$$||\gamma||_1 \leq 1. \tag{2.7}$$

This condition should always be fulfilled to attenuate output signals. It is known that studying norms in the time domain is more challenging, whereas working with transfer function norms is relatively simple. Hence, the frequency domain approach is more preferable in the analysis. From linear systems theory, it is known that

$$|\Gamma(0)| \leq ||\Gamma||_\infty \leq ||\gamma||_1. \tag{2.8}$$

where $||\Gamma||_\infty = \sup_\omega |\Gamma(j\omega)|$, and (2.9) is written according to the Laplace transform,

$$|\Gamma(0)| = \left| \int_0^\infty \gamma(t) dt \right| \leq \int_0^\infty |\gamma(t)| dt = ||\gamma||_1. \tag{2.9}$$

If the impulse response of the system $\gamma(t)$ stays positive, (2.9) is arranged as

$$||\Gamma||_\infty = ||\gamma||_1 \quad \text{where} \quad \gamma(t) \geq 0. \tag{2.10}$$

Proceeding from here, three notions of string stability are defined:

1. L_2 string stability: The energy of the output signal represented by L_2 norm is smaller than the energy of the input signal: $||y_i||_2 \leq ||y_{i-1}||_2$. This holds if

$$||\Gamma||_\infty \leq 1. \tag{2.11}$$

2. L_∞ string stability: Inequality in (2.12) is concluded from the fact that maximum magnitude of the output signal is smaller than the maximum magnitude of the input signal.

$$||\gamma||_1 \leq 1 \tag{2.12}$$

3. String stability without overshoot: It involves both inequality in (2.11) and $\gamma(t) \geq 0$ for all t. As a result, there is no overshoot in the ouput signal.

In this thesis, we want to

1. make sure that the output signal energy is decreased

2. overshooting behavior in the output signal is avoided.

Hence, the condition of string stability without overshoot

$$||\Gamma||_\infty \leq 1, \ \gamma(t) \geq 0. \qquad (2.13)$$

is considered.

To illustrate the string stability property, we conduct an analysis of a homogeneous vehicle string using MATLAB/Simulink. Input/output traffic throughout the string is realized according to the schematic in Fig. 3.
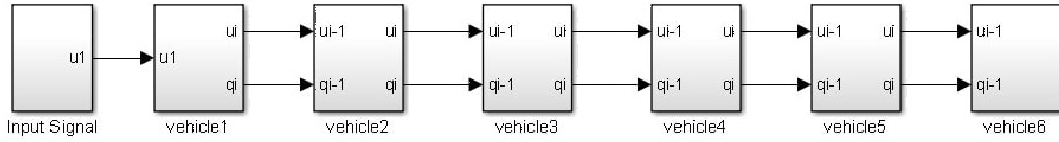
Figure 3: Input and output realization with six vehicle.

To do this, the generated input signal in Fig. 4 is applied to the leader vehicle and the output of the leader vehicle is transferred to the follower vehicles as an input signal. Illustration of string stability is given in Fig. 5. Here, the relevant output signals are
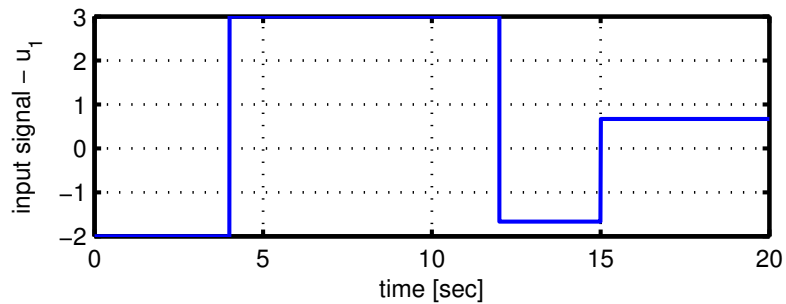
Figure 4: Generated input signal applied to the leader vehicle.

velocity and acceleration. At first, the leader vehicle (blue line), accelerates and decelerates between 3 m/s^2 and -2 m/s^2 (right-hand side). Each vehicle in the string follows its predecessor vehicle. Since string stability is fulfilled in this example, vehicles do

not exceed the defined acceleration/deceleration bounds. Moreover, the velocity along the platoon is attenuated as shown in the velocity plot (center). Eventually, the position plot (left-hand side) demonstrates that platooning of vehicles allows keeping a safe inter-vehicle spacing.
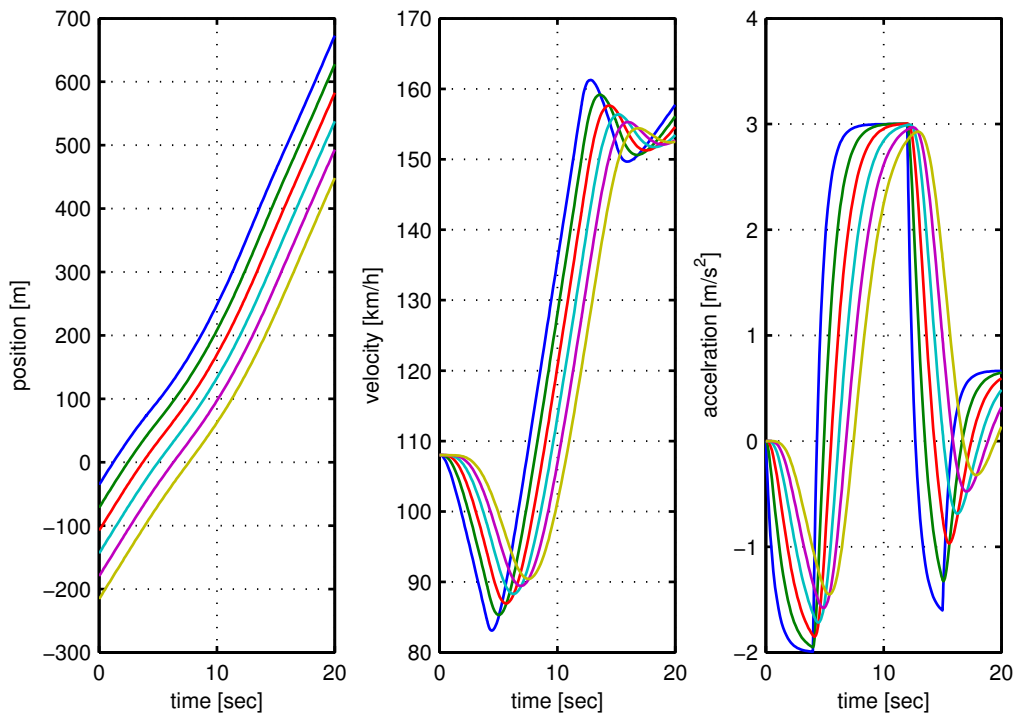
Figure 5: Simulation results of six CACC-equipped vehicles that achieve string stability.

In contrast to Fig. 5, where string stability is satisfied, signal amplification is observed in Fig. 6, where string stability is violated. Even if the leader vehicle accelerates and decelerates between 3 m/s^2 and -2 m/s^2 (right-hand side), the acceleration of the following vehicles is increased significantly. The same situation is observed in the velocity plot (centered), where the following vehicle is moving faster or slower compared to its leader vehicle. Lastly, the position plot shows that the vehicle distance is not always safe for vehicles in the platoon.
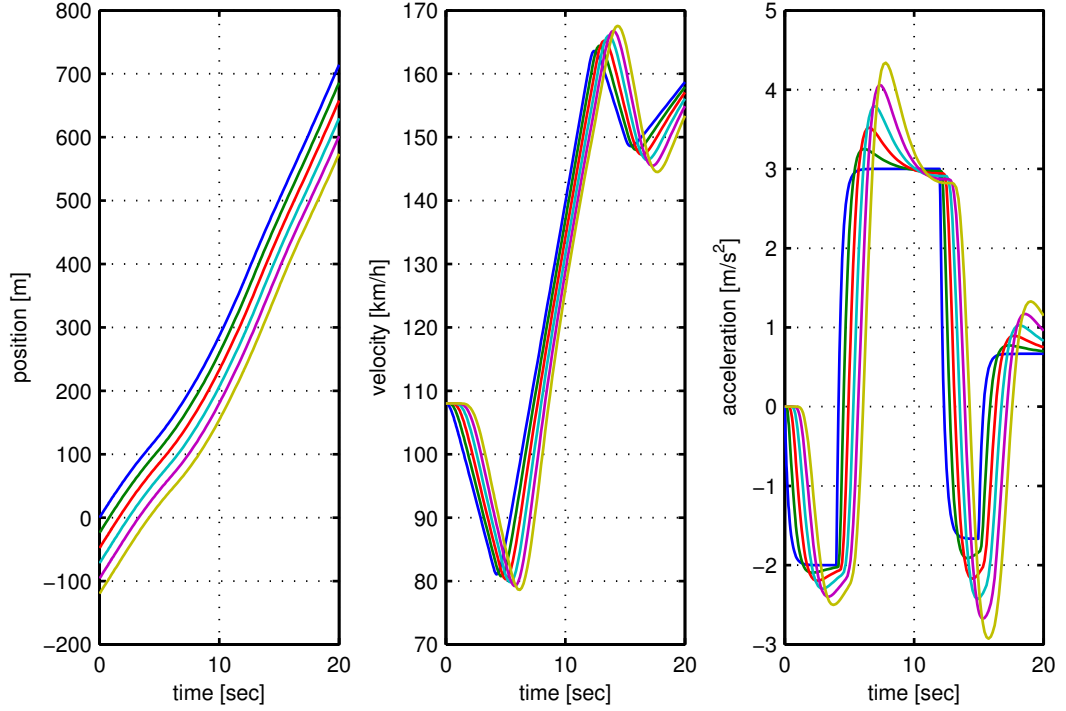
Figure 6: Simulation results of six CACC-equipped vehicle that not achieved string stability.

2.2 Controller Design and Model For Linear Systems

In the literature, authors have developed many CACC designs for a variety of purposes [9, 17, 19, 32, 33]. At this point, we only explain the controller design for the case of a linear plant model in a homogeneous string, where each vehicle has the same dynamics. Due to this reason, each vehicle is represented by the same plant transfer function and uses the same CACC controller. Based on the spacing policy equation in (2.2) and recent studies in the literature, the plant transfer function is given as

$$G_i(s) = \frac{e^{-\theta_i s}}{(1 + s\,\tau_i)\,s^2}. \tag{2.14}$$

Here θ_i, τ_i represent a possible plant delay and the time constant of the low-level drive line dynamics, respectively. By then, vehicle following can be realized according to the feedback loop in Fig. 7 [9]. Here, D represents a potential communication delay with the transfer function $D = e^{-\theta_i s}$. The controller transfer function block is represented by $K = \begin{bmatrix} K_{ff} & K_{fb} \end{bmatrix}$, in which K_{ff} is a feed-forward controller transfer function to obtain acceleration data from the predecessor vehicle and K_{fb} is a feed-back controller transfer function to control the spacing error. In this CACC model, the controller $K(s)$

10
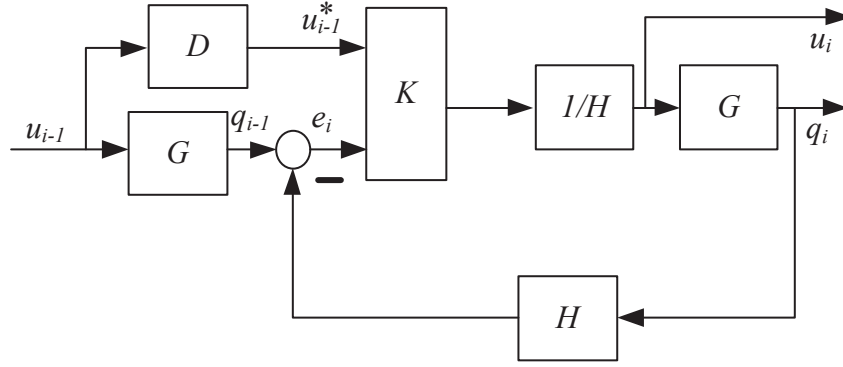
Figure 7: CACC Design for Linear Systems.

is designed using H_∞ control. The spacing policy is implemented by the $H = 1 + hs$ block with the constant headway h. u_{i-1} is an input signal of vehicle $i - 1$ and it is transmitted to vehicle i via V2V.

As mentioned before, if the CACC model is designed for the homogeneous case, it holds that $\tau_i = \tau_{i-1}$ and $\theta_i = \theta_{i-1}$ for all vehicles i. Thus, the transfer function $\Gamma(s)$ is computed for all vehicles in the platooning as shown

$$\Gamma_i(s) = \frac{U_i(s)}{U_{i-1}(s)} = \frac{DK_{ff} + G_i K_{fb}}{H(1 + G_i K_{fb})}. \tag{2.15}$$

To analyze CACC for the homogeneous case, we conduct an analysis of a vehicle string as in Fig.8. The generated input signal in Fig. 4 is applied to the string. In this exper-
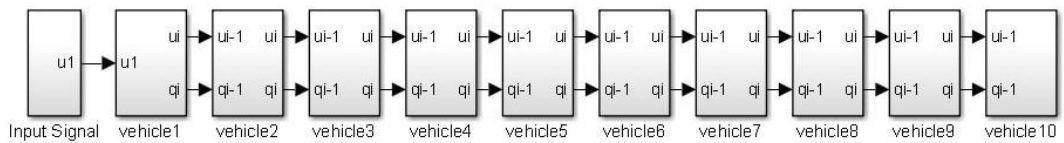
Figure 8: Input and output realization with ten vehicle

iment, the desired results are obtained by values of $h = 0.7$ s and $\tau_i = 0.3$ s for each vehicle i. As seen from the acceleration plot (left-hand side), the acceleration of the leader vehicle between $2\,\text{m/s}^2$ and $-4\,\text{m/s}^2$ and it is attenuated along the string. The initial velocity of the vehicles is approximately $110\,\text{km/h}$ and all vehicles attenuate the signals of their predecessor vehicles as is for example seen in the velocity plot (centered). Also, the position plot (right-hand side) shows that vehicles follow each other

at the desired distance. From these simulation results, it can be seen that string stability is fulfilled for this CACC design.
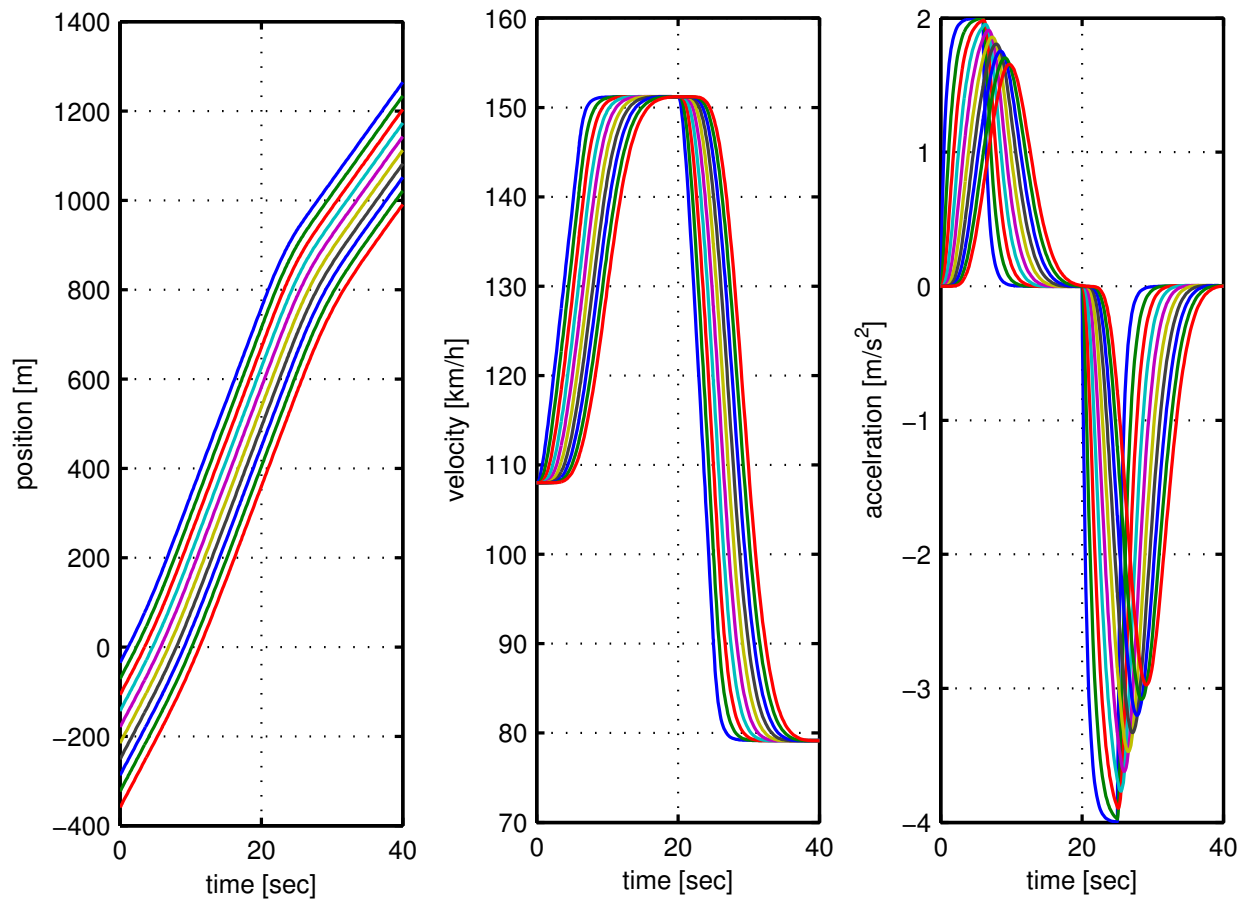
Figure 9: CACC design with ten vehicle string.

CHAPTER 3

ANALYSIS OF CACC UNDER SATURATION

The main problem considered in this thesis is presented in this chapter. A nonlinear plant model and feedback linearization are explained in Section 3.1. After that, the potential saturation of the engine force is discussed in Section 3.2. The application of reach-ability analysis for confirming string stability is explained in Section 3.3.

3.1 Nonlinear Model and Feedback Linearization

As explained in Chapter 2, the CACC controller is designed considering linear system models. Even though the vehicle behavior indicates nonlinear dynamics in practice, the internal dynamics of vehicles is usually ignored by the CACC model in Fig. 7. Proceeding from here, we establish a new string stability analysis using nonlinear model equations, where each vehicle in the string is equipped with the proposed controller. The dynamics of vehicle i can be modeled by the following nonlinear differential equations that we get from literature [34, 35, 36, 37, 38, 39, 40].

$$\begin{bmatrix} \dot{q}_i(t) \\ \dot{v}_i(t) \\ \dot{a}_i(t) \end{bmatrix} = \begin{bmatrix} v_i \\ a_i \\ f_i(v_i, a_i) + g_i(v_i)c_i \end{bmatrix} \tag{3.1}$$

q_i, v_i, and a_i denote the position, velocity and acceleration of vehicle i, respectively. f_i and g_i are defined as

$$f_i(v_i, a_i) = -\frac{1}{\tau_i}a_i - \frac{1}{m_i \tau_i}\left(\frac{\sigma A_i c_{di}}{2}v_i^2 - d_{mi} - \tau_i \sigma A_i c_{di} v_i a_i\right). \tag{3.2}$$

$$g_i(v_i) = \frac{1}{m_i \tau_i}. \tag{3.3}$$

13

where σ, A_i, c_{di}, d_{mi}, m_i, and τ_i denote the specific mass of the air, the cross-sectional area, drag coefficient, mechanical drag, mass, and engine time constant of vehicle i, respectively. The time derivative of $a_i(t)$ along the equations in (3.2), (3.3) is given by

$$\dot{a}_i = -\frac{1}{\tau_i}\,a_i - \frac{1}{m_i\,\tau_i}\left(\frac{\sigma A_i c_{di}}{2}v_i^2 - d_{mi} - \tau_i \sigma A_i c_{di} v_i a_i\right) + \frac{1}{m_i \tau_i}c_i. \tag{3.4}$$

From this point, the following control law c_i (engine input) in (3.5) with control input u_i is adopted as

$$c_i = u_i m_i + \frac{\sigma A_i c_{di}}{2}v_i^2 + d_{mi} + \tau_i \sigma A_i c_{di} v_i a_i. \tag{3.5}$$

It is obvious that, feedback linearization is achieved by using this control law. Substituting (3.5) into (3.4), we obtain

$$\dot{a}_i = -\frac{1}{\tau_i}a_i + \frac{1}{\tau_i}u_i \tag{3.6}$$

The feedback linearization law c_i defined in (3.5) helps us to achieve

1. Linearization of the vehicle dynamics

2. Simplification of the closed-loop model by excluding some characteristic parameters of the vehicle from its dynamics

As a consequence of linearization of the vehicle model equations, we design a new CACC model denoted in Fig.10. The basic difference between the models in Fig. 7
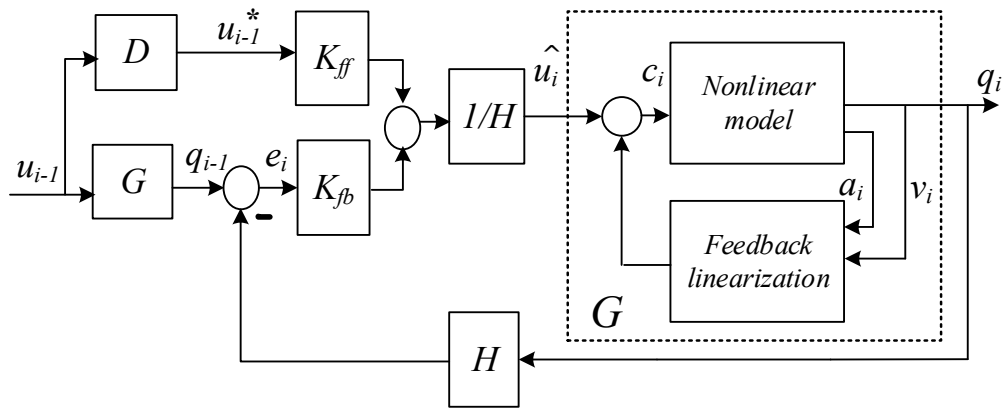
Figure 10: CACC model based on the non-linear model.

and Fig. 10 is the feedback linearization block. In this model, the inner control loop is designed to eliminate the internal vehicle dynamics. Moreover, it has to be pointed out

that c_i is defined as an exogeneous input and u_i is not a physical signal anymore in the model. After the feedback linearization, the same plant transfer function $G_i(s)$ is found for each vehicle i as defined in (2.14). From this point, it is determined that the plant transfer function $G_i(s)$ is linear, however; internally, the system is nonlinear.

To fulfill the string stability notions in (2.13), we use a CACC controller for the parameters $\tau_i = 0.1$ s and $h = 0.7$ s [9]. The feedforward controller and feedback controller transfer functions are evaluated as

$$K_{ff,i} = \frac{1431s^3 + 1.214\,10^4 s^2 + 3.219\,10^4 s + 2.538\,10^4}{s^4 + 1437s^3 + 1.215\,10^4 s^2 + 3.22\,10^4 s + 2.58\,10^4} \tag{3.7}$$

$$K_{fb,i} = \frac{3019s^3 + 2.041\,10^4 s^2 + 2.799\,10^4 s + 7143}{s^4 + 1437s^3 + 1.215\,10^4 s^2 + 3.22\,10^4 s + 2.58\,10^4} \tag{3.8}$$

According to controller $K_{ff,i}$, $K_{fb,i}$ and model in Fig.10, the closed loop transfer function

$$\Gamma_i(s) = \frac{U_i(s)}{U_{i-1}(s)} = \frac{D K_{ff} + G_i K_{fb}}{H(1 + G_i K_{fb})}. \tag{3.9}$$

is found for each vehicle i in the platoon. Furthermore, the impulse response of the designed system has to be positive to satisfy the string stability condition in (2.13). In this CACC design, the resulting $\gamma(t) \geq 0$ is shown in Fig. 11.
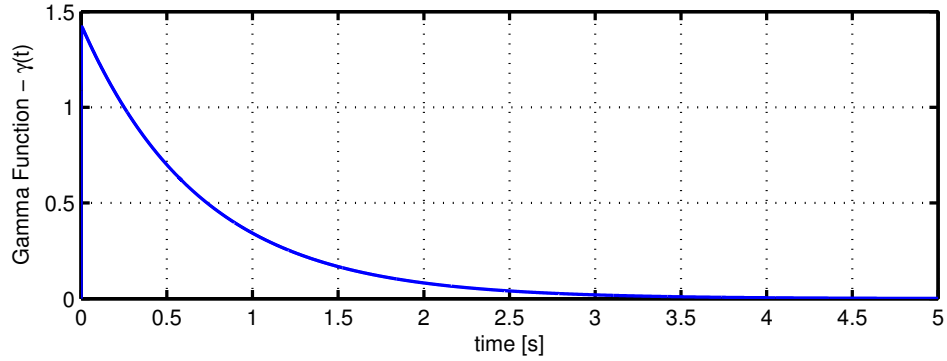
Figure 11: Impulse response of the system - $\gamma(t)$.

We conclude that the CACC design achieves the essential property of string stability as long as the feedback loop linearization can be applied. In the next section, we discuss the case where feedback linearization fails due to actuator saturation.

3.2 Saturation of the Engine Force

Using feedback linearization in Section 3.1, we demonstrate that the CACC model also can be used with nonlinear model equations. In the nonlinear model, c_i represents the traction force provided by the engine in case $c_i > 0$ and the braking force in case $c_i < 0$.

In practice, both forces are limited by both the engine power/brake pressure and the road adhesion [55]. In this work, we focus on the dependency of the traction/brake force on the road adhesion, considering that all homogeneous vehicles in a string are faced with the same road conditions. The maximum road adhesion force for longitudinal acceleration of a vehicle with front actuation is given by [55]

$$c_{\max} = \frac{\mu \, W_{front}}{1 + \frac{h}{L}\mu}. \tag{3.10}$$

μ is the peak coefficient of friction (ratio between traction/braking force and normal force), W is the weight on the front wheels and L is distance between wheels. Similarly, the maximum road adhesion for braking is computed as

$$c_{\min} = W_{total}\,\mu. \tag{3.11}$$

Noting that braking leads to deceleration, the maximum road adhesion leads to a negative force.

Typical values for the coefficient of friction are $\mu = 0.85$ (dry asphalt) or $\mu = 0.3$ (wet asphalt) [53, 56, 57]. Considering (3.5), (3.10) and (3.11), it holds that the vehicle string complies with the linear state space model in (4.6) and (4.7) as long as

$$c_{\min} \le c_i \le c_{\max} \text{ for all } i = 0, \dots, N. \tag{3.12}$$

Under this condition, string stability for the architecture in Fig.10 is ensured. However, if this condition is violated, string stability can no longer be guaranteed since the assumption of linearity of the plant model in (2.14) becomes invalid. Accordingly, the main purpose of this section is to investigate maneuvers of the leader vehicle that ensure (3.12) for all the follower vehicles. As a result, saturation will be avoided for each vehicle.

In order to demonstrate the saturation effect, we perform a first experiment. The engine force parameters are chosen as $\mu = 0.3$, $m_{total} = 1406\,\text{kg}$, $m_{front} = 884\,\text{kg}$, $h = 0.48\,\text{m}$

and $L = 2.66\,\text{m}$. Based on these values, the maximum and minimum engine forces are determined as $c_{max} = 2470\,\text{N}$ and $c_{min} = \text{-}4140\,\text{N}$. To analyze the effect of the engine force saturation on the vehicle motion, we make a simulation using the nonlinear model parameters in Table 1.

Table 1: Nonlinear model parameters for engine force simulations

Parameters	Definition	Quality
A_i	cross-sectional area	$2.2\ m^2$
c_{di}	drag coefficient	$0.3\ m^2$
d_{mi}	mechanical drag	$150\ N$
τ	engine time constant	$0.2\ s$
σ	specific mass of the air	$1\ \frac{kg}{m^3}$

As depicted in Fig. 12, the vehicle with the red line changes its position more quickly as compared to the vehicle with blue line in the position plot (a). This effect occurs because of the engine force saturation as indicated in plot (b). In the velocity plot in (c) it is indicated that the vehicle without saturation reduces its velocity more rapidly compared to the vehicle with saturation. Lastly, the vehicle with red line decelerates more slowly if the engine force without saturation is applied to the vehicle in plot (d).
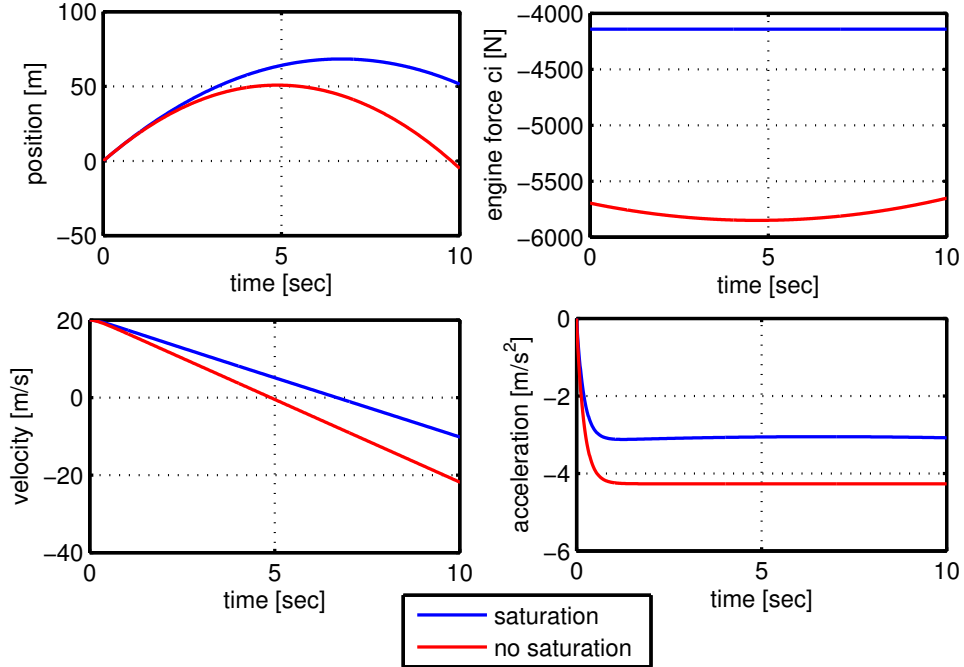
Figure 12: Vehicle motion with saturation and without saturation: a) position b) engine force c) velocity d) acceleration.

In the next simulations, we point what happened if an undesired engine force is applied to a string with ten vehicles. The initial value of velocity and acceleration is set to $v_i = 30$ m/s and $a_i = 0$ m/s^2. In the simulation, the engine force of the leader vehicle is limited by -4140 N shown with blue line. On the other hand, the engine force of the following vehicle with green line exceeds the desired engine force value as seen in Fig. 13. Similarly, the engine force of the other following vehicles saturates. That is, the exacct feedback linearization is no longer achieved, leading to nonlinear behavior of the system. In this case, string stability defined in Section 2.1.2 can no longer be confirmed.
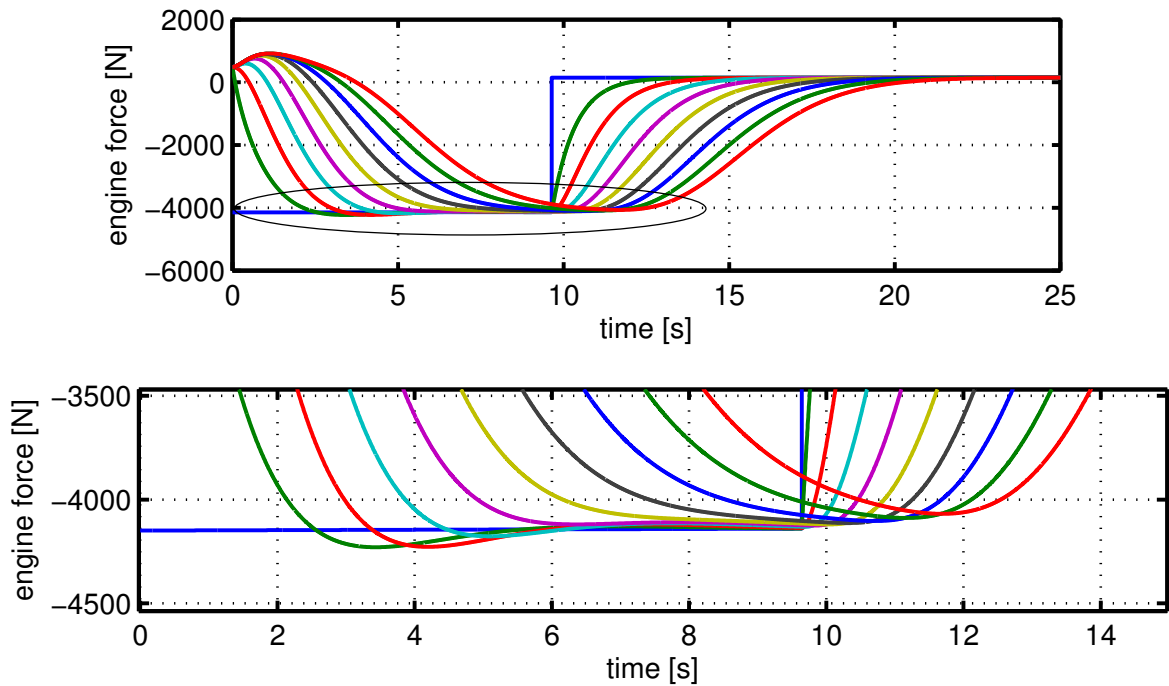
Figure 13: Engine force of ten vehicle with saturation

In following simulation, the same initial velocity, acceleration and engine force values are set for ten vehicle string. As indicated plots of Fig. 14, the engine force saturation is attenuated. For example, engine force of the leader vehicle with blue line is bounded by -4140 N. Further, all vehicles stay in defined engine force limits and string stability notion is accomplished for homogeneous CACC model. It means that system shows the linear behavior if engine force of the vehicles is not violated.
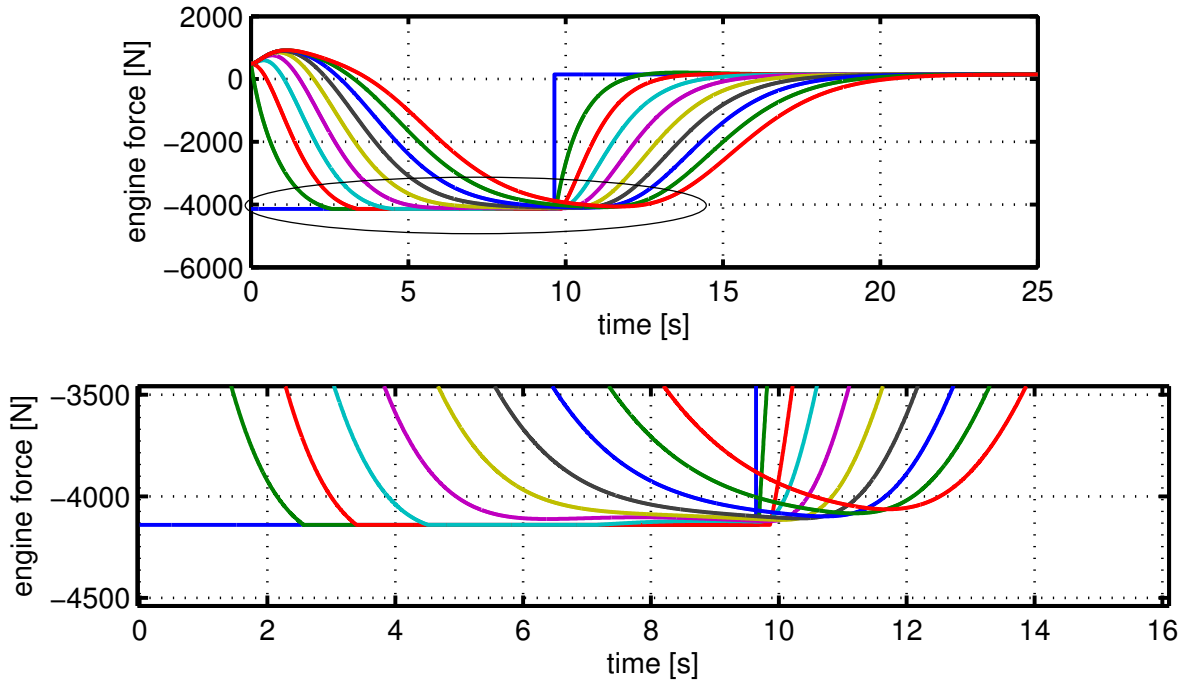
Figure 14: Engine force of ten vehicle without saturation.

3.3 Reach-ability Analysis for Confirming String Stability (Level Set Method)

As emphasized in Section 3.1, our plant transfer function $G_i(s)$ is linear after feedback linearization. However, the system is internally represented by a nonlinear model.

In order to ensure that the nonlinear system indeed behaves like a linear system, it has to be guaranteed that the feedback linearization is successful. That is, none of the vehicles should violate its limit on the minimum/maximum engine force. One important fact is that the engine force of all follower vehicles in a vehicle string only depends on the motion of the leader vehicle. In addition, the engine force of the leader force can be chosen arbitrarily between the saturation limits c_{min} and c_{max}. In addition, it is usually

desired that the leader vehicle performs comfortable driving. That is, its acceleration and velocity should stay between given limits a_{min}, a_{max} and v_{min}, v_{max}. In summary, the motion of the leader vehicle is subject to the constraints

$$c_{min} \leq c_1(t) \leq c_{max}, \tag{3.13}$$

$$v_{min} \leq v_1(t) \leq v_{max}, \tag{3.14}$$

$$a_{min} \leq a_1(t) \leq a_{max}. \tag{3.15}$$

According to this discussion, two problems can be formulated to address the saturation problem. First, it can be verified if the following condition is true

Given some initial condition of the vehicles in a vehicle string and applying an arbitrary input force within the bounds in (3.13) *to* (3.15) *to the leader vehicle, which states of the follower vehicles can be reached.*

From the vehicle states, it is possible to compute the engine force of each vehicle and verify if the saturation limit is violated for any follower vehicle.

Second, a converse problem can be formulated.

Given all bad states of the follower vehicles such that the engine force saturates and the acceleration and velocity limits are violated, determine all bad states of the leader vehicle and an engine force input such that the bad states can be reached.

Having found the bad states of the leader vehicle, it can then be checked if these states are reachable.

The two problems formulated above are reach-ability problems for nonlinear systems under input and state constraints. Depending on the specification of initial and final condition, two types of reachable sets are defined in the literature. Backward reach-ability and forward reach-ability as depicted in Fig. 15.

In forward reach-ability, we seek all states that are reached by trajectories which start from the specified initial condition. The first problem above is a forward reach-ability problem. For backward reach-ability, the final set is defined and we seek for states from which this defined final set can be reached. The second problem above is a backward reach-ability problem.
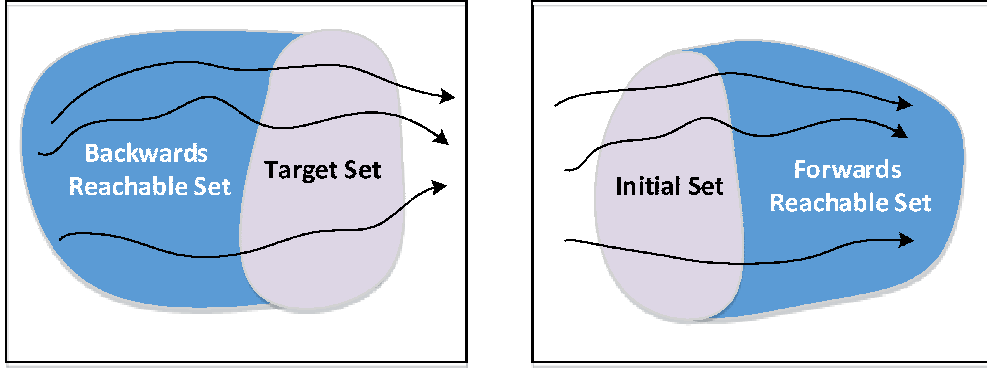
Figure 15: Backwards and Forwards Reachable Set.

3.3.1 Problem Formulation

The literature on reach-ability problems under state constraints is scarce. In general, the problem is formulated as a Hamilton-Jacobi equation. Then, the reachable set is determined from the viscosity solution of this Hamilton-Jacobi equation [42, 44, 45, 46, 47, 48]. In this thesis, we use the formulation in [44], which has the advantage that a unique continuous viscosity solution exists. In our model, we consider the reachable set from a target set T of a continuous system with dynamics

$$\dot{x} = f(x, u),$$

where $x \in R^d$ is the state space of our system and $T \subset R^d$. $u : (0, +\infty) \to A$ is the control input where $A \subset R^{d_u}$. The level set function along the continuous state space model is expressed by $J(x,t) : R^d \times R \to R$ and the initial data is represented by $J(x,0)$. Also, we consider a Lipschitz continuous function $g : R^d \longrightarrow R$ in order to formulate a state constraint as

$$g(x) \leq 0 \Leftrightarrow x \in T. \tag{3.16}$$

It is desired to find the unique viscosity solution $J(x,t)$ of the partial differential Hamilton-Jacobi for $t > 0$ and $x \in R^d$

$$\min(\partial_t J(x,t) + H(x, \Delta J(x,t)), J(x,t) - g(x)) = 0. \tag{3.17}$$

$$J(x,0) = \max(J_0(x), g(x)). \tag{3.18}$$

$\partial_t J$ is the partial derivative of J with respect to t, $\Delta J(x,t)$ is the gradient of J respect to state space variables x.

The evolution of the level set function $J(x,t)$ is defined by the Hamiltonian Jacobi equation in (3.19). The solution $J(x,t)$ of (3.16) represents the reachable set at each time instant t [44]: all states x with $J(x,t) \leq 0$ are reachable until time t, whereas states with $J(x,t) > 0$ are not reachable from the initial set T. That is, if we are interested in computing the reachable set, we need to solve (3.16) for a large enough time interval.

Our reach-ability computation is implemented using a variant of the level set method to find an efficient computation of the reach-ability set boundary as stated in [44]. The level set function approach leads to a characterization via a Hamilton-Jacobi equation and it is formulated as

$$H(x,p) \quad = \quad max_{u \in U} \left(f(x,u) \cdot p \right) = H(x, \Delta J(x,t)). \tag{3.19}$$

For the solution of (3.16), the toolbox for level set methods in [49] is suitable. This toolbox is only realized for the case without state constraints and was extended to include state constraints in the scope of this thesis. In addition a relaxation coefficient is needed in the toolbox, which requires to realize

$$\alpha_{dim}(x) = max_p \left| \frac{\partial H(x,p)}{\partial p_{dim}} \right|. \tag{3.20}$$

and it can be written as

$$\alpha_i(x) \quad = \quad max_p \left| \frac{\partial}{\partial p_i} H(x,p) \right|$$
$$= \quad max_p \left| \frac{\partial}{\partial p_i} [max_{u \in A} p f(x,u)] \right|. \tag{3.21}$$

The general evaluation of (3.21) is difficult. Nevertheless, our system dynamics can be represented as

$$f(x,u) = f^x(x) + F^u(x)u. \tag{3.22}$$

where $f^x : R^d \longrightarrow R^d$ and $F^u : R^d \longrightarrow R^{d_u}$. The important point in (3.22) is that input of the nonlinear system is linearly taken. Also, the input constraint is

$$a_i \in A_i = [\underline{A_i}, \overline{A_i}], \quad A = \prod_{i_1}^{n_a} A_i. \tag{3.23}$$

22

where $A_i^{max} = max(|\underline{A_i}|, |\overline{A_i}|)$. Analytically, inputs of the Hamiltonian Jacobian (3.19) are verified

$$a_i^*(x, p) = \begin{cases} \underline{A_i}, & \text{if } \sum_{j=1}^d p_j F_{ji}^a(x) \leq 0 \\ \overline{A_i} & \text{otherwise} \end{cases} \tag{3.24}$$

Furthermore, (3.21) is estimated as

$$\alpha_j(x) \leq |f_j^x(x)| + \sum |F_{ji}^a(x)| A_i^{max} \tag{3.25}$$

Based on these equations the reach-ability computation for our nonlinear system is performed numerically using the MATLAB toolbox in [49].

3.3.2 Solution for the Leader Vehicle

For our system, we first consider the nonlinear dynamics of the leader vehicle in (3.26)

$$\dot{x} = \begin{bmatrix} \dot{v}_0(t) \\ \dot{a}_0(t) \end{bmatrix} = \begin{bmatrix} a_0 \\ -\frac{1}{\tau_i}(a_0 + \frac{\sigma A_i c_{di}}{2m_i}v_0^2 + \frac{d_{mi}}{m_i}) - \frac{\sigma A_i c_{di}}{m_i}v_0 a_0 + \frac{1}{\tau m_i}c_0 \end{bmatrix} = f(x, u) \tag{3.26}$$

where $v_0 \in R$ velocity of the leader vehicle, $a_0 \in R$ acceleration of the leader vehicle and the engine force $c_0 \in A \subset R$ is the control input. Assume that $v_0 > 0$, $A = [-A^{max}, A^{max}]$ and for our system A is computed as $[2470, -4140]$ as defined briefly in Section 3.2. The model in (3.26) is simply arranged according to (3.22)

$$f^x(x) = \begin{bmatrix} a_0 \\ -\frac{1}{\tau_i}(a_0 + \frac{\sigma A_i c_{di}}{2m_i}v_0^2 + \frac{d_{mi}}{m_i}) - \frac{\sigma A_i c_{di}}{m_i}v_0 a_0 \end{bmatrix}, \quad F^a(x) = \begin{bmatrix} 0 \\ \frac{1}{\tau m_i} \end{bmatrix}. \tag{3.27}$$

From (3.24) and (3.27), it is concluded that

$$a^*(x, p) = A^{max} abs(p_2). \tag{3.28}$$

In addition to this, from (3.21) α is evaluated as shown

$$\alpha_1(x) \leq |a_0| \tag{3.29}$$

$$\alpha_2(x) \leq |-\frac{1}{\tau_i}(a_0 + \frac{\sigma A_i c_{di}}{2m_i}v_0^2 + \frac{d_{mi}}{m_i}) - \frac{\sigma A_i c_{di}}{m_i}v_0 a_0| + |A^{max}\frac{1}{m_i \tau}|. \tag{3.30}$$

23

Thus, the optimal Hamiltonian Jacobian for our non-linear dynamic model is governed by

$$
\begin{aligned}
H(x,p) \;=\; & p_1 a_0 - p_2 a_0 \frac{1}{\tau} \\
& + \; p_2 \frac{1}{\tau m_i} \left(-d_{mi} - \frac{\sigma A_i c_{di}}{2} v_0^2 - \tau A_i c_{di} v_0 a_0 \right) \\
& + \; A^{max} \left(2470\, p_2, -4140\, p_2 \right).
\end{aligned}
\tag{3.31}
$$

According to (3.35) to (3.31), we computed the reachable set for non-linear model equations in (3.26). Reach-ability computation is only applied to two states and reliable results are obtained for forward and backward reach-ability set. Computation is done using MATLAB tool and results are depicted in Fig. 16 and Fig. 17.

In the implementation, state constraints are determined as 0 m/s $\leq v_0 \leq 30$ m/s and 0 m/s$^2 \leq a_0 \leq 2$ m/s^2. An initial set rectangle for the forwards reach-ability set $J(x,0)$ is defined with the corners $[0\,0]$ and $[0.01\,0.01]$. The reachable states of the leader vehicle are shown in Fig. 16. The reachable set starts from the initial set rectangle and ends where $a_0 \leq 2$ m/s^2 and $v_0 \leq 0.2$ m/s.

The initial set rectangle for the backwards reach-ability set $J(x,0)$ is defined by the corners $[29.94\,0]$ and $[31\,2.1]$ in Fig.17. Starting from this point, the level set function $J(x,t)$ is evaluated according to state and input constraints. The level set function is positive outside the backwards reachable set, zero on its limits and negative inside the backwards reachable set. That is, we are only interested in states x with negative values of $J(x,t)$. From any such state, it is possible to find an input signal that makes the leader vehicle violate the given velocity and/or acceleration constraints.

3.3.3 Full CACC Model

The reach-ability computation in the previous section is implemented only for the leader vehicle with two states. On the other hand, the full CACC model with a leader
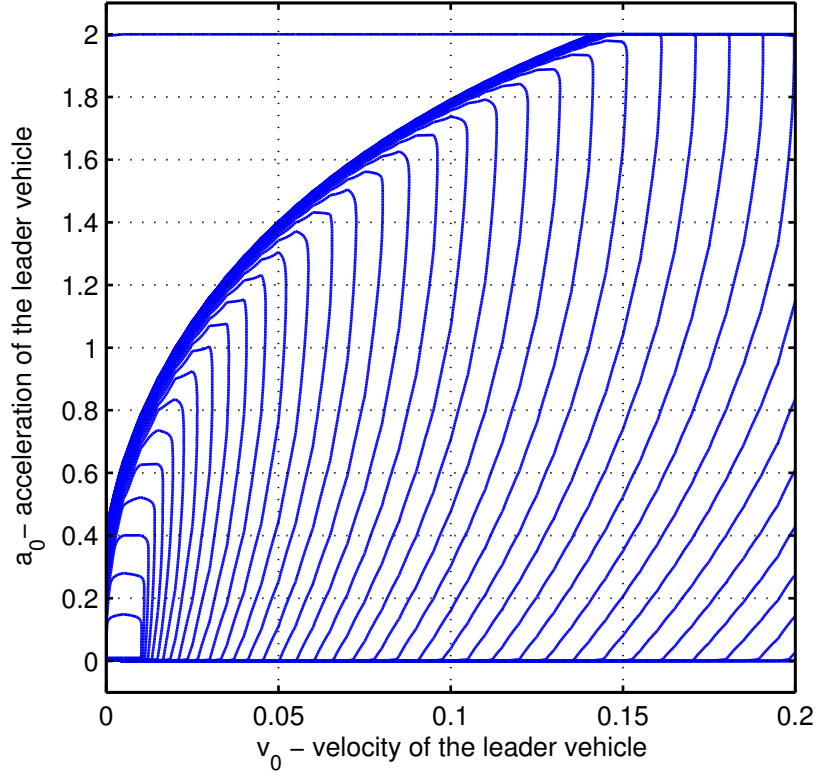
Figure 16: Forwards Reach-ability Set

and one follower vehicle has at least 6 states when using a simple PD controller [33]:

$$
\begin{bmatrix}
\dot{v}_0(t) \\
\dot{a}_0(t) \\
\dot{e}_1(t) \\
\dot{v}_1(t) \\
\dot{a}_1(t) \\
\dot{u}_1(t)
\end{bmatrix}
=
\begin{bmatrix}
a_0 \\
-\frac{1}{\tau_i}a_0 + \frac{1}{\tau_i}u_0 \\
v_0 - v_1 - h a_1 \\
a_1 \\
-\frac{1}{\tau_i} a_1 + \frac{1}{\tau_i} u_1 \\
\frac{k_d}{h} v_0 + \frac{k_p}{h} e_2 - \frac{k_p}{h} v_1 - k_d a_1 - \frac{1}{h} u_1 + \frac{1}{h m_i} u_0
\end{bmatrix}.
\tag{3.32}
$$

where $u_0 = \frac{1}{m_i}(\frac{\sigma A_i c_{di}}{2} v_0^2 + d_{mi} - \sigma A_i c_{di} v_0 a_0 + \frac{1}{\tau_i} c_0)$.

25
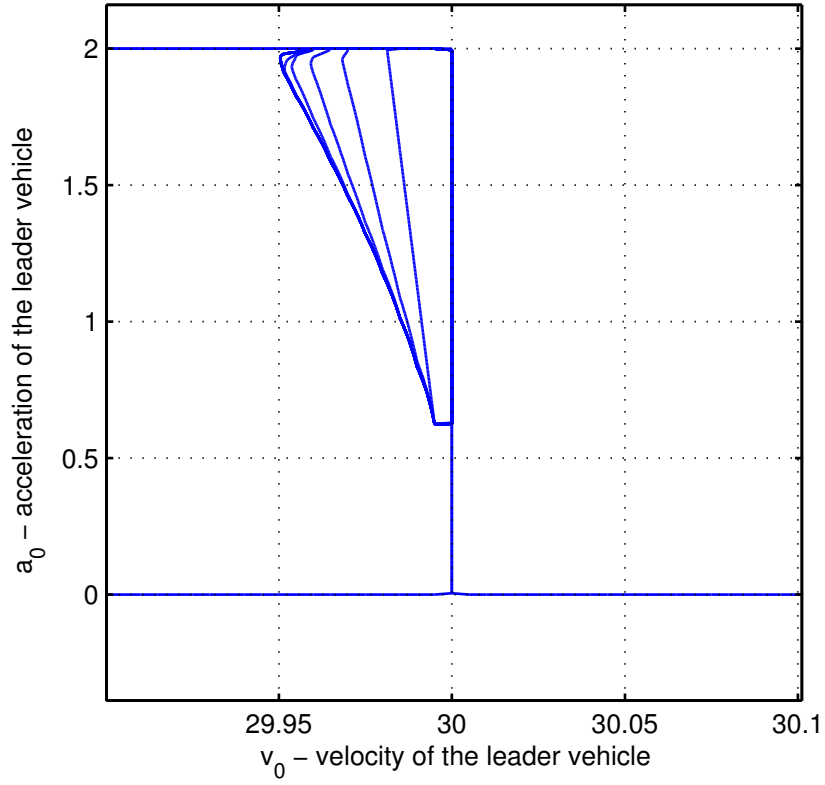
Figure 17: Backwards Reach-ability Set

According to definition of Hamiltonian Jacobian in (3.22), $f^x(x)$ is formulated as

$$f^x(x) = \begin{bmatrix} a_0 \\ -\frac{1}{\tau_i}\left(a_0 + \frac{\sigma A_i c_{di}}{2m_i}v_0^2 + \frac{d_{mi}}{m_i}\right) - \frac{\sigma A_i c_{di}}{m_i}v_0 a_0 \\ v_0 - v_1 - h a_1 \\ a_2 \\ -\frac{1}{\tau}a_1 \\ \frac{k_d}{h}v_0 + \frac{k_p}{h}e_1 - \frac{k_p}{h}v_1 - k_d a_1 - \frac{1}{h}u_1 - \frac{1}{\tau_i}\left(\frac{\sigma A_i c_{di}}{2m_i}v_0^2 + \frac{d_{mi}}{m_i}\right) - \frac{\sigma A_i c_{di}}{m_i}v_0 a_0 \end{bmatrix}.$$

$$(3.33)$$

Also, $F^a(x)$ is governed by

$$
F^a(x) = \begin{bmatrix} 0 \\ \frac{1}{\tau_i} c_0 \\ 0 \\ 0 \\ 0 \\ \frac{1}{h m_i} c_0 \end{bmatrix}
\tag{3.34}
$$

From (3.21), the function α is computed as

$$
\begin{aligned}
\alpha_1(x) &\leq |a_0| \\
\alpha_2(x) &\leq |-\frac{1}{\tau_i}(a_0 + \frac{\sigma A_i c_{di}}{2 m_i} v_0^2 + \frac{d_{mi}}{m_i}) - \frac{\sigma A_i c_{di}}{m_i} v_0 a_0| + |A^{max} \frac{1}{m_i \tau}| \\
\alpha_3(x) &\leq |v_0 - v_1 - h a_1| \\
\alpha_4(x) &\leq |a_1| \\
\alpha_5(x) &\leq |-\frac{1}{\tau} a_1 + \frac{1}{\tau} u_1| \\
\alpha_6(x) &\leq |\frac{k_d}{h} v_0 + \frac{k_p}{h} e_1 - \frac{k_p}{h} v_1 - k_d a_1 - \frac{1}{h} u_1| + |-\frac{1}{\tau_i}(\frac{\sigma A_i c_{di}}{2 m_i} v_0^2 + \frac{d_{mi}}{m_i}) \\
&\quad - \frac{\sigma A_i c_{di}}{m_i} v_0 a_0| + |A^{max} \frac{1}{h m_i} c_0|
\end{aligned}
\tag{3.35}
$$

Then, the Hamiltonian Jacobian equation is written for six states as represented in (3.36).

$$
\begin{aligned}
H(x,p) = \;& p_1 a_0 - p_2 a_0 \frac{1}{\tau} \\
&+ p_2 \frac{1}{\tau m_i}(-d_{mi} - \frac{\sigma A_i c_{di}}{2} v_0^2 - \tau A_i c_{di} v_0 a_0) \\
&+ A^{max}(2470 p_2, -4140 p_2) \\
&+ p_3 (v_0 - v_1 - h a_1) + p_4 a_1 - p_5 a_1 \frac{1}{\tau} \\
&+ p_6 (\frac{k_d}{h} v_0 + \frac{k_p}{h} e_1 - \frac{k_p}{h} v_1 - k_d a_1 - \frac{1}{h} u_1) \\
&+ p_6 \frac{1}{h m_i}(-d_{mi} - \frac{\sigma A_i c_{di}}{2} v_0^2 - \tau A_i c_{di} v_0 a_0) \\
&+ A^{max}(2470 p_6, -4140 p_6).
\end{aligned}
\tag{3.36}
$$

Using this formulation, it is in principle desired to determine the backwards reachable

set representing all states from where there exists an input signal to violate the constraints of any vehicle similar to Section 3.3.2. Unfortunately, it is realized that the computation of the level set function takes a considerable time even for systems with two states (two dimension) in the MATLAB implementation. In addition to this, the level set toolbox highlights that dimensions greater than five are likely to be unsuccessful. Since our model has six states, it was not possible to obtain a meaningful result using the level-set method.

Based on these outcomes it is concluded that, although the reachablitiy set computation is a suitable method for verifying saturation of the engine force, it is not applicable due to the computational complexity. Thus, we focus our attention on a direct analysis of the nonlinear system equations in the subsequent chapter.

CHAPTER 4

STRING STABILITY CONDITIONS UNDER ACTUATOR SATURATION

This chapter is concerned with different conditions on the input signal of the leader vehicle so as to maintain string stability even in the case of actuator saturation. To this end, we first discuss velocity change maneuvers of the vehicle string in Section 4.1. Then, several important relations between signals of different vehicles are established in Section 4.2. The thesis derives two types of conditions on the input signal of the leader vehicle. The first type in Section 4.3, 4.4 and 4.5 is computed based on an optimal control formulation, leading to conditions that depend on the respective velocities. An extensive simulation study in Section 4.6 and 4.7 illustrates the derived input signal constraints. Then, Section 4.8 determines velocity-independent constraints on the input signal of the leader vehicle that are further evaluated by simulations in Section 4.9 and 4.10.

4.1 Equilibrium Points of the State Space Model

The system $\dot{x} = f(x, u)$ possesses an equilibrium point if $f(x, u) = 0$. We next derive a state space model for the feedback loop in Fig. 10 for vehicle $i = 0, 1, \ldots, N$. To this end, we use the state-space model of the plant in (2.14)

$$
\begin{bmatrix} \dot{q}_i \\ \dot{v}_i \\ \dot{a}_i \end{bmatrix} = \begin{bmatrix} v_i \\ a_i \\ -\frac{1}{\tau} a_i + \frac{1}{\tau} u_i \end{bmatrix} = \underbrace{\begin{bmatrix} 0 & 1 & 0 \\ 0 & 0 & 1 \\ 0 & 0 & -\frac{1}{\tau} \end{bmatrix}}_{A} \begin{bmatrix} q_i \\ v_i \\ a_i \end{bmatrix} + \underbrace{\begin{bmatrix} 0 \\ 0 \\ \frac{1}{\tau} \end{bmatrix}}_{B} u_i. \tag{4.1}
$$

In addition, we determine a state-space model of the controller transfer matrix $K = \begin{bmatrix} K_{\text{ff}} & K_{\text{fb}} \end{bmatrix}$ using the controller state vector η_i, the controller output $\hat{u}_i$ and the controller

input $\begin{bmatrix} u_{i-1}^\star & e_i \end{bmatrix}^T$ of vehicle i:

$$\dot{\eta}_i = A_K\,\eta_i + \begin{bmatrix} b_{K,1} & b_{K,2} \end{bmatrix} \begin{bmatrix} u_{i-1}^\star \\ e_i \end{bmatrix}, \tag{4.2}$$

$$\hat{u}_i = C_K\,\eta_i + \begin{bmatrix} d_{K,1} & d_{K,2} \end{bmatrix} \begin{bmatrix} u_{i-1}^\star \\ e_i \end{bmatrix} \tag{4.3}$$

We finally respect that the controller output in (4.3) is the input of the filter $1/H$ in Fig. 10, which can be written as

$$\dot{u}_i = -\frac{1}{h}\,u_i + \frac{1}{h}\,\hat{u}_i \tag{4.4}$$

for $i = 1, 2, \ldots, N$. Considering that the leader vehicle is operated in the open loop since it does not follow any other vehicle, the overall state space model for a vehicle string is given by

$$\dot{q}_0 = v_0 \tag{4.5}$$

$$\begin{bmatrix} \dot{v}_0 \\ \dot{a}_0 \end{bmatrix} = \begin{bmatrix} 0 & 1 \\ 0 & -\frac{1}{\tau} \end{bmatrix} \begin{bmatrix} v_0 \\ a_0 \end{bmatrix} + \begin{bmatrix} 0 \\ \frac{1}{\tau} \end{bmatrix} u_0. \tag{4.6}$$

$$\begin{bmatrix} \dot{e}_i \\ \dot{v}_i \\ \dot{a}_i \\ \dot{u}_i \\ \dot{\eta}_i \end{bmatrix} = \begin{bmatrix} 0 & -1 & -h & 0 & 0 \\ 0 & 0 & 1 & 0 & 0 \\ 0 & 0 & -\frac{1}{\tau} & \frac{1}{\tau} & 0 \\ d_{K,2} & 0 & 0 & -\frac{1}{h} & \frac{1}{h}C_K \\ b_{K,2} & 0 & 0 & 0 & A_K \end{bmatrix} \begin{bmatrix} e_i \\ v_i \\ a_i \\ u_i \\ \eta_i \end{bmatrix} + \begin{bmatrix} 1 & 0 \\ 0 & 0 \\ 0 & 0 \\ 0 & \frac{d_{K,1}}{h} \\ 0 & b_{K,1} \end{bmatrix} \begin{bmatrix} v_{i-1} \\ u_{i-1}^\star \end{bmatrix} \quad \text{for } i = 1, \ldots, N.$$
$$\tag{4.7}$$

It is readily observed that the model in (4.6) and (4.7) has an equilibrium point for $a_0 = u_0 = 0$, $a_i = e_i = u_i = 0$ and $\eta_i = 0$ for $i = 1, \ldots, N$ and $v_i = v$ for $i = 0, \ldots, N$. Assuming that the feedback controller K_{fb} ensures that the feedback loop in Fig. 10 is asymptotically stable, this implies that the velocity of each follower vehicle $i = 1, \ldots, N$ in a vehicle string converges to the constant velocity v of the leader vehicle if the input signal is $u_0 = 0$. In this thesis, we are interested in maneuvers, where the leader vehicle changes its velocity. That is, we focus on transitions of the state space model in (4.6) and (4.7) between equilibrium points.

4.2 General Signal Relations Between Successive Vehicles

We first establish general relations between signals of successive vehicles in a string. We assume that, initially, all vehicles travel at a constant velocity v such that the vehicle string is in an equilibrium point as discussed in Section 4.1.

We further respect that the minimum allowable velocity is zero such that none of the vehicles travels backwards. Next consider that an input signal $u_{\max,v,0}(t)$ is applied to the leader vehicle starting from an initial velocity v such that

$$c_i(t) \leq c_{\max}$$

for all t and for vehicles $i = 0, \ldots, N$. The trajectory of leader vehicle when applying $u_{\max,v,0}(t)$ is given by $v_{\max,v,0}(t)$ and $a_{\max,v,0}(t)$. The corresponding trajectories and input signals of the follower vehicles when applying $u_{\max,v,0}(t)$ to the leader vehicle are denoted as $v_{\max,v,i}(t)$, $a_{\max,v,i}(t)$ and $u_{\max,v,i}(t)$ for $i = 1, \ldots, N$.

Likewise, assume that $u_{\min,v,0}(t)$ is an input signal such that

$$c_i(t) \geq c_{\min}, \quad v_i(t) \geq 0 \text{ and } u_{\min,v,0}(t) \leq u_{\max,v,0}(t)$$

for all t and for all vehicles $i = 0, \ldots, N$. Then, the trajectory of the leader vehicle for $u_{\min,v,0}(t)$ is given by $v_{\min,v,0}(t)$ and $a_{\min,v,0}(t)$. The corresponding trajectories and input signals of all follower vehicles when applying $u_{\min,v,0}(t)$ to the leader vehicle are denoted as $v_{\min,v,i}(t)$, $a_{\min,v,i}(t)$ and $u_{\min,v,i}(t)$.

That is, for each initial velocity v, $u_{\max,v,0}(t)/u_{\min,v,0}(t)$ represent an input signal that can be applied to the leader vehicle without violating the force saturation constraint $c_{\max}/c_{\min}$ of any vehicle and without obtaining a negative velocity for any vehicles $i = 0, \ldots, N$.

Using the maximum and minimum signals defined above, it is now possible to establish several signal relations between successive vehicles. To this end, we recall that a controller design for L_∞ string stability without overshoot in the feedback loop in Fig. 10 leads to a non-negative impulse response $\gamma(t) \geq 0$ of the transfer function Γ in (3.9). We further emphasize that the assumption of homogeneous vehicle strings implies that

$$\Gamma(s) = \frac{U_{i+1}(s)}{U_i(s)} = \frac{A_{i+1}(s)}{A_i(s)} = \frac{V_{i+1}(s)}{V_i(s)}. \tag{4.8}$$

In the time domain, this leads to the relations

$$u_{i+1}(t) = \gamma(t) \star u_i(t), \tag{4.9}$$

$$a_{i+1}(t) = \gamma(t) \star a_i(t), \tag{4.10}$$

$$v_{i+1}(t) = \gamma(t) \star v_i(t). \tag{4.11}$$

Using the defined signals, the following general result can be derived.

Lemma 1. *Consider a vehicle string with $N+1$ vehicles in the feedback loop in Fig. 10 and with the state space model in (4.6) and (4.7). Assume that K_{ff} and K_{fb} are designed such that $||\Gamma||_\infty \leq 1$ and $\gamma(t) \geq 0$. Let $u_{\max,v,i}(t)$ and $u_{\min,v,i}(t)$ be defined as above for $i = 0,\dots,N$. Assume that the vehicle string starts from an equilibrium point with velocity v and let u_0 be an input signal of the leader vehicle with*

$$u_{min,v,0}(t) \leq u_0(t) \leq u_{max,v,0}(t), \forall t \geq 0.$$

Then, it holds for all vehicles $i = 0,\dots,N$ and for all times $t \geq 0$ that

$$v_{min,v,i}(t) \leq v_i(t) \leq v_{max,v,i}(t) \tag{4.12}$$

$$a_{min,v,i}(t) \leq a_i(t) \leq a_{max,v,i}(t) \tag{4.13}$$

$$u_{min,v,i}(t) \leq u_i(t) \leq u_{max,v,i}(t) \tag{4.14}$$

Proof. We first show (4.14) in Lemma 1 for u_i, $i = 0,\dots,N$ by induction. Initially, let $i = 0$. Then, (4.14) holds by assumption. For the induction step, assume that (4.14) is true for all $k \leq i$. We have to show that (4.14) also holds for $i+1$. We compute

$$
\begin{aligned}
u_{min,v,i+1}(t) \quad &= \quad \int_{-\infty}^{\infty} \gamma(t-\xi) u_{min,v,i}(\xi)\,d\xi = \int_0^t \gamma(t-\xi) u_{min,v,i}(\xi)\,d\xi \\[2mm]
&\overset{(4.14),\gamma(t)\geq 0}{\leq} \int_0^t \gamma(t-\xi) u_i(\xi)\,d\xi = u_{i+1}(t) \\[2mm]
&\overset{(4.14),\gamma(t)\geq 0}{\leq} \int_0^t \gamma(t-\xi) u_{max,v,i}(\xi)\,d\xi = u_{max,v,i+1}(t). \tag{4.15}
\end{aligned}
$$

An analogous computation shows that also (4.12) and (4.13) hold. $\qquad\square$

4.3 Velocity-Dependent Conditions for Maximum Engine Force

In this section, we focus on the upper bound $u_{\max,v,0}(t)$ starting from an equilibrium point with the velocity v. For each $i = 0, \ldots, N$, we define

$$c_{\max,v,i}(t) = m\, u_{\max,v,i}(t) + \frac{\sigma A c_d}{2} v^2_{\max,v,i}(t) + d_m + \tau\, \sigma A c_d\, v_{\max,v,i}(t)\, a_{\max,v,i}(t) \quad (4.16)$$

as the traction force of vehicle i that is obtained when applying the maximum input signal. As in Section 4.2, we assume that $u_{\max,v,0}(t)$ is determined such that for all $i = 0, \ldots, N$

$$c_{\max,v,i}(t) \leq c_{\max}. \tag{4.17}$$

In addition, we require that

$$a_{\max,v,i}(t) \geq 0. \tag{4.18}$$

We show that the engine force of each successor vehicle $i = 1, \ldots, N$ is bounded by $c_{\max}$ as long as the input signal of the leader vehicle remains below $u_{\max,v,0}(t)$ for all $t \geq 0$.

Theorem 1. *Consider a vehicle string with a leader vehicle and N vehicles in the feedback loop in Fig. 10 and with the state space model in (4.6) and (4.7). Assume that K_{ff} and K_{fb} are designed such that $||\Gamma||_\infty \leq 1$ and $\gamma(t) \geq 0$ and that (4.17), (4.18) are fulfilled. Let $u_0(t) \leq u_{max,v,i}(t)$ be an input signal of the leader vehicle and let $v_i(0) = v$ for all $i = 0, \ldots, N$. Then, it holds for all $i = 0, \ldots, N$ and $t \geq 0$ that*

$$c_i(t) \leq c_{max}.$$

Proof. Consider any i. We have to show that $c_i(t) \leq c_{\max}$ for all $t \geq 0$. Referring to Lemma 1, $v_i(t) \geq 0$ and (4.18), it holds that

$$m_i u_i(t) \leq m_i u_{max,v,i}(t) \tag{4.19}$$

$$v_i^2(t) \leq v_{\max,v,i}{}^2(t) \tag{4.20}$$

$$a_i(t) v_i(t) \leq v_{max,v,i}(t) a_{max,v,i}(t) \tag{4.21}$$

is computed. According to the results in (4.19), (4.20), (4.21) imply that

$$c_i \leq \underbrace{m_i u_{i,max} + d_{mi} + \frac{\sigma A_i c_{di}}{2} v_{i,max}{}^2(t) + \tau_i \sigma A_i c_{di} v_{i,max}(t) a_{i,max}(t)}_{c_{i,max}(t)} \leq c_{max}. \quad (4.22)$$

Thus, $c_i(t) \leq c_{max}$ is achieved as defined in (4.17). $\qquad \square$

Remark 2. *We note that the result in Theorem 1 depends on several conditions. The maximum input signal $u_{max,v,0}(t)$ has to be chosen such that (4.17) and (4.18) are fulfilled. In addition, any input signal $u_0(t)$ applied to the leader vehicle has to ensure that $v_i(t) \geq 0$ for all $i = 0, \ldots, N$ and $t \geq 0$. Appropriate maximum input signals can be found using optimal control as discussed in Section 4.6.*

4.4 Velocity-Dependent Condition for Minimum Braking Force

In this section, we focus on the maximum braking force that is given by c_{min}. It is desired to derive conditions for the input signal $u_0(t)$ of the leader vehicle such that the braking force of none of the follower vehicles falls below c_{min}. To this end, we use the minimum input signal $u_{min,v,i}(t)$ for $i = 0, \ldots, N$ that was introduced in Section 4.2. Theorem 1 gives sufficient conditions for avoiding saturation of all vehicles.

Theorem 2. *Consider a vehicle string with a leader vehicle and N vehicles in the feedback loop in Fig.10 and with the state space model in (4.6) and (4.7). Assume that K_{ff} and K_{fb} are designed such that $||\Gamma||_\infty \leq 1$ and $\gamma(t) \geq 0$ is fulfilled. Assume that the vehicle string starts from an initial velocity of $v_i(0) = v$ and $a_i(0) = 0$. Let $u_{min,v,i}(t)$ be minimum input signals for $i = 0, \ldots, N$ as defined in Section 4.2. Assume that the input signal of the leader vehicle is chosen such that $u_0(t) \geq u_{min,v,0}(t)$ for all $t \geq 0$. Then, it holds for all $i = 1, \ldots, N$ and $t \geq 0$ that*

$$c_{min} \leq c_i(t) \quad (4.23)$$

if

$$v + \int_0^t u_{min,v,i}(\xi)d\xi \geq 0 \quad (4.24)$$

Proof. Let $u_0(t) \geq u_{\min,v,0}(t)$ for all $t \geq 0$ by assumption. Then, we know that

$$
\begin{aligned}
m u_i(t) &\geq m u_{\min,v,i}(t) \\
a_i(t) v_i(t) &\geq a_{\min,v,i}(t) v_i(t).
\end{aligned}
\tag{4.25}
$$

because of Lemma 1 and since $v_i(t) \geq 0$. According to (4.25), we can write

$$
\begin{aligned}
c_i(t) \geq{}& m u_{\min,v,i} + d_m + \frac{\sigma A c_d}{2} v_i^2(t) + \tau \sigma A c_d v_i(t) a_{\min,v,i}(t) \\
={}& \underbrace{m u_{\min,v,i} + d_m + \frac{\sigma A c_d}{2} v_{\min,v,i}^2(t) + \tau \sigma A c_d v_{\min,v,i}(t) a_{\min,v,i}(t)}_{c_{\min,v,i}(t)} \\
&+ \frac{\sigma A c_d}{2} v_i^2(t) + \tau \sigma A c_d v_i(t) a_{\min,v,i}(t) - \frac{\sigma A c_d}{2} v_{\min,v,i}^2(t) \\
&- \tau \sigma A c_d v_{\min,v,i}(t) a_{\min,v,i}(t)
\end{aligned}
\tag{4.26}
$$

At this point, we define

$$
\begin{aligned}
\Delta c_i(v_i(t)) ={}& \frac{\sigma A_i c_{di}}{2} v_i^2(t) + \tau_i \sigma A_i c_{di} v_i(t) a_{i,min}(t) \\
&- \frac{\sigma A_i c_{di}}{2} v_{i,min}^2(t) - \tau_i \sigma A_i c_{di} v_{i,min}(t) a_{i,min}(t)
\end{aligned}
\tag{4.27}
$$

From (4.26) - (4.27), it is hold that

$$
c_i = c_{min,v,i}(t) + \Delta c_i(v_i(t)) \geq c_{\min} + \Delta c_i(v_i(t)).
\tag{4.28}
$$

It is obvious that, we need that $\Delta c_i(v_i(t)) \geq 0$. It holds that $\Delta c_i(v_i(t))$ is a parabola in $v_i(t)$ with a minimum at $v_i(t) = \tau_i a_{min,v,i}(t)$ and we know that $\Delta c_i(v_i(t)) = 0$. That is, if $v_{min,v,i}(t) \geq -\tau_i a_{min,v,i}(t)$, then $\Delta c_i(v_i(t)) \geq 0$ for all $v_i(t) \geq v_{min,v,i}(t)$.

Hence, we only need to show that $v_{min,v,i}(t) \geq -\tau_i a_{min,v,i}(t)$ or equivalently $v_{i,min}(t) + \tau_i a_{i,min}(t) \geq 0$.

Consider that the expression for $\dot{a}_i(t)$ in (3.6) can be arranged as

$$
\tau_i \dot{a}_i + a_i(t) = u_i(t).
\tag{4.29}
$$

After integrating both sides of (4.29), the equation becomes

$$\tau_i a_i(t) + v_i(t) = \int u_i(\xi) d\xi + v_i(0). \tag{4.30}$$

Noting that $v_i(0) = v$, it directly follows that

$$\tau a_{\min,v,i}(t) + v_{\min,v,i}(t) = \int_0^t u_{\min,v,i}(\xi) d\xi + v \geq 0. \tag{4.31}$$

That is, (4.24) indeed ensures (4.23). □

Theorem 2 applies to maneuvers, where a vehicle string starts from an equilibrium point with velocity v. Then, for each v, it is required to find a minimum input signal $u_{\min,v,0}(t)$ for the leader vehicle such that for all $i = 1, \ldots, N$

$$\int_0^t u_{i,min}(\xi) d\xi + v \geq 0.$$

Then, saturation of the engine force of all vehicles is avoided if the conditions in the theorem are fulfilled. String stability is also preserved in this case.

If a suitable $u_{\min,v,0}(t)$ is found, it only needs to be ensured that the input signal of the leader $u_0(t)$ stays above $u_{\min,v,0}(t)$.

4.5 Additional Constraints for Vehicle Signals

Theorem 2 is derived without any assumptions on the remaining signals of the leader vehicle. However, in practice, it is usually desired that the velocity, acceleration and jerk of vehicles stays between certain bounds. For example, in order to realize comfortable driving, the literature suggest accelerations between $a_{min} = -2 \, \text{m/s}^2$ and $a_{max} = 2 \, \text{m/s}^2$ and jerk values between $j_{min} = -5 \, \text{m/s}^2$ and $j_{max} = 5 \, \text{m/s}^2$ [50, 51, 52, 53, 54]. Due to the properties of the CACC design with L_∞ string stability without overshoot, it holds that any constraint imposed on the leader vehicle signals is also fulfilled for all successor vehicles.

Theorem 3. *Consider a vehicle string with a leader vehicle and N vehicles in the feedback loop in Fig.10 and with the state space model in (4.6) and (4.7). Assume that K_{ff} and K_{fb} are designed such that $||\Gamma||_\infty \leq 1$ and $\gamma(t) \geq 0$ is fulfilled. Let $u_0(t)$ be an*

input signal for the leader vehicle such that

$$v_{min} \le v_0(t) \le v_{max}, \quad a_{min} \le a_0(t) \le a_{max}, \quad j_{min} \le \dot{a}_0(t) \le j_{max}$$

Then, it holds that for all $i = 1, \ldots, N$

$$v_{min} \le v_i(t) \le v_{max}, \quad a_{min} \le a_i(t) \le a_{max}, \quad j_{min} \le \dot{a}_i(t) \le j_{max} \tag{4.32}$$

Proof. We first show that $\int_0^\infty \gamma(\xi) d\xi = 1$. To this end, consider the transfer function $\Gamma(s)$ in (3.9) with the plant model in (2.14). It holds that

$$\Gamma(s) = \frac{DK_{\mathrm{ff}} + GK_{\mathrm{fb}}}{H(1 + GK_{\mathrm{fb}})} = \frac{D(1 + s\tau)s^2 K_{\mathrm{ff}} + K_{\mathrm{fb}}}{H((1 + s\tau)s^2 + K_{\mathrm{fb}})}.$$

That is,

$$\Gamma(0) = \frac{K_{\mathrm{fb}}(0)}{H(0) K_{\mathrm{fb}}(0)} = 1.$$

Further, using the definition of the Laplace transform, we compute

$$\int_0^\infty \gamma(\xi) d\xi = \lim_{s \to 0} \int_0^\infty \gamma(\xi) e^{-s\xi} d\xi = \lim_{s \to 0} \Gamma(s) = 1.$$

Now, it is possible to prove Theorem 3 by induction. Let $i = 0$. Then, (4.32) holds by assumption. Now assume that (4.32) holds for all $k \le i$. It has to be shown that also (4.32) holds for $i + 1$. Consider the signals $a_i(t)$ and $a_{i+1}(t)$. Recalling that $\gamma(t) \ge 0$, we compute

$$a_{i+1}(t) = \int_0^t \gamma(\xi) a(t - \xi) d\xi \le \int_0^t \gamma(\xi) a_{\max} d\xi \le a_{\max} \int_0^\infty \gamma(\xi) d\xi = a_{\max}.$$

Likewise,

$$a_{i+1}(t) = \int_0^t \gamma(\xi) a(t - \xi) d\xi \ge \int_0^t \gamma(\xi) a_{\min} d\xi \ge a_{\min} \int_0^\infty \gamma(\xi) d\xi = a_{\min}.$$

That is, $a_{\min} \le a_{i+1}(t) \le a_{\max}$ is confirmed. The conditions for v_{i+1} and j_{i+1} follow analogously. That is, (4.32) is valid for all $i = 0, \ldots, N$. $\qquad\square$

Theorem 3 has an important consequence for vehicle strings in practice. It is sufficient to design the leader input signal $u_0(t)$ according to Theorem 1 and Theorem 2 in order to avoid saturation. If, additionally, $u_0(t)$ is chosen such that velocity, acceleration, jerk are bounded, the same conditions are automatically valid for all the follower vehicles. In this context, it is important to note that the latter condition depends on the fact that

$\gamma(t) \geq 0$. That is, the sufficient conditions for L_∞-string stability without overshoot should be fulfilled.

4.6 Simulation Results for Maximum Input Signal - Theorem 1

Theorem 1 allows ensuring a bound on the maximum traction force under the assumption of a suitable maximum input signal $u_{\mathrm{max},v,0}(t)$ of the leader vehicle for a given initial velocity v. Such input signal must fulfill (4.17) and (4.18). In addition, bounds on the maximum acceleration and jerk can be added for driving comfort as discussed in Section 4.5. The aim of this section is the computation of such input signal under the assumption of a given maximum velocity v_{max} of the vehicle string. In this case, it is desired to solve the optimal control problem that transfers the leader vehicle from an initial velocity v to a final velocity in the shortest time while meeting all state constraints:

$$\min_{T} \int_0^T 1 \, dt \tag{4.33}$$

subject to

$$\dot{v}_0 = a_0 \tag{4.34}$$

$$\dot{a}_0 = -\frac{1}{\tau} a_0(t) + \frac{1}{\tau} u_0(t) \tag{4.35}$$

$$v_0(0) = v \text{ and } a_0(0) = 0 \text{ and } v_0(T) = 0 \text{ and } a_0(T) = 0 \tag{4.36}$$

$$c_0(t) = m u_0(t) + d_{\mathrm{m}} + 0.5 \sigma A c_{\mathrm{d}} v_0^2(t) + \tau \sigma A c_{\mathrm{d}} v_0(t) a_0(t) \leq c_{\mathrm{max}} \tag{4.37}$$

$$v_0(t) \leq v_{\mathrm{max}} \tag{4.38}$$

$$a_0(t) \leq a_{\mathrm{max}} \tag{4.39}$$

$$\dot{a}_0(t) \leq j_{\mathrm{max}}. \tag{4.40}$$

This optimal control problem is explained as follows.

- The objective function in (4.33) minimizes the time for the maneuver.

- (4.34) to (4.35) represent the dynamic equations of the leader vehicle.

- (4.36) represents the initial and final conditions.

- (4.37) states the constraint on the maximum force.

- (4.38) to (4.40) pose additional constraints on velocity, acceleration and jerk.

The optimal control problem in (4.33) to (4.40) can be solved using available optimal control solvers. In this work, the PROPT solver [**?**] of the Tomlab optimization environment is used.

We next illustrate the presented results by computing maximum input signals for different maneuvers and using different constraints. The first example considers velocity changes of the leader vehicle starting from $0, 5, 10, 15, 20, 25, 30, 35$ m/s to a maximum velocity of $v_{\max} = 40$ m/s. A vehicle model with the parameters in Table 2 is considered. Also, two different maximum engine forces are computed as $c_{\max} = 2470$ N and $c_{\max} = 6395$ N for different friction coefficient values such as $\mu = 0.3$ (wet asphalt) and $\mu = 0.85$ (dry asphalt).

Table 2: Nonlinear model parameters for string stability simulations

Parameters	Definition	Quality
A_i	cross-sectional area	$2.2\,\mathrm{m}^2$
c_{di}	drag coefficient	0.3
d_{mi}	mechanical drag	150 N
m_i	mass of vehicle	1406 kg
τ_i	engine time constant	0.8 s
σ_i	specific mass of air	$1\,\frac{\mathrm{kg}}{\mathrm{m}^3}$

4.6.1 Maximum Input Signal Without State Constraint

For the evaluation in this section, the maximum input signal $u_{\max,v,0}$ trajectory is generated by optimal control without additional state constraints. This signal is then applied to the platoon. Simulations are done with different $c_{\max}$ and τ values.

First, $c_{\max} = 2470\,\text{N}$, $\tau = 0.1\,\text{s}$ are used for each vehicle in the platoon. The plots for vehicle 1, vehicle 5 and vehicle 10 are shown in Fig. 18, Fig. 19 and Fig. 20, respectively. The maximum input signal $u_{\max,v,0}$ with different final velocity values is represented in Fig. 18. In the velocity subplots, it can be seen that the vehicles reach different final velocities within different time durations, which is an expected result. The force plots further show that the engine force is only applied during a short time period. As expected, there are no bounds for acceleration and jerk signals.

Figure 18: Maximum trajectories of the leader vehicle with $c_{\max} = 2470\,\text{N}$, $\tau = 0.1$

Figure 19: Maximum trajectories of the 5. vehicle with $c_{max} = 2470\,\text{N}$, $\tau = 0.1$

Figure 20: Maximum trajectories of the 10. vehicle with $c_{max} = 2470\,\text{N}$, $\tau = 0.1$

In the next simulations, $c_{max} = 6395\,\mathrm{N}$ and $\tau = 0.1\,\mathrm{s}$ are chosen for each vehicle and the generated maximum input signal is applied to the string. The simulation figures for the selected vehicles are indicated in Fig. 21, Fig. 22 and Fig. 23. The generated input signal with different final velocity values is applied to the leader vehicle as shown in Fig. 21. As expected, the engine force of the vehicles in the string does not violate the specified bound since the conditions in Theorem 1 hold. In the velocity plots, the vehicles reach the different final velocities in different time intervals. Since the maximum engine force is larger compared to the previous experiment, the maneuvers are performed in less time. Since acceleration and jerk signal are not bounded, the obtained values are greater than $j_{min} = -5\,\mathrm{m/s^3}$, $a_{min} = -2\,\mathrm{m/s^2}$ as can be seen in the figures.
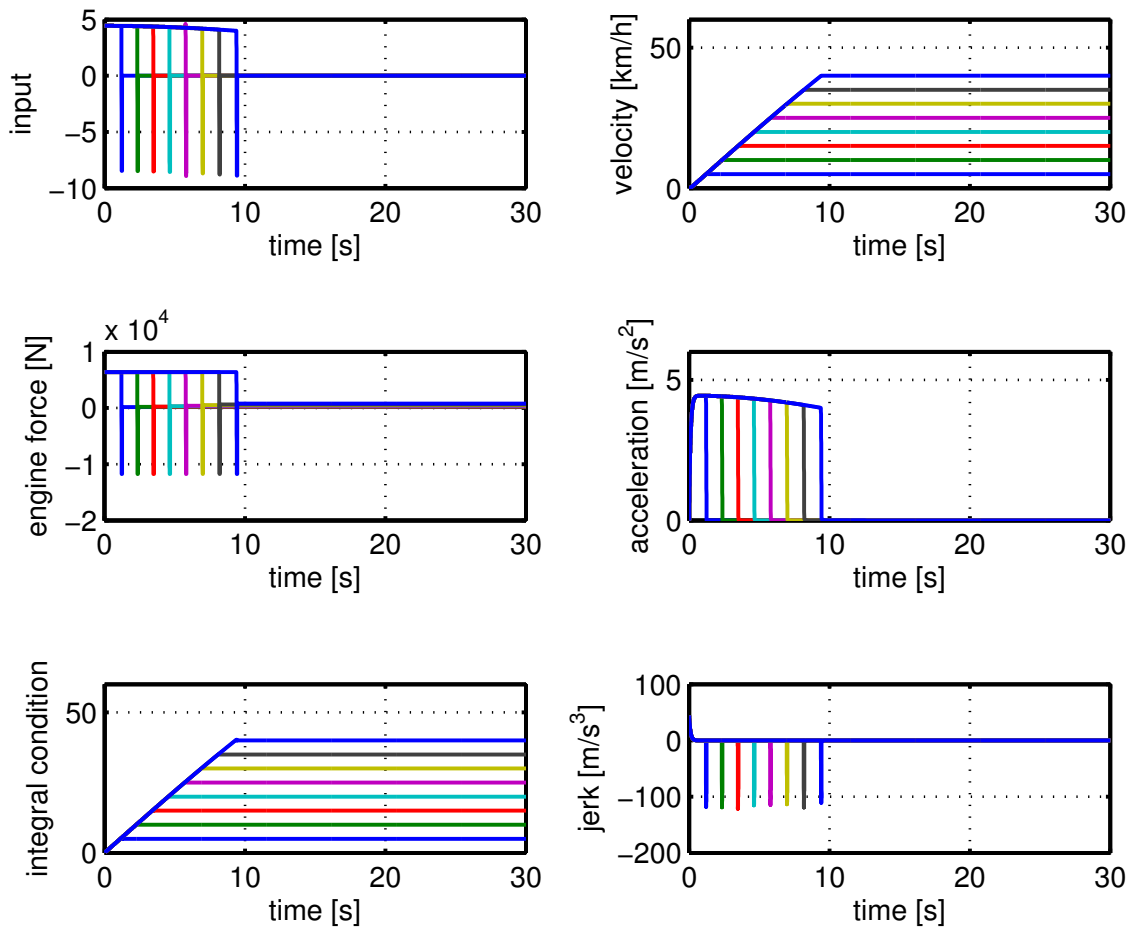
Figure 21: Maximum trajectories of the leader vehicle with $c_{max} = 6395\,\mathrm{N}$, $\tau = 0.1$

43
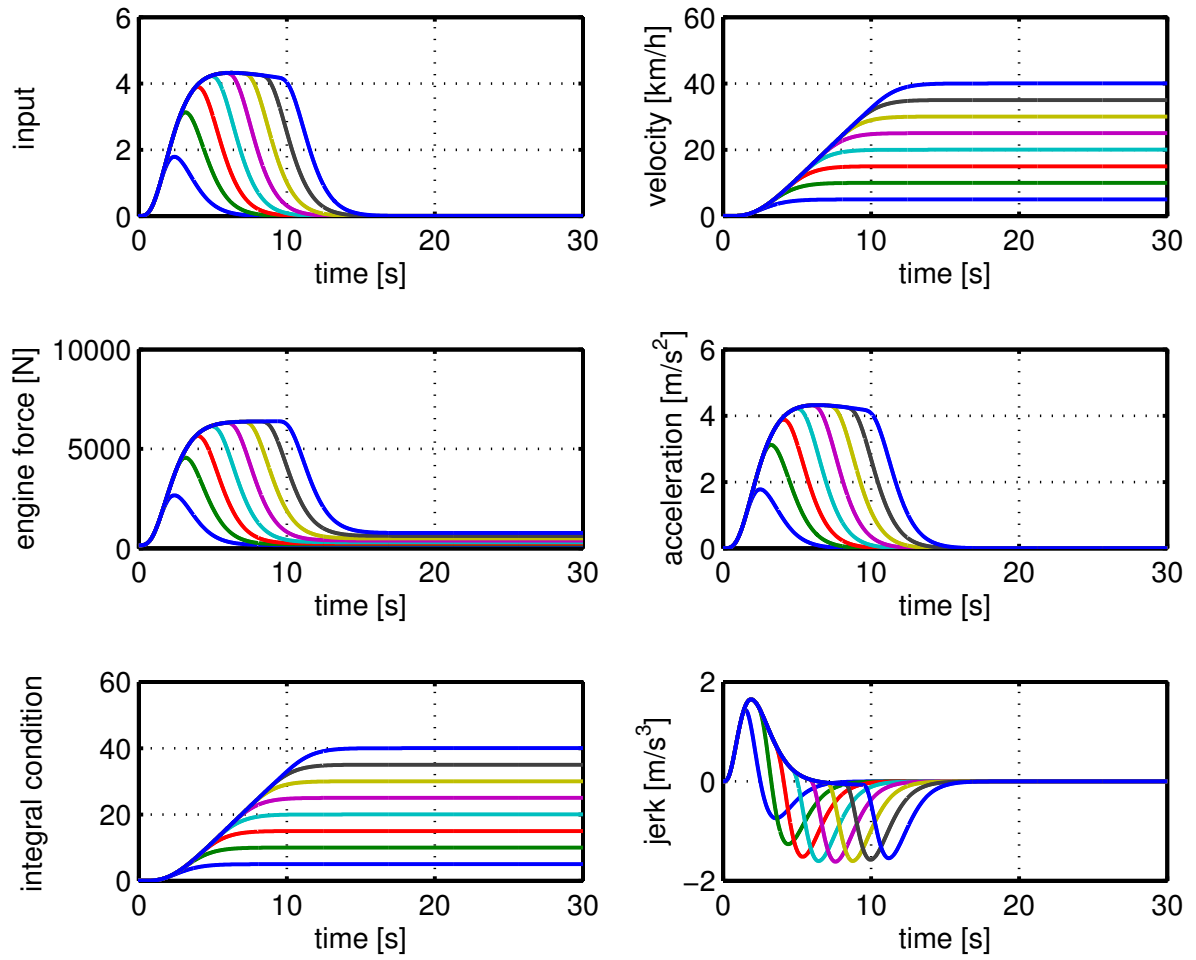
Figure 22: Maximum trajectories of the 5. vehicle with $c_{max} = 6395\,\text{N}$, $\tau = 0.1$
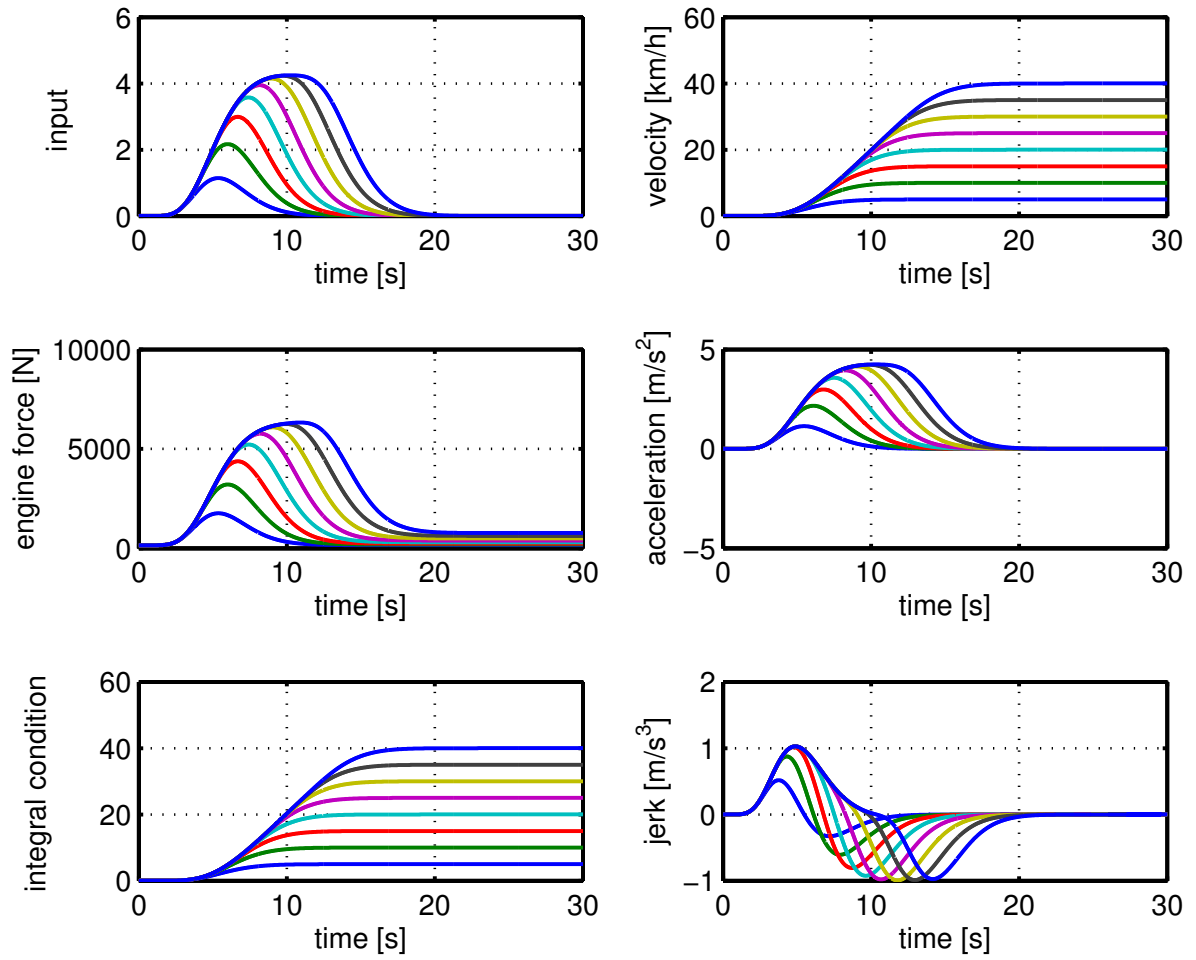
Figure 23: Maximum trajectories of the 10. vehicle with $c_{\max} = 6395\,\text{N}$, $\tau = 0.1$

In last simulation for this type of experiment, $c_{max} = 6395\,\text{N}$ and $\tau = 0.8\,\text{s}$ are used for each vehicle. The simulation results are shown in Fig. 24 to Fig. 26. The computed maximum input signal is can be seen in Fig. 24 for different final velocity values. As expected, none of the vehicles violates the force constraint since the conditions in Theorem 1 hold. In the velocity plots, the vehicles reach different the final velocities in different times as expected. Compared to the previous experiment, the durations are slightly larger since the vehicle time constant is now $\tau = 0.8\,\text{s}$. Referring to Theorem 1, there is no constraint for acceleration and jerk as shown in Fig. 24 to Fig. 26.
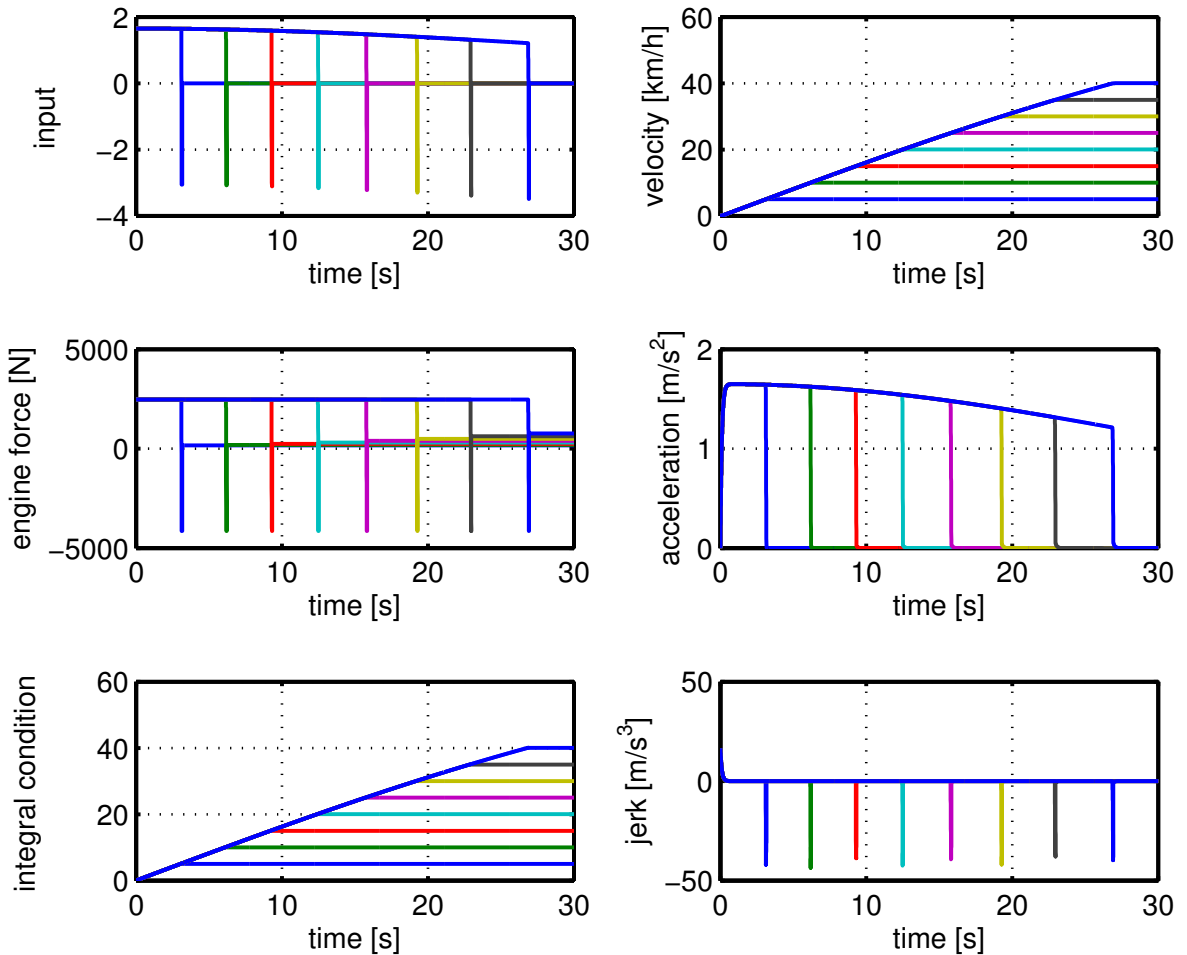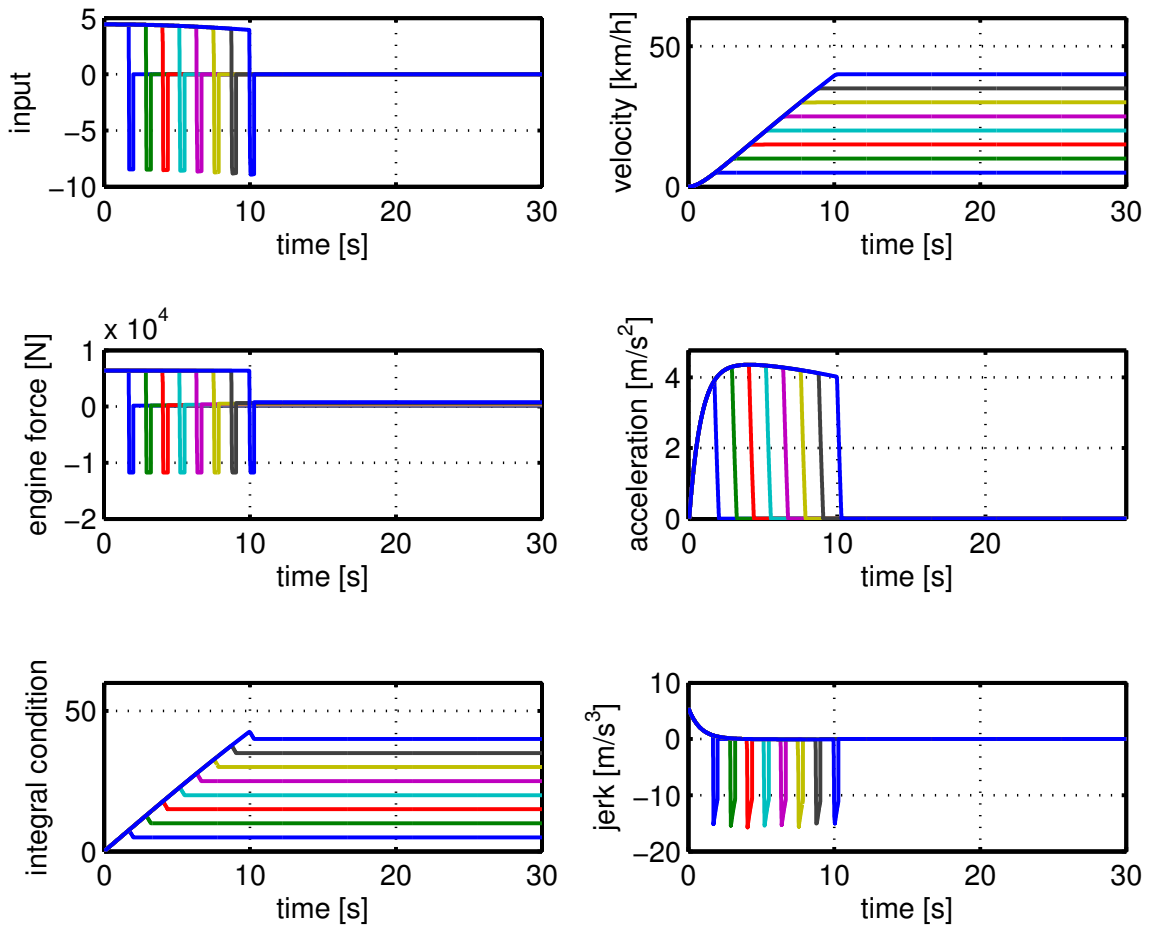

Figure 24: Maximum trajectories of the leader vehicle with $c_{max} = 6395\,\text{N}$, $\tau = 0.8$
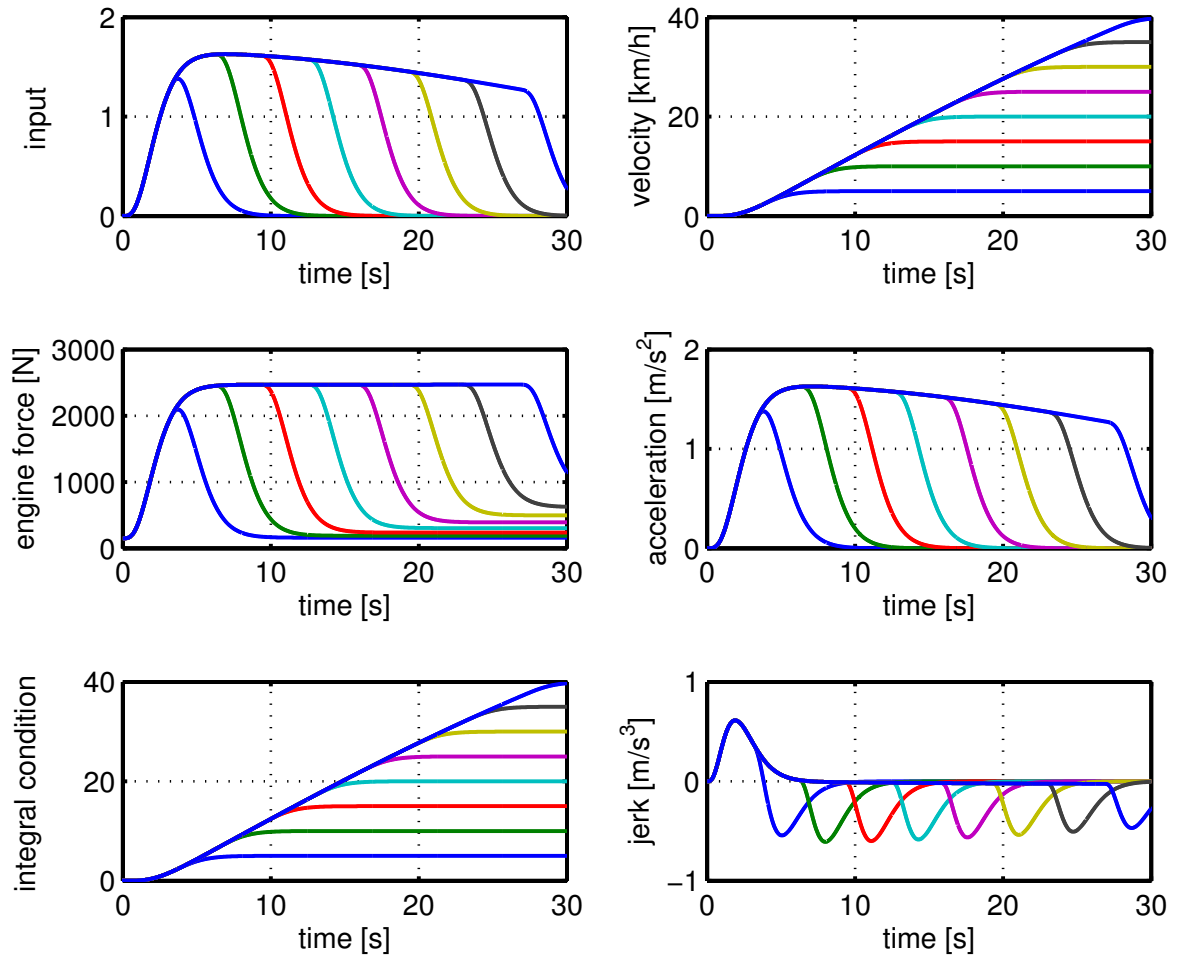
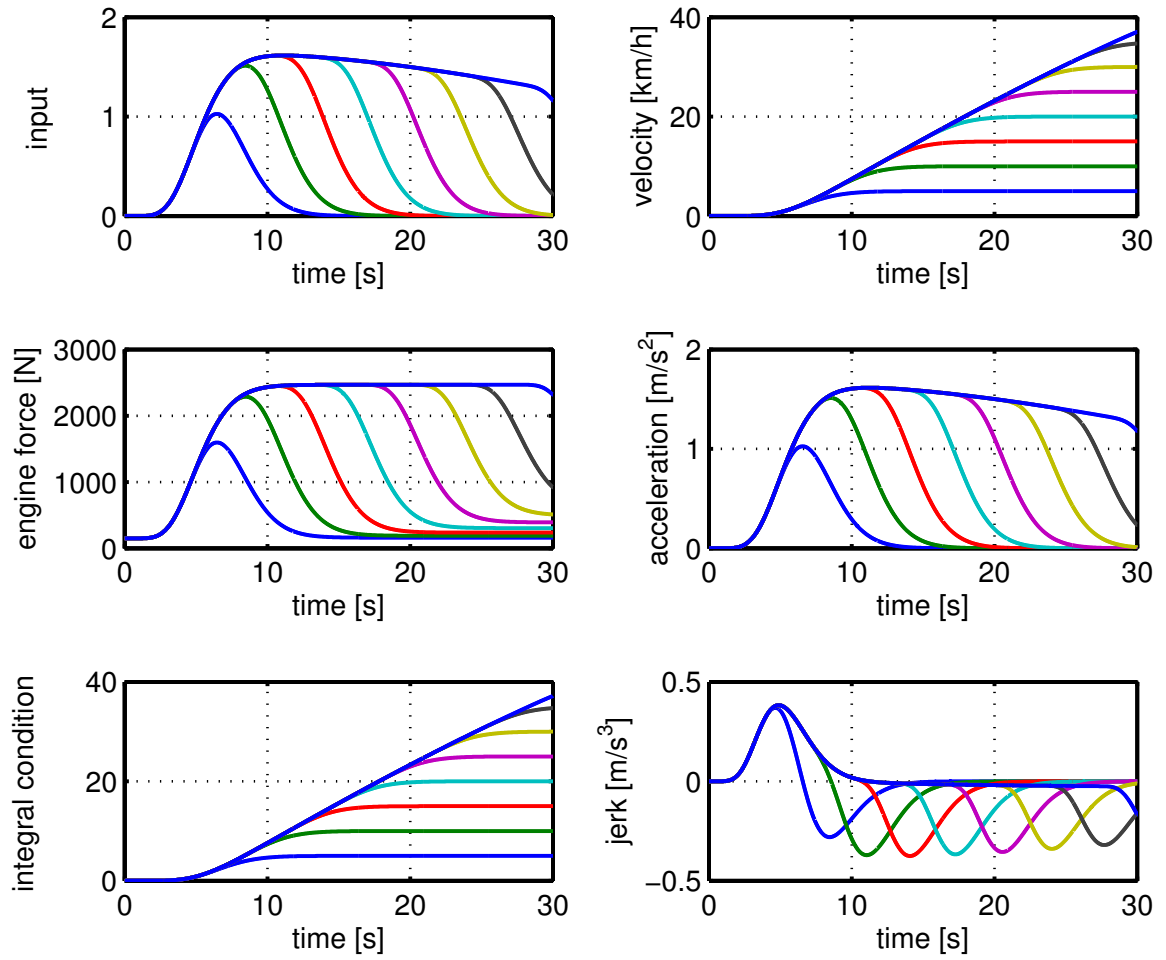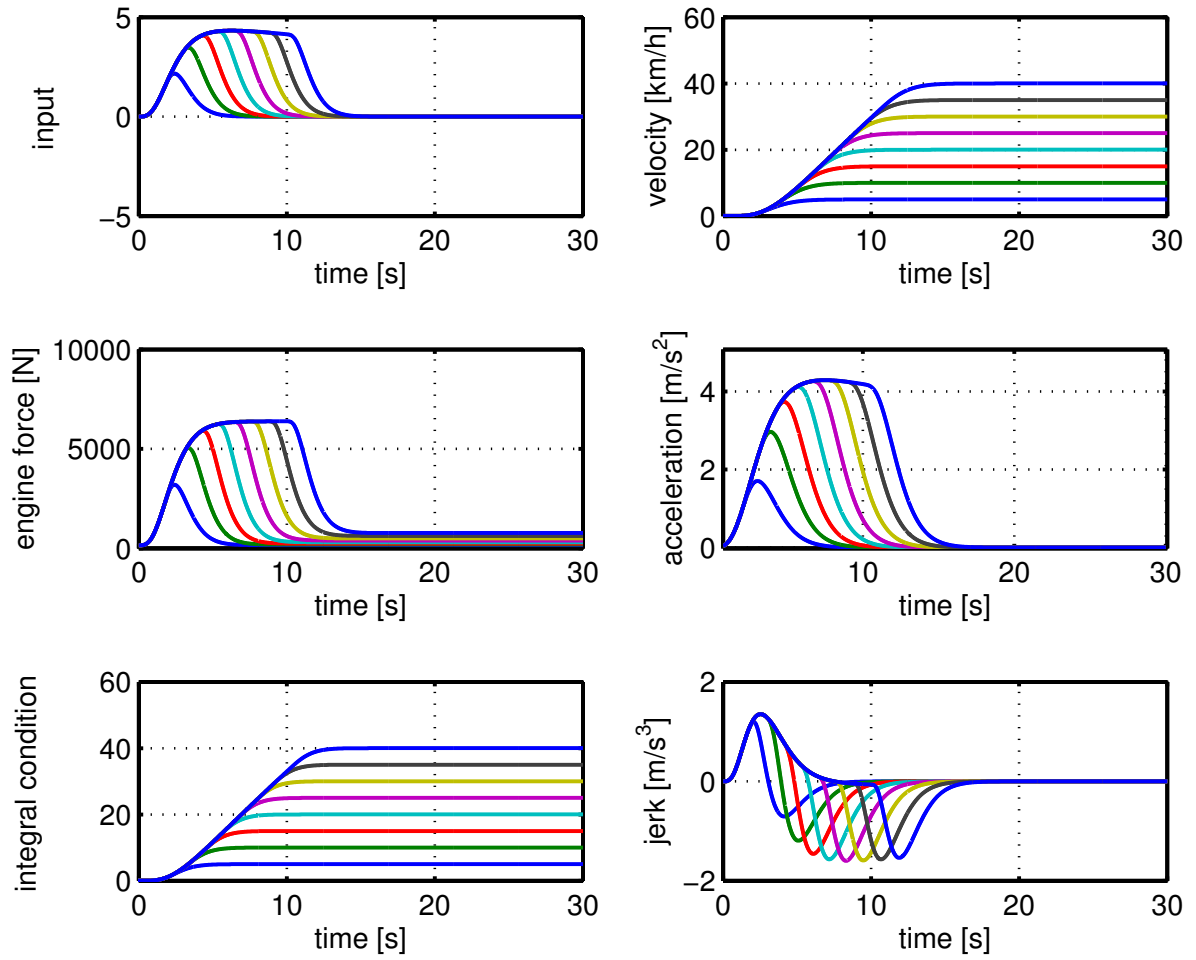**Figure 25:** Maximum trajectories of the 5. vehicle with $c_{max} = 6395\,\text{N}$, $\tau = 0.8$
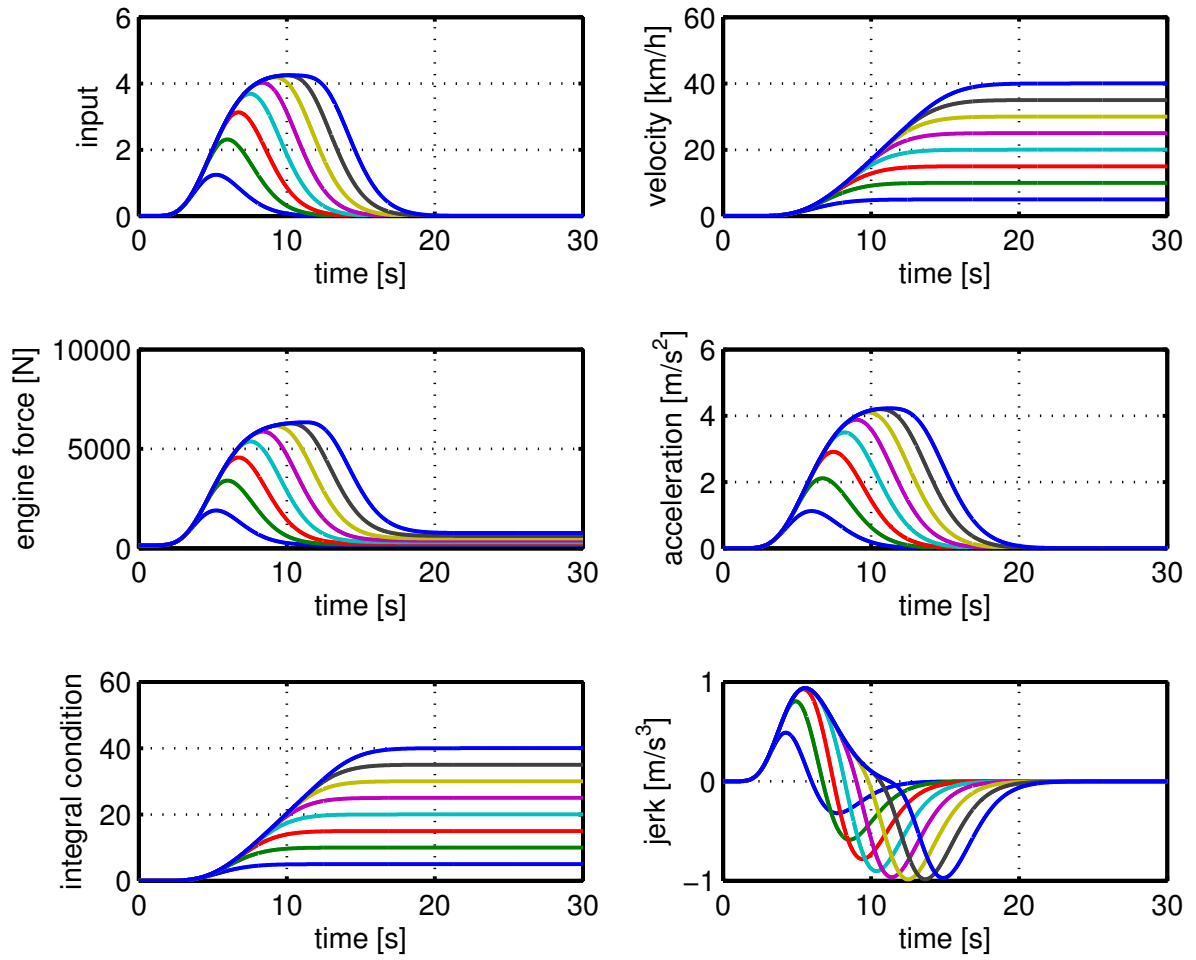
Figure 26: Maximum trajectories of the 10. vehicle with $c_{\max} = 6395\,\mathrm{N}$, $\tau = 0.8$

4.6.2 Maximum Input Signal With Jerk and Acceleration Constraints

In this section, the optimal control problem for $u_{max,v,0}$ is solved with the additional state constraints $j_{max} = 5 \, \mathrm{m/s^3}$, $a_{max} = 2 \, \mathrm{m/s^2}$.

For the subsequent simulations, $c_{max} = 2470 \, \mathrm{N}$, $\tau = 0.1 \, \mathrm{s}$ are arranged for each vehicles in the platoon. The simultion results for selected vehicles are shown in Fig. 27, Fig. 28 and Fig. 29. The observations for these simulations are in analogy to Section 4.6.1. It is further interesting to note that the maneuver duration for each velocity change is slightly longer compared to the corresponding duration in Section 4.6.1. This is due to the additional acceleration and jerk constraints. It further follows from Theorem 3 that, since $a_0 \leq a_{max}$ is bounded, the acceleration signal of all vehicles stays within the defined limits as indicated in the figures. Similarly, $j_0 \leq j_{max}$ implies that the jerk signal of the vehicles does not exceed the jerk bound.
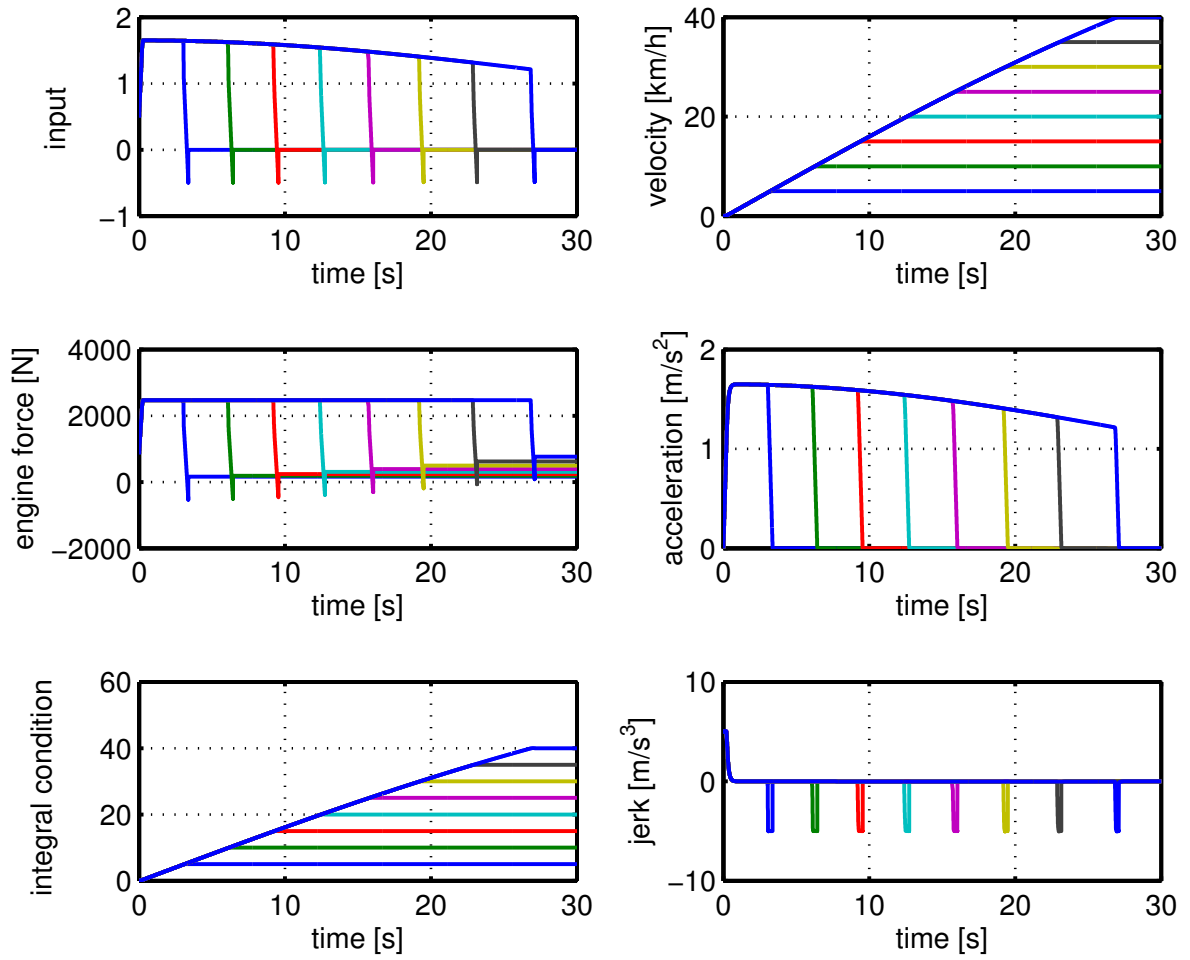
Figure 27: Maximum trajectories of leader vehicle with $j_{max} = 5 \text{ m/s}^3$, $a_{max} = 2 \text{ m/s}^2$, $c_{max} = 2470 \text{ N}$, $\tau = 0.1$
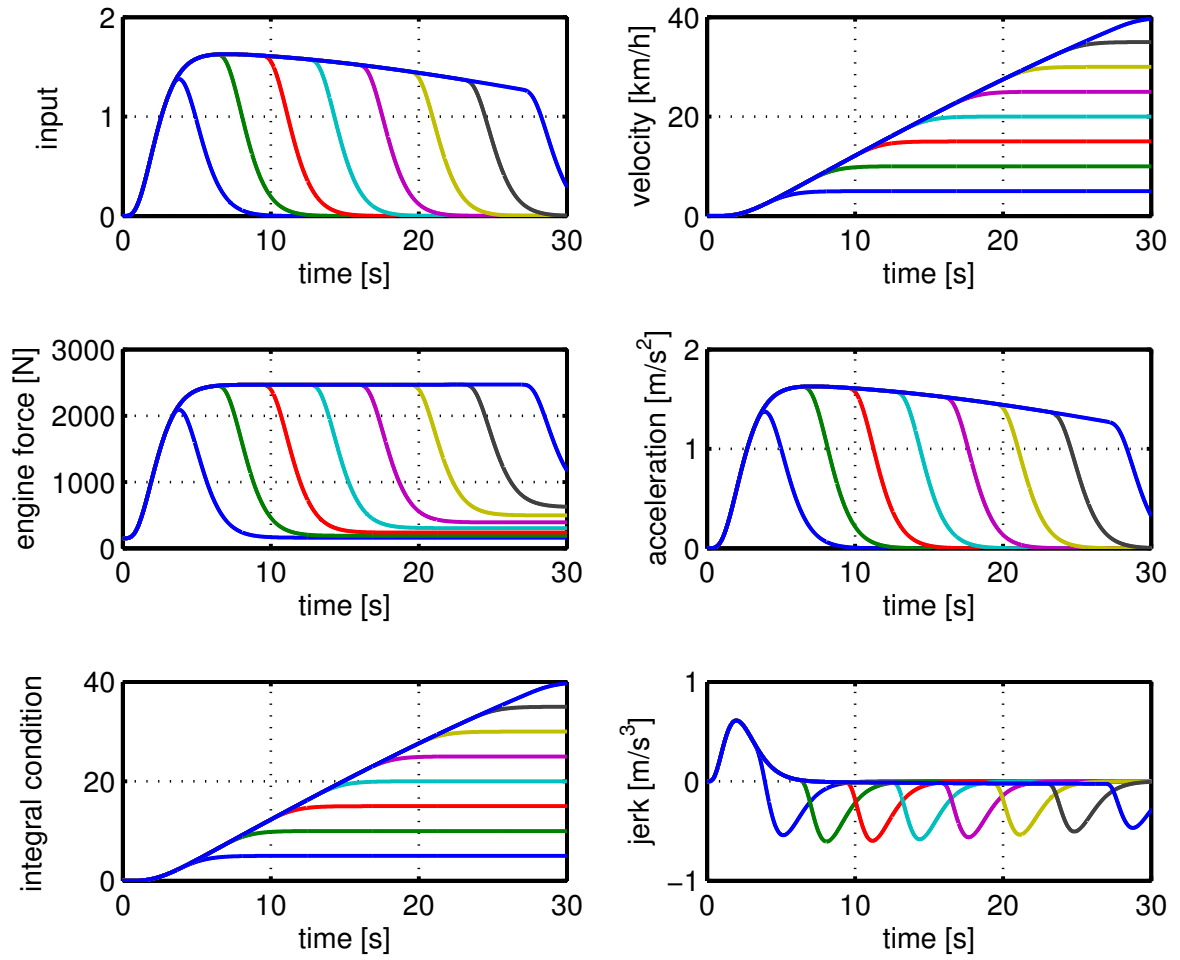
Figure 28: Maximum trajectories of 5. vehicle with $j_{max} = 5\,\text{m/s}^3$, $a_{max} = 2\,\text{m/s}^2$, $c_{max} = 2470\,\text{N}$, $\tau = 0.1$
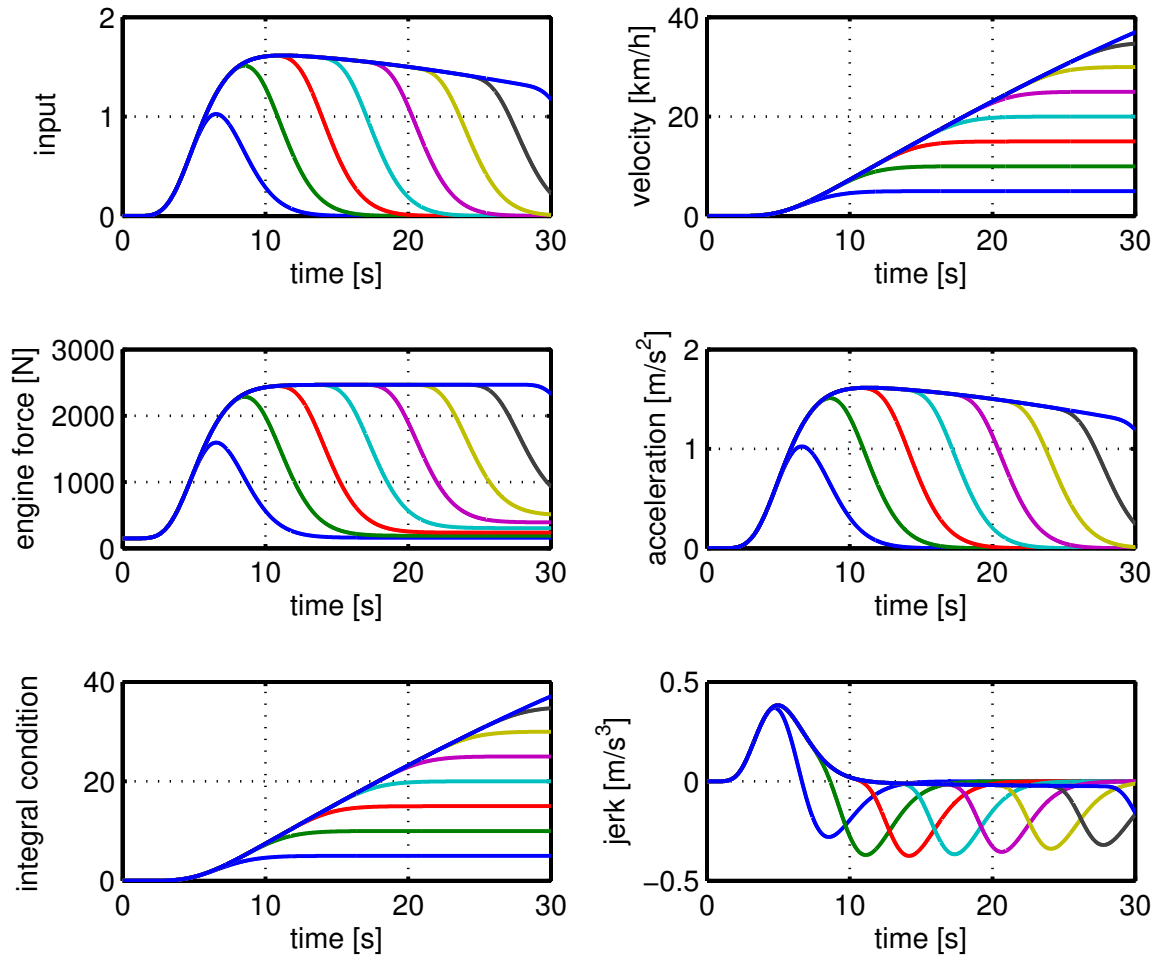
Figure 29: Maximum trajectories of 10. vehicle with $j_{max} = 5\,\mathrm{m/s^3}$, $a_{max} = 2\,\mathrm{m/s^2}$, $c_{max} = 2470\,\mathrm{N}$, $\tau = 0.1$

For following simulations, $c_{max} = 6395\,\text{N}$, $\tau = 0.1\,\text{s}$ are set for each vehicle in the platoon. The selected plots are shown in Fig. 30, Fig. 31 and Fig. 32. The generated maximum input signal for different velocity changes can be seen in Fig. 30. Again, the engine force bound is not violated. It can further be observed that the engine force does not come close to the force limit due to the imposed jerk and acceleration constraints. As stated in Theorem 1, $a_0 \leq a_{max}$ is bounded and all vehicle stay below this bound. Also, $j_0 \leq j_{max}$ is bounded such that the jerk signals of all vehicles do not exceed defined limit. In summary, the simulations confirm that all conditions of Theorem 1 and 3 are fulfilled and string stability is preserved.
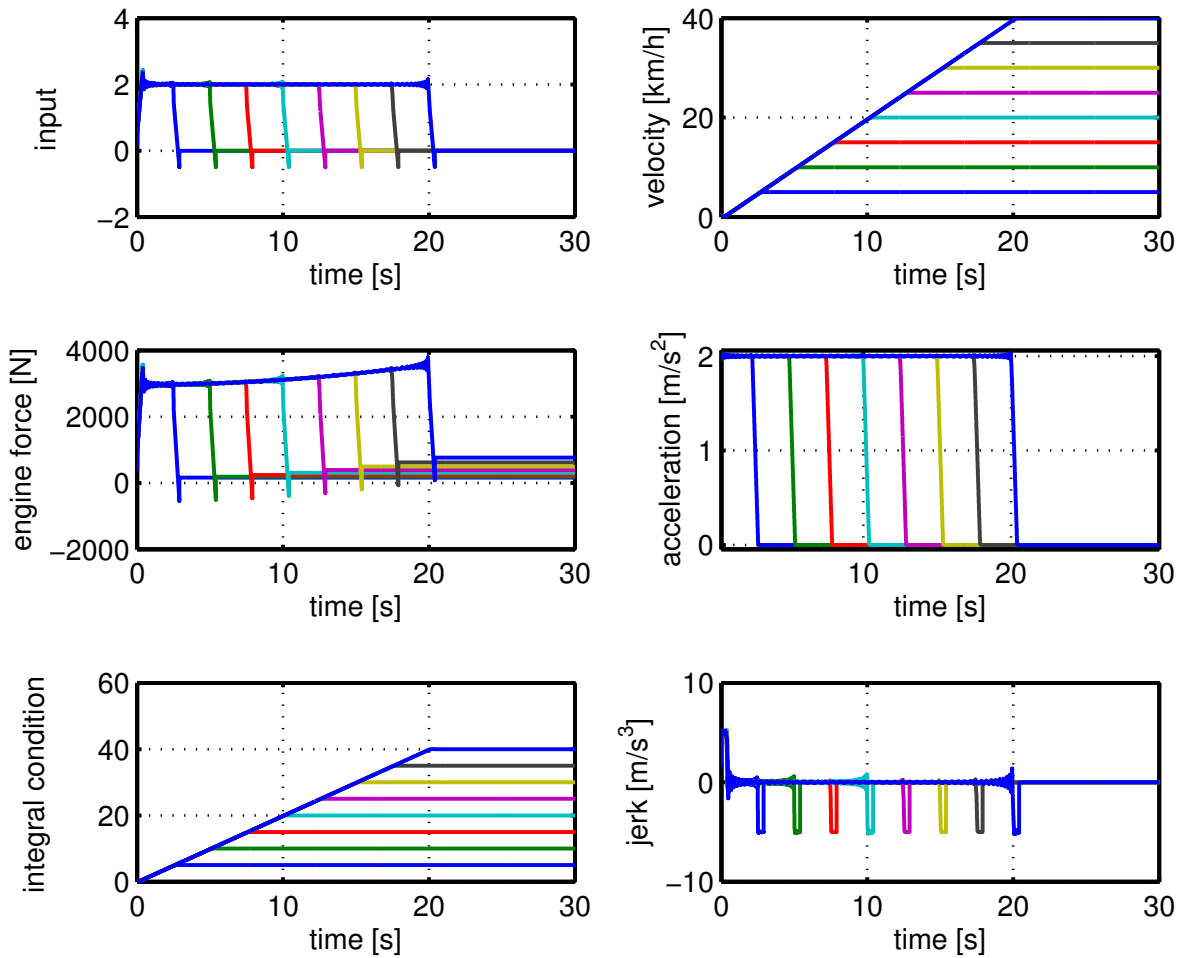
Figure 30: Maximum trajectories of leader vehicle with $j_{max} = 5\,\text{m/s}^3$, $a_{max} = 2\,\text{m/s}^2$, $c_{max} = 6395\,\text{N}$, $\tau = 0.1$
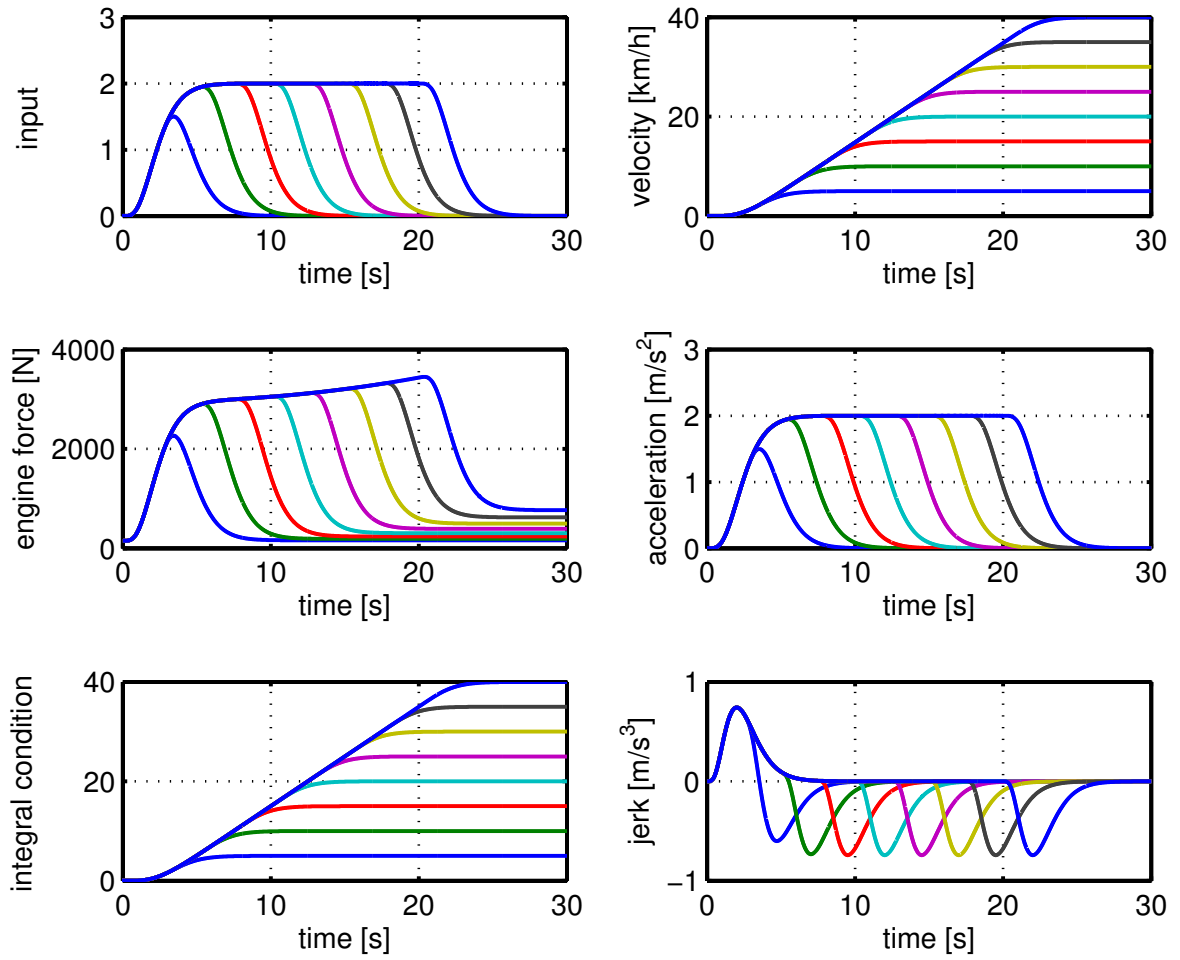
Figure 31: Maximum trajectories of 5. vehicle with $j_{max} = 5\,\text{m/s}^3$, $a_{max} = 2\,\text{m/s}^2$, $c_{max} = 6395\,\text{N}$, $\tau = 0.1$
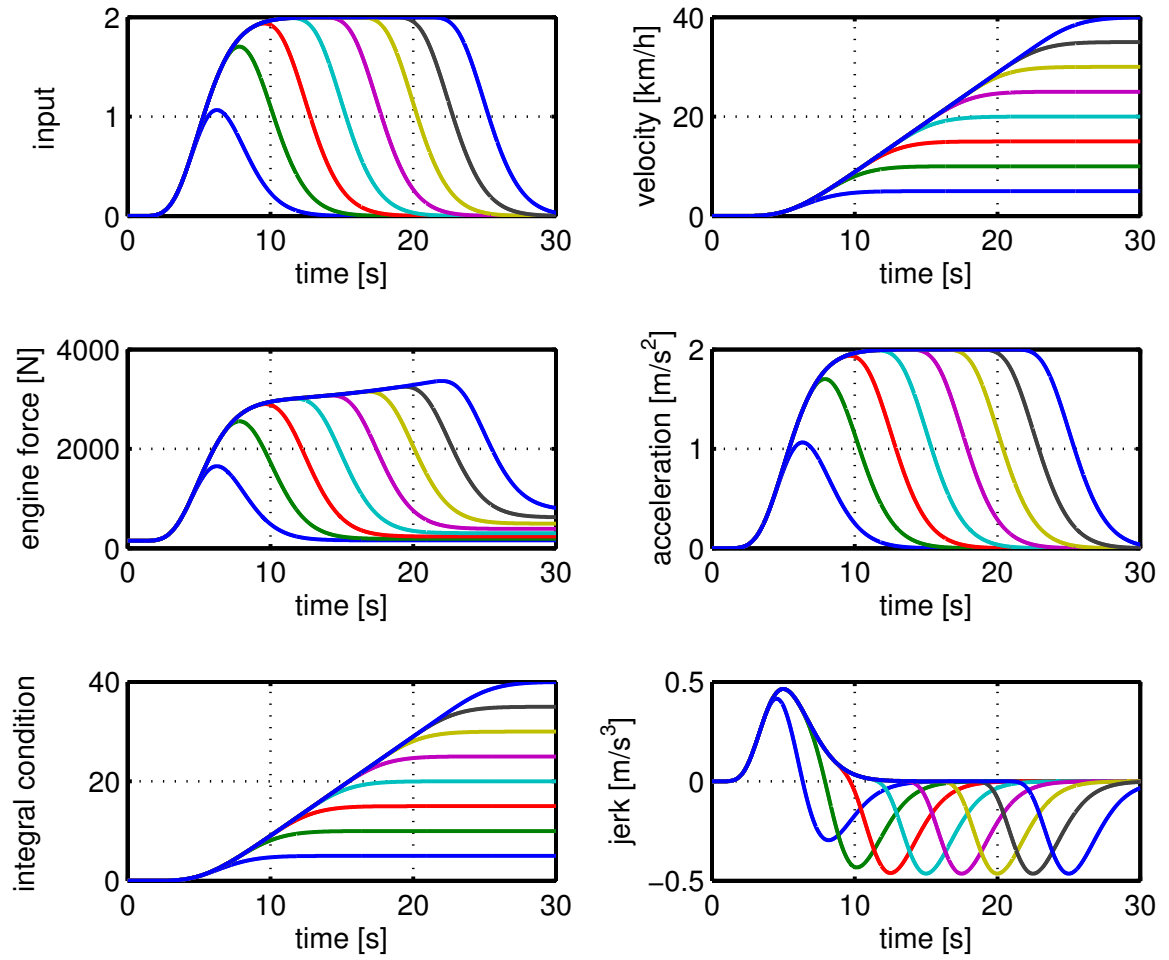
Figure 32: Maximum trajectories of 10. vehicle with $j_{max} = 5\,\text{m/s}^3$, $a_{max} = 2\,\text{m/s}^2$, $c_{max} = 6395\,\text{N}$, $\tau = 0.1$

In the last simulations related to the maximum input signal, $c_{max} = 6395\,\text{N}$, $\tau = 0.8\,\text{s}$ are set for each vehicle in the platoon. The simulation results are shown in Fig. 33, Fig. 34 and Fig. 35. The input plot of Fig. 33 shows the generated input signal with different final velocity values. The observations in this case are analogous to the previous cases. In particular, the engine force bound is not violated. Further, since $a_0 \leq a_{max}$ and $j_0 \leq j_{max}$ are bounded, the corresponding signals of all vehicles do not exceed the defined limits.
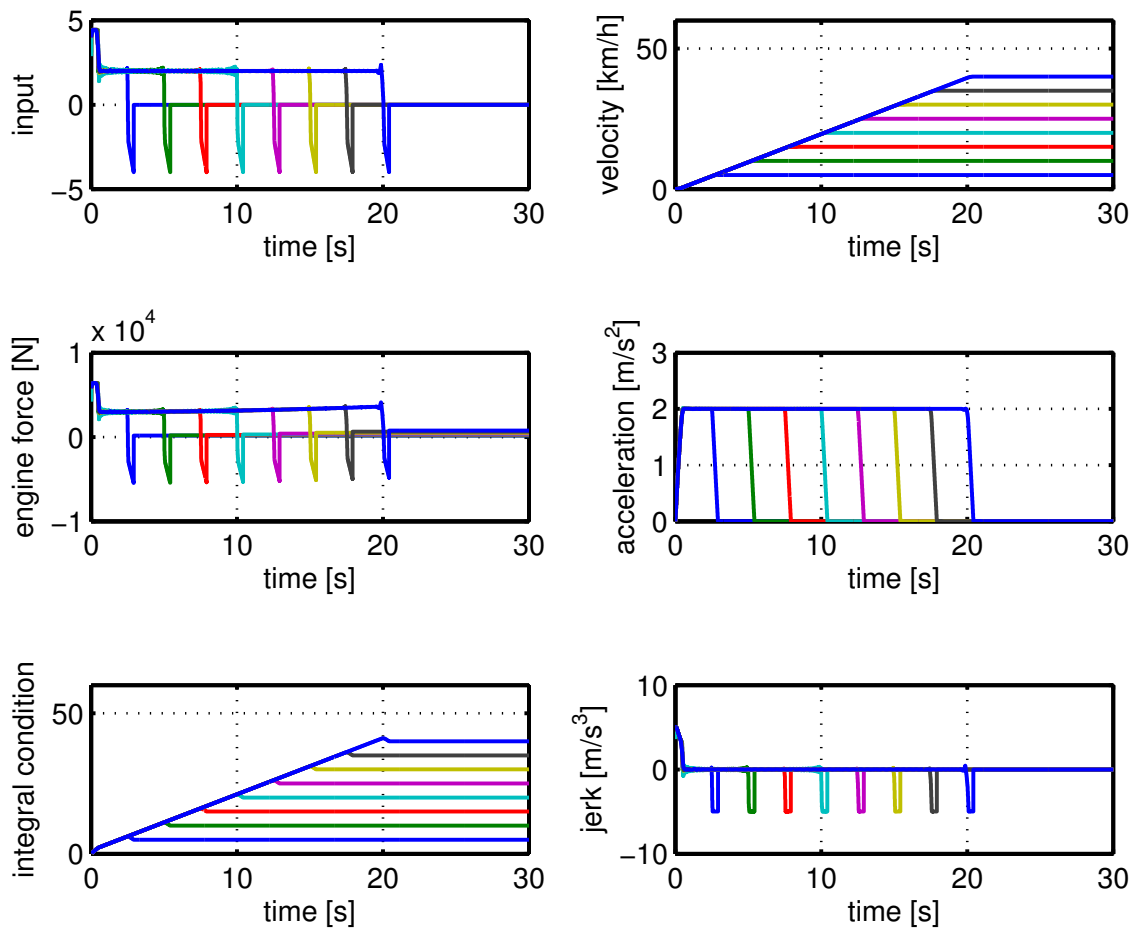
Figure 33: Maximum trajectories of leader vehicle with $j_{max} = 5\,\text{m/s}^3$, $a_{max} = 2\,\text{m/s}^2$, $c_{max} = 6395\,\text{N}$, $\tau = 0.8$
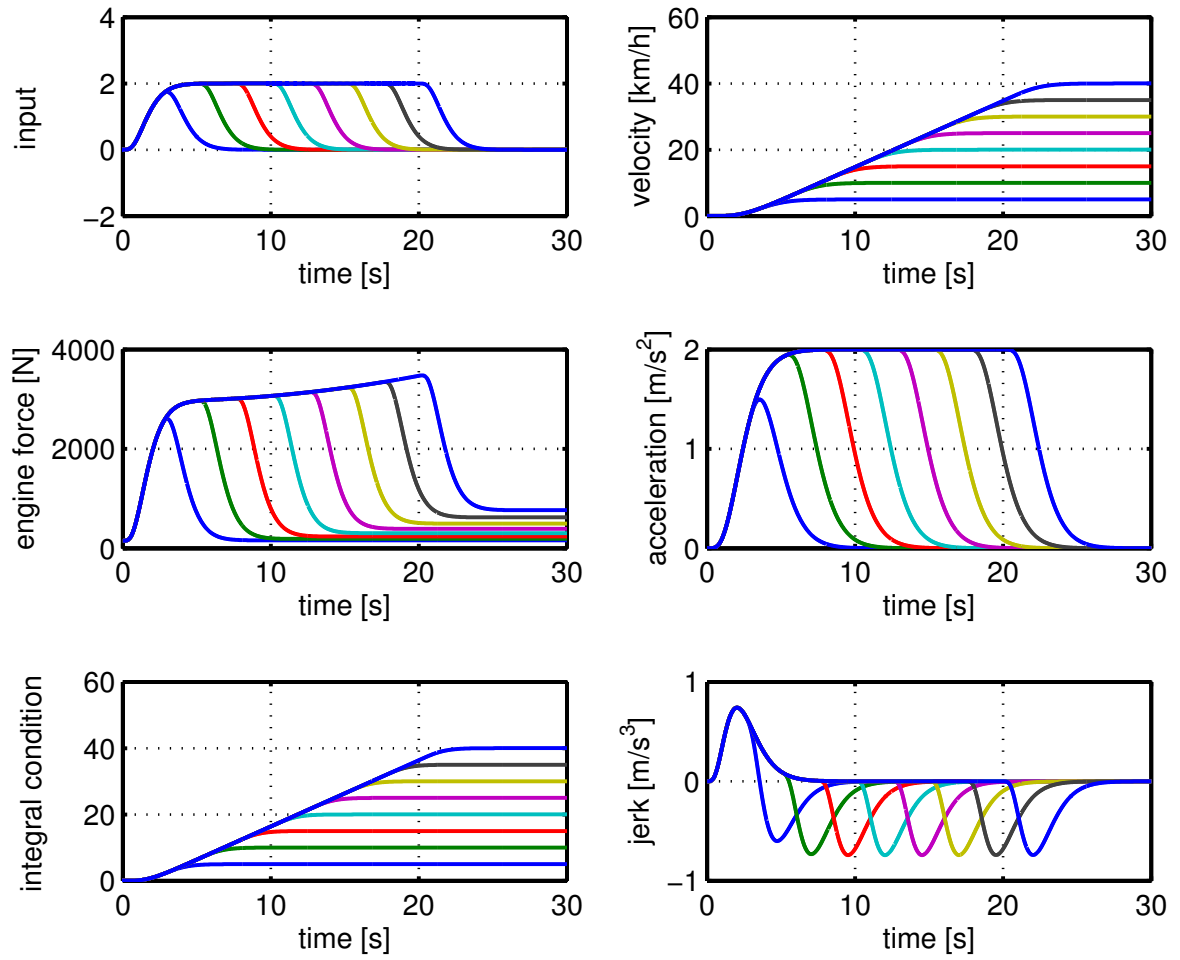
Figure 34: Maximum trajectories of 5. vehicle with $j_{\max} = 5\,\mathrm{m/s^3}$, $a_{\max} = 2\,\mathrm{m/s^2}$, $c_{\max} = 6395\,\mathrm{N}$, $\tau = 0.8$
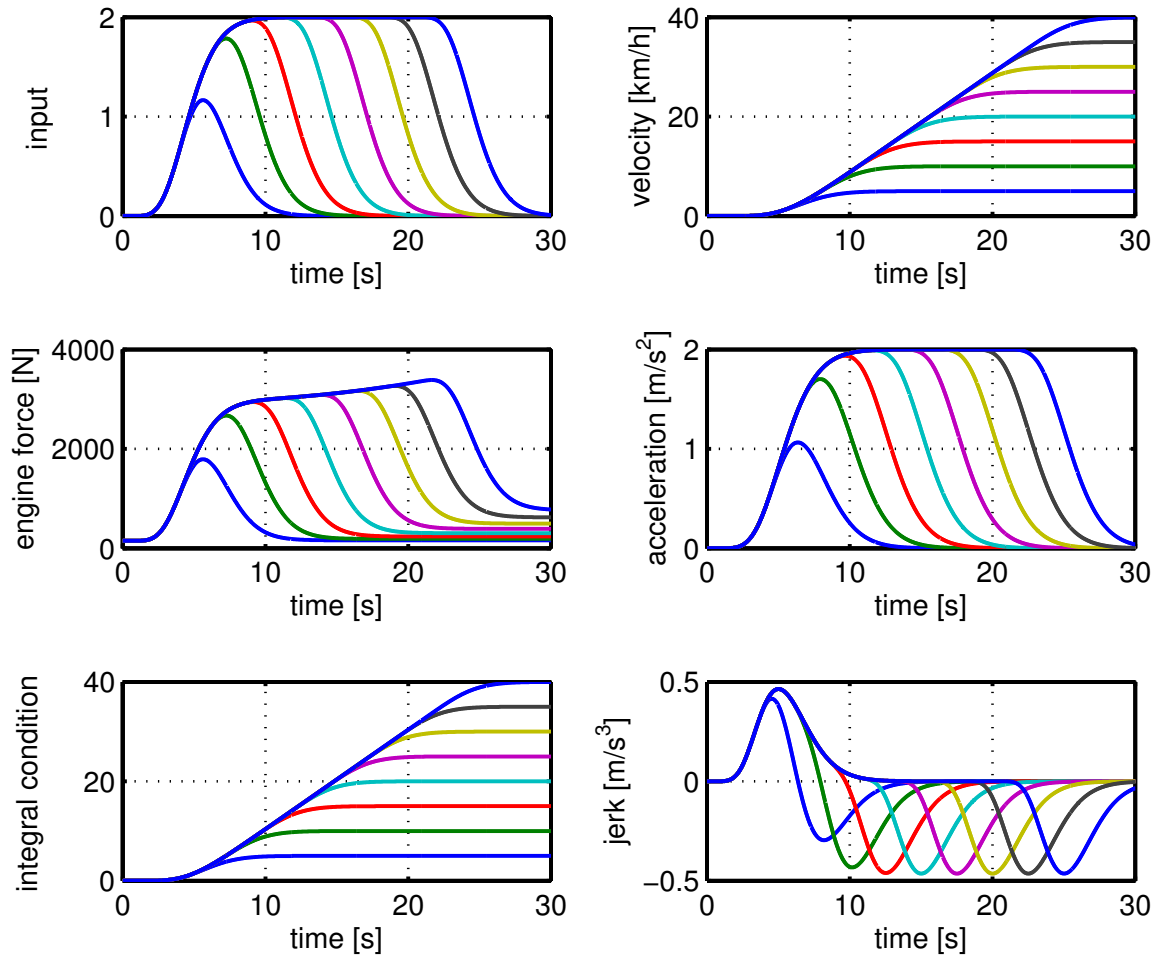
Figure 35: Maximum trajectories of 10. vehicle with $j_{max} = 5\,\text{m/s}^3$, $a_{max} = 2\,\text{m/s}^2$, $c_{max} = 6395\,\text{N}$, $\tau = 0.8$

4.7 Simulation Results for Minimum Input Signal - Theorem 2-3

Similar to the maximum input signal in Section 4.6, a minimum input signal $u_{\min,v,0}(t)$ has to be determined for the leader vehicle 0 such that the conditions in Theorem 2 are fulfilled. That is, it must be the case for each $i = 0,\ldots,N$ and for all $t \geq 0$ that

$$v + \int_0^t u_{\min,v,i}(\xi)\,d\xi \geq 0. \tag{4.41}$$

We next show that it is sufficient to require (4.41) for $i = 0$.

Lemma 2. *Consider a vehicle string with $N+1$ vehicles in the feedback loop in Fig. 10 and with the state space model in (4.6) and (4.7). Assume that K_{ff} and K_{fb} are designed such that $||\Gamma||_\infty \leq 1$ and $\gamma(t) \geq 0$ is fulfilled. Assume that (4.41) is fulfilled for $i = 0$. Then, (4.41) also holds for $i = 1,\ldots,N$*

Proof. We prove the assertion by induction. We know by assumption that (4.41) is fulfilled for $i = 0$. Now assume that (4.41) is fulfilled for $k = 0,\ldots,i-1$. We need to show that the condition is also fulfilled for i.

Considering that $\dot{a}_i(t) = -\frac{1}{\tau}a_i(t) + \frac{1}{\tau}u_i(t)$, we can write

$$u_i(t) = \tau \dot{a}_i(t) + a_i(t).$$

We know from $u_i(t) = \gamma(t) \star u_{i-1}(t)$ that $\int_0^t u_i(\xi)\,d\xi = \gamma(t) \star \int_0^t u_{i-1}(t-\xi)\,d\xi$. Let $\hat{u}_{\min} = \min_t \int_0^t u_{i-1}(\xi)\,d\xi$ be the minimum value of $\int_0^t u_{i-1}(\xi)\,d\xi$. It holds that $\hat{u}_{\min} + v \geq 0$. Then, $\gamma(t) \geq 0$ and $\int_0^\infty \gamma(\xi)\,d\xi = 1$ imply that

$$\int_0^t u_i(\xi)\,d\xi + v \geq \int_0^t \gamma(\xi)\hat{u}_{\min}\,d\xi + v = \hat{u}_{\min} + v \geq 0.$$

$\square$

Using Lemma 2, it is possible to formulate the same optimal control problem as in Section 4.6 with the additional condition

$$\int_0^t u_0(\xi)\,d\xi + v \geq 0$$

.

$$\min_{T} \int_0^T 1\, dt \qquad (4.42)$$

subject to

$$\dot{v}_0 = a_0 \qquad (4.43)$$

$$\dot{a}_0 = -\frac{1}{\tau} a_0(t) + \frac{1}{\tau} u_0(t) \qquad (4.44)$$

$$v_0(0) = v \text{ and } a_0(0) = 0 \text{ and } v_0(T) = 0 \text{ and } a_0(T) = 0 \qquad (4.45)$$

$$c_0(t) = m u_0(t) + d_{\mathrm{m}} + 0.5\,\sigma A c_{\mathrm{d}} v_0^2(t) + \tau \sigma A c_{\mathrm{d}} v_0(t) a_0(t) \geq c_{\min} \qquad (4.46)$$

$$v_0(t) \geq 0 \qquad (4.47)$$

$$a_0(t) \geq a_{\min} \qquad (4.48)$$

$$\dot{a}_0(t) \geq j_{\min} \qquad (4.49)$$

$$\int_0^t u_0(\xi)\, d\xi + v \geq 0. \qquad (4.50)$$

This optimal control problem is explained as follows.

- The objective function in (4.42) minimizes the time for maneuver.

- (4.43) to (4.44) represent the dynamic equations.

- (4.45) represents the initial and final conditions.

- (4.46) formulates the constraint for the maximum braking force.

- (4.47) to (4.49) pose additional constraints on velocity, acceleration and jerk.

- (4.50) is the additional constraint that is needed because of Lemma 2.

We next perform example computations for the minimum input signal. In the first example, we consider velocity changes from $v = 40$ m/s to different final velocities of $35, 30, 25, 20, 15, 10, 5, 1$ m/s. The same vehicle parameters as in Table 2 are used and the minimum force is computed as $c_{\min} = -11730$ N for $\mu = 0.85$ and $c_{\min} = -4140$ N for $\mu = 0.3$.

4.7.1 Minimum Input Signal Without State Constraints

The initial velocity is set to $v_i = 40\,\text{m/s}$ and $a_i = 0\,\text{m/s}^2$ in optimal control problem. In addition to these parameters, $c_{\min} = -4140\,\text{N}$ and $\tau = 0.1$ are set for the following simulations.
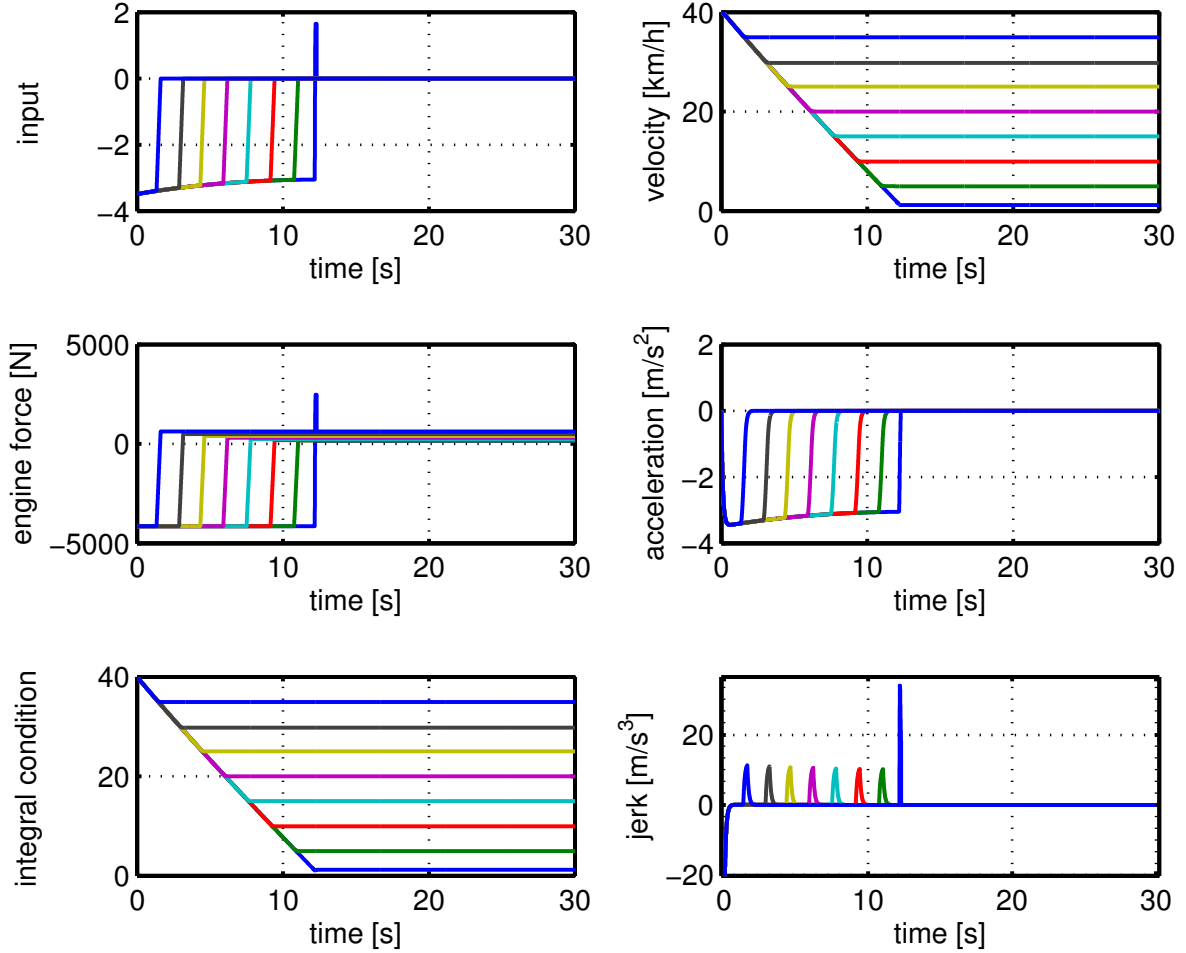
Figure 36: Minimum trajectories of leader vehicle with $c_{min} = -4140\,\text{N}$, $\tau = 0.1$

The leader vehicle signal plots are shown in Fig. 36. The generated input signal by the optimal control solution and its integral is shown in by the blue line in the figure. Even for large changes in the final velocity of the leader vehicle, the integral condition in (4.24) is fulfilled. At this point, we focus on the difference between the initial velocity $v_i = 40\,\text{m/s}$ and final velocity values. As expected, if the velocity difference is smaller, the vehicle reaches the final velocity faster. It can be seen in these figures that all vehicles meet the force constraint. However, since there are no state constraints, large

acceleration and jerk values are observed, which impairs the driving comfort.
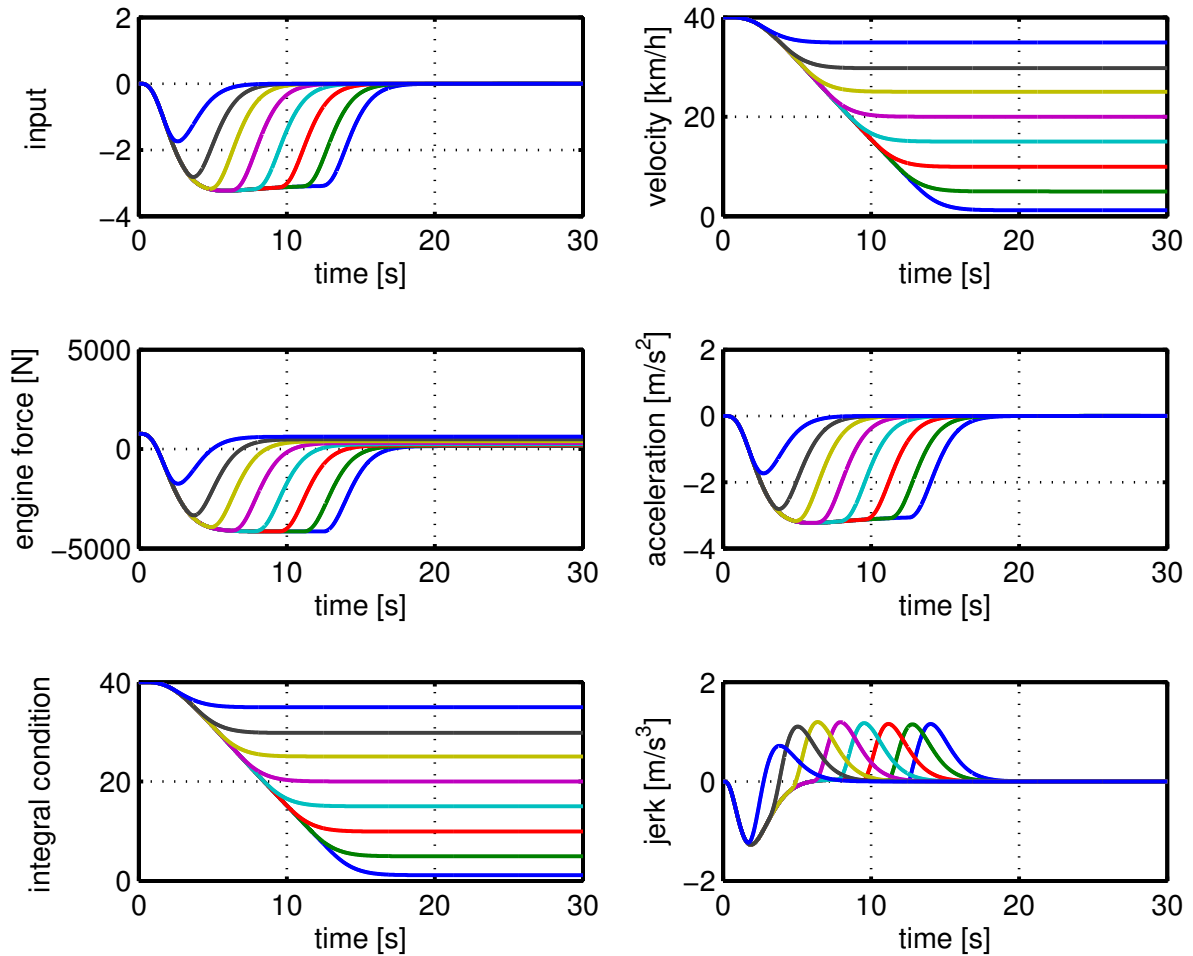
Figure 37: Minimum trajectories of 5. vehicle with $c_{\min} = -4140\,\text{N}$, $\tau = 0.1$

Fig. 37 indicates the 5. vehicle. The input signal with the greatest velocity difference is represented by a blue line. As seen in the velocity plots, if the velocity difference is getting smaller then the vehicle reach the final velocity earlier and the engine force has to be applied to the vehicle for a shorter time duration if velocity difference is getting smaller. Even if different final velocity values are set for the vehicle, the engine force $c_{\min}$ stays above the defined limit of $-4140\,\text{N}$.

The simulation for the last vehicle is shown Fig. 38. Again, the engine force of the vehicle does not exceed the minimum limit $c_{\min} = -4140\,\text{N}$. Furthermore, the acceleration, jerk plots of the last vehicle give reasonable results.
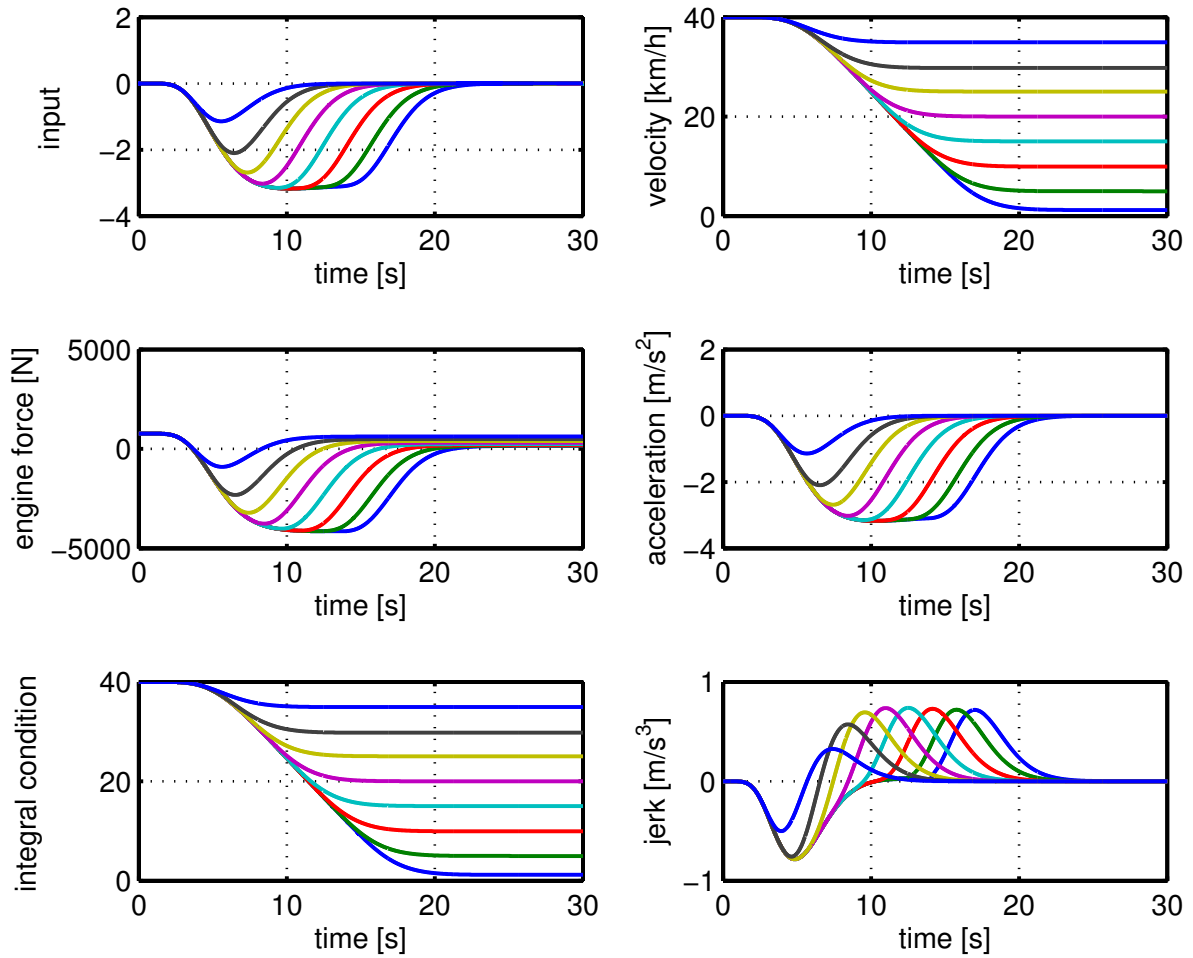
Figure 38: Minimum trajectories of 10. vehicle with $c_{min} = -4140\,\text{N}$, $\tau = 0.1$

For next simulation, $c_{min} = -11730\,\text{N}$ is used. Fig. 39 to Fig. 41 correspond to the 1. vehicle, 5. vehicle and 10. vehicle in the platoon, respectively. The input signal plot in Fig. 39 shows the input signal generated by optimal control. As can be seen from the velocity plot of the figures, the arrival time of the vehicles changes with the final velocity. Accordingly, the braking force is applied to the vehicles in different time intervals as displayed in figures. Since the minimum braking force is smaller compared to the previous experiment, faster maneuvers are achieved. The acceleration and jerk plots of the figures also show that high accelerations and jerk values are observed since no constraint on these signals is imposed.
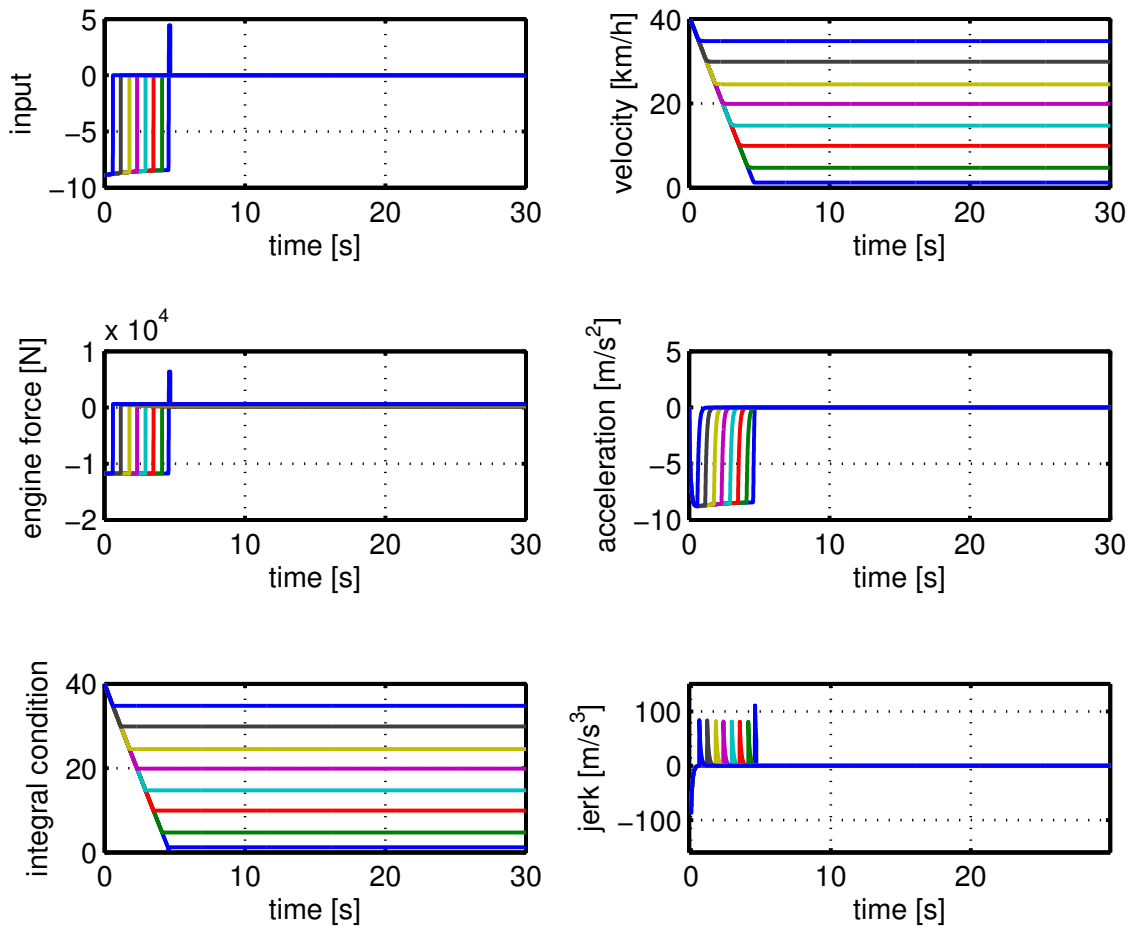
Figure 39: Minimum trajectories of leader vehicle with $c_{min} = -11730\,\mathrm{N}$, $\tau = 0.1$
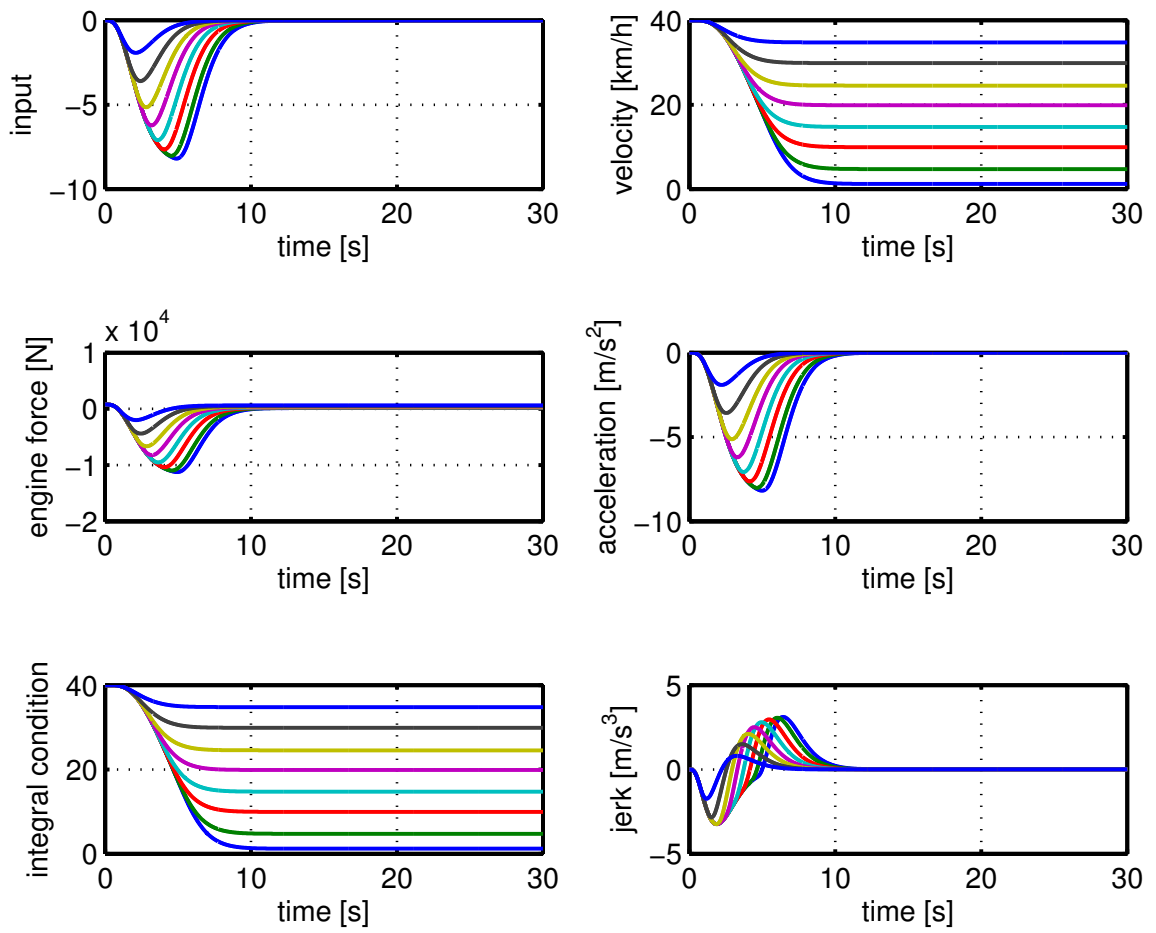
Figure 40: Minimum trajectories of 5. vehicle with $c_{min} = -11730\,\mathrm{N}$, $\tau = 0.1$
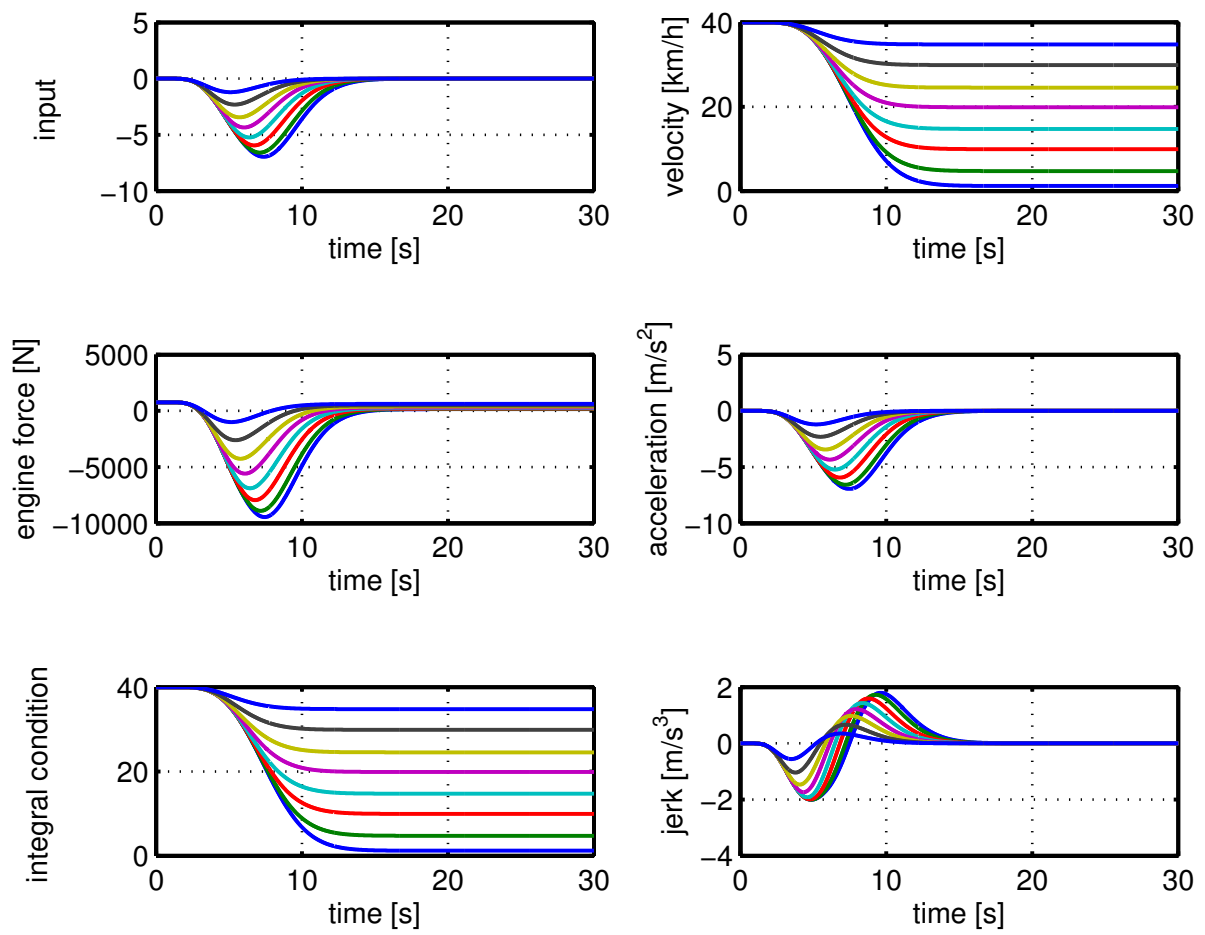
Figure 41: Minimum trajectories of 10. vehicle with $c_{min} = -11730\,\text{N}$, $\tau = 0.1$

In the following experiment, $\tau = 0.8$ is set for each vehicle in the string and $c_{\min} = -11730\,\mathrm{N}$. The plots for the selected vehicles are shown in Fig. 42, Fig. 43 and Fig. 44. The input signal generated by optimal control problem can be seen in Fig. 42. All the observations are analogous to the previous experiment, whereby the maneuvers times are slightly larger due to the larger vehicle time constant $\tau = 0.8$.
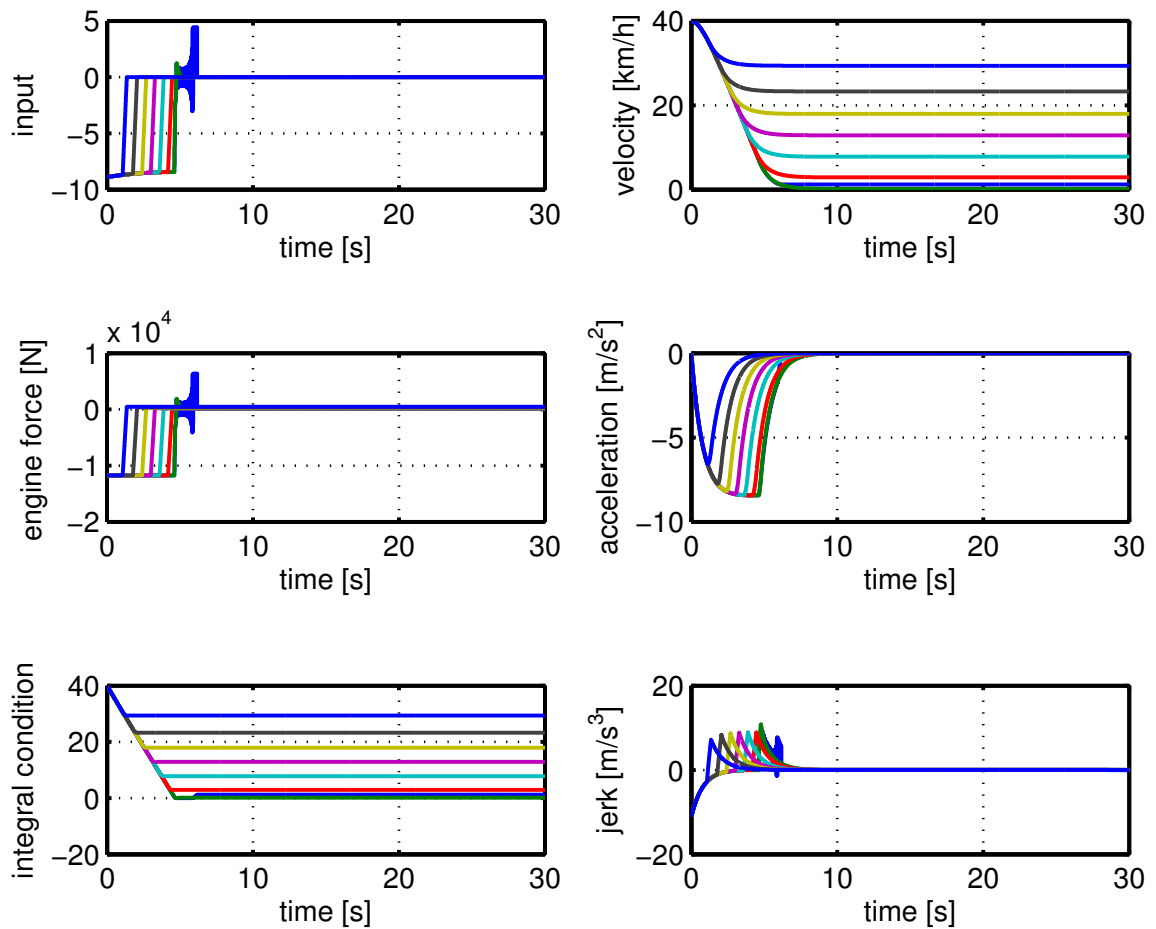
Figure 42: Minimum trajectories of leader vehicle with $c_{\min} = -11730\,\mathrm{N}$, $\tau = 0.8$
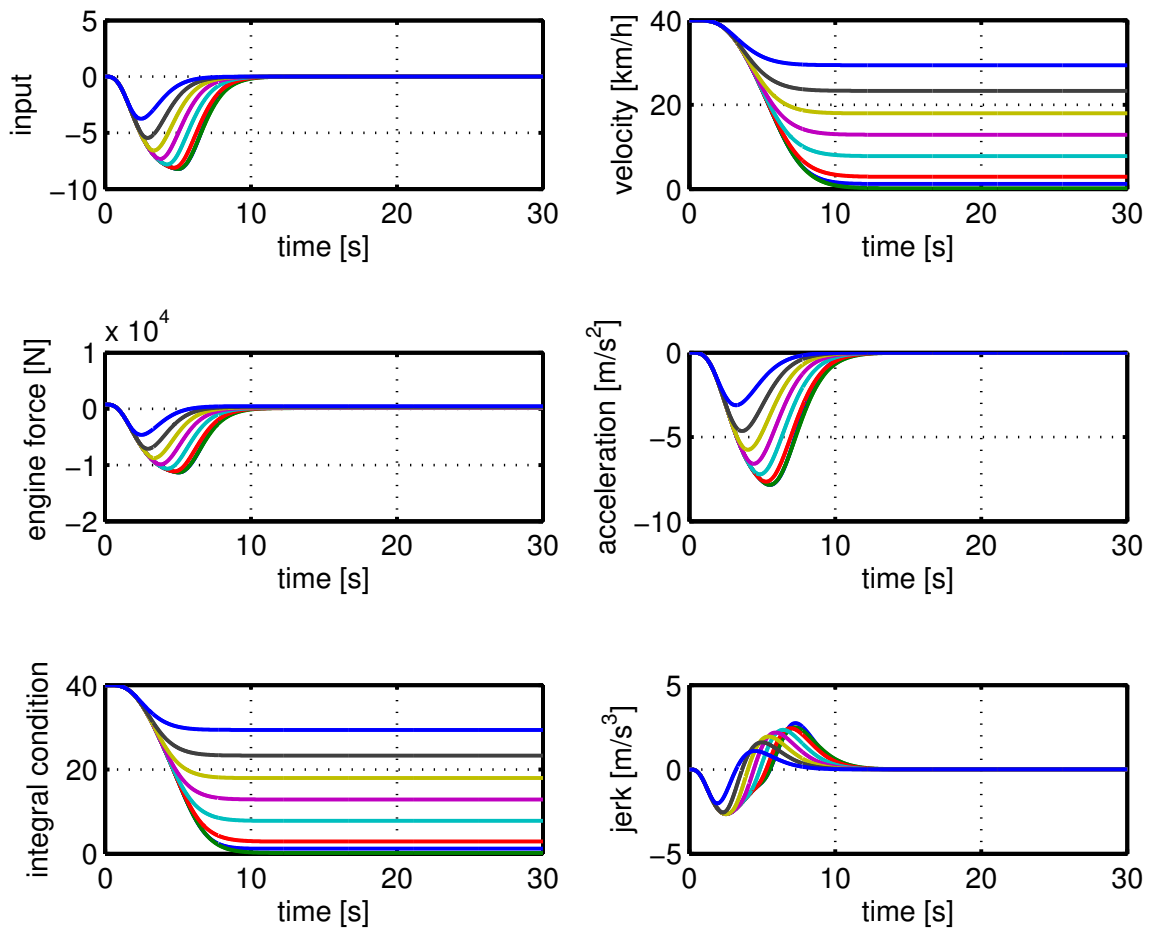
Figure 43: Minimum trajectories of 5. vehicle with $c_{min} = -11730\,\text{N}$, $\tau = 0.8$
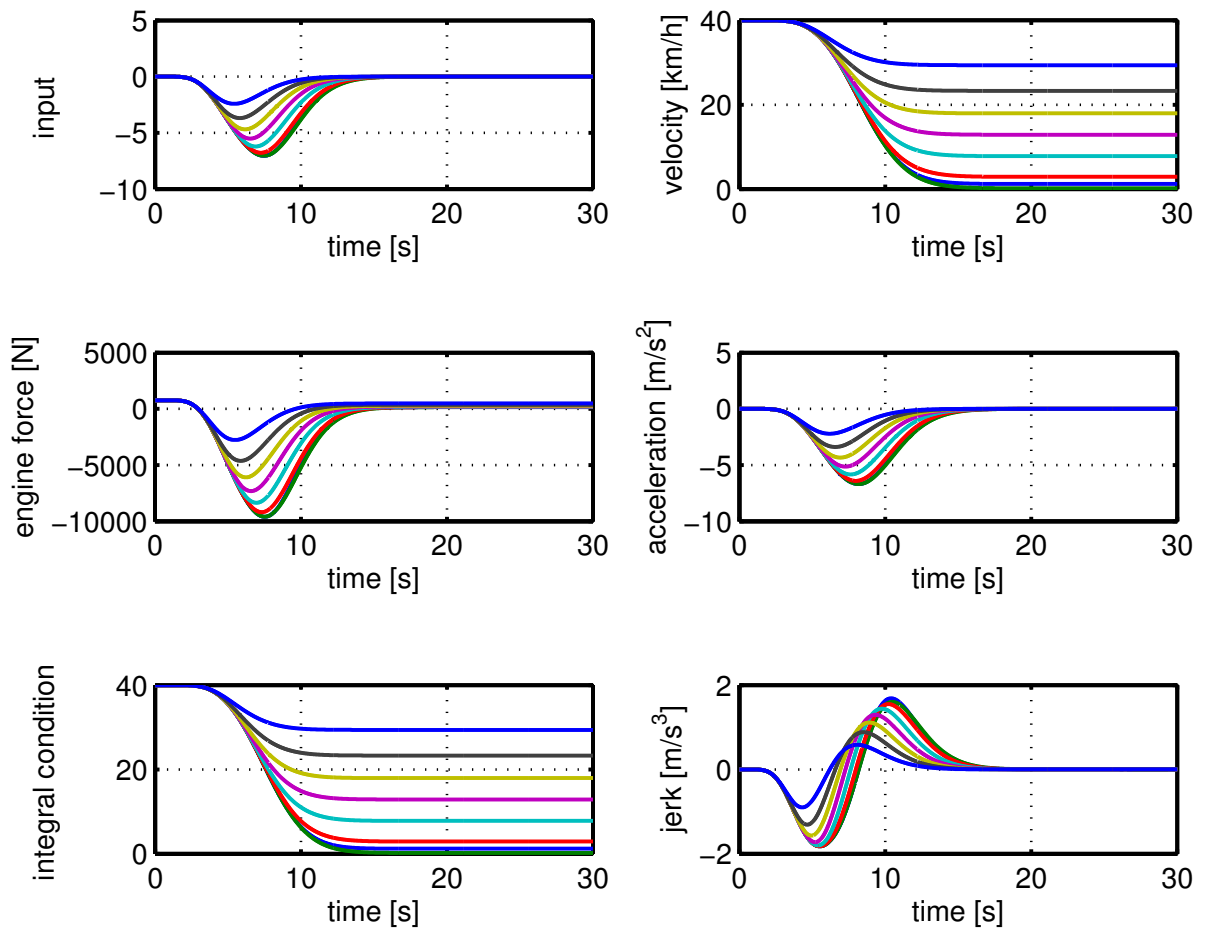
Figure 44: Minimum trajectories of 10. vehicle with $c_{\min} = -11730\,\text{N}$, $\tau = 0.8$

4.7.2 Minimum Input Signal With Acceleration and Jerk Constraints

To generate $u_{0,min}$, the additional state constraints are set as $-2\,\text{m/s}^2 \leq a_{min}$ and $-5\,\text{m/s}^3 \leq j_{min}$. Also, $v_i(0) = 40\,\text{m/s}$ and $a_i(0) = 0\,\text{m/s}^2$ are chosen for each vehicle in string.

For the following simulation, $c_{min} = -4140\,\text{N}$ and $\tau = 0.1$ are used. The btained simulation results of the selected vehicles are displayed in Fig. 45, Fig. 46 and Fig. 47. The generated input signal is shown in Fig. 45 for different final velocity values. It can further be seen that the integral constraint in (4.24) is fulfilled. Since acceleration and jerk constraints are imposed according to Theorem 3, the acceleration and jerk values do not exceed the defined limit values.
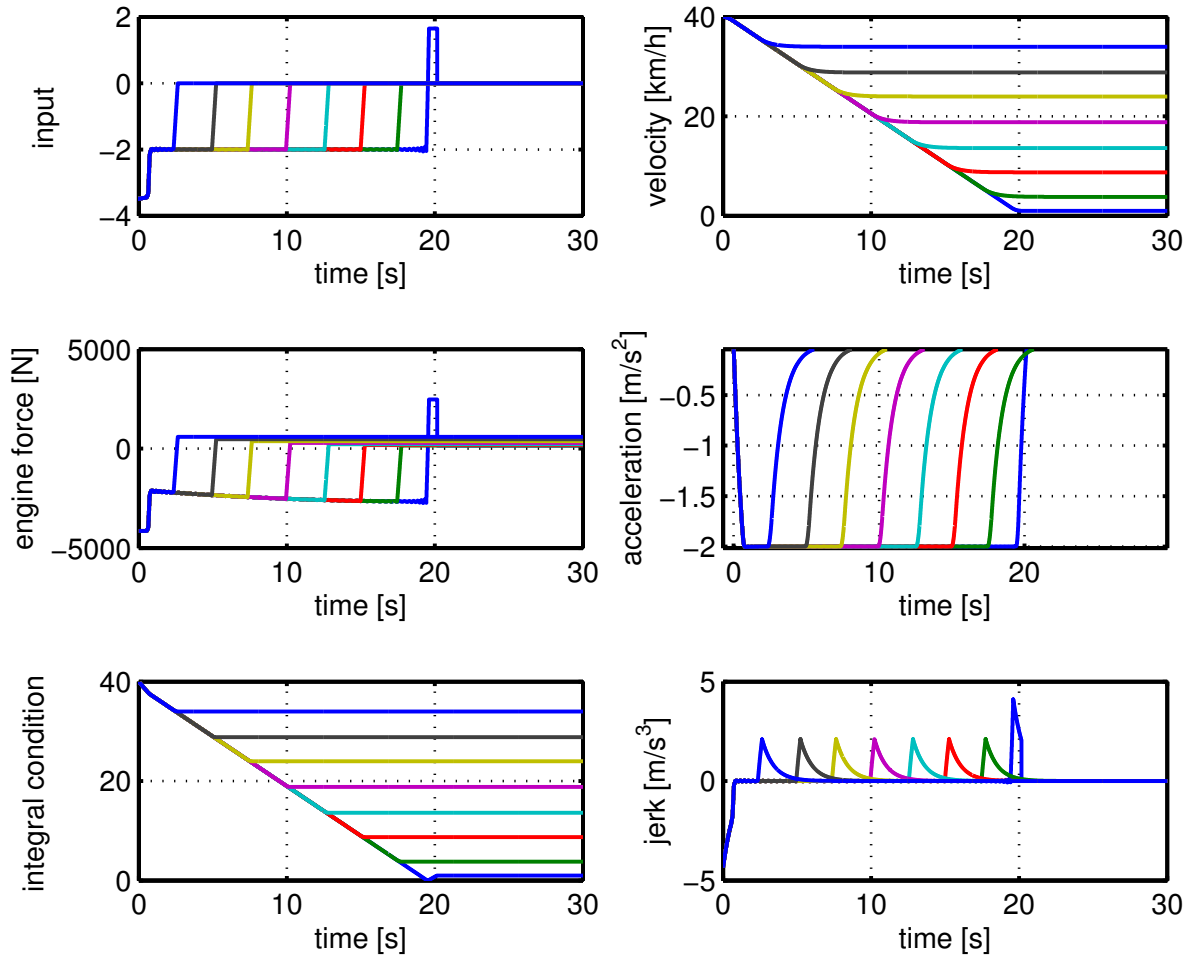
Figure 45: Minimum trajectories of leader vehicle with $j_{min} = -5\,\text{m/s}^3$, $a_{min} = -2\,\text{m/s}^2$, $c_{min} = -4140\,\text{N}$, $\tau = 0.1$
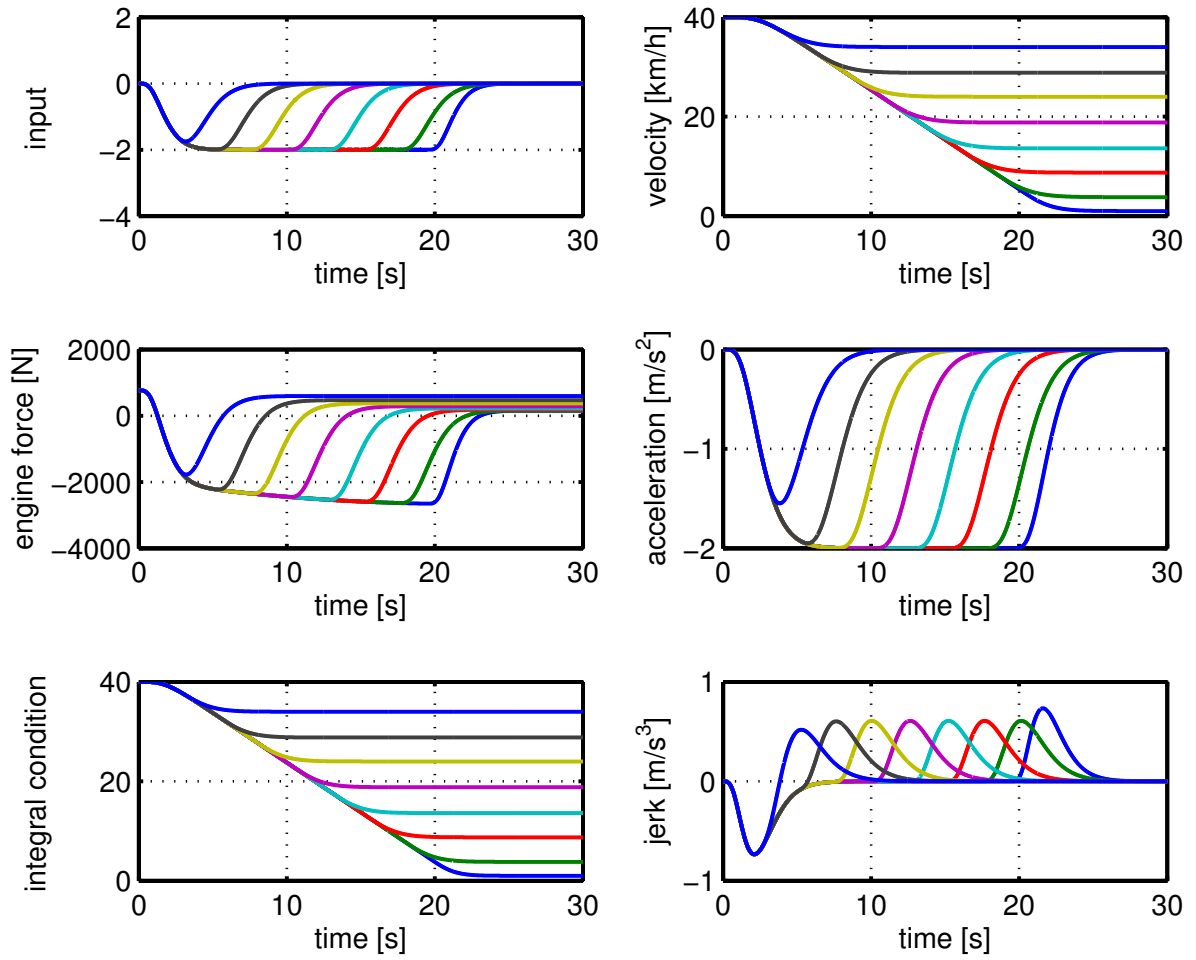
Figure 46: Minimum trajectories of 5. vehicle with $j_{min} = -5 \, \text{m/s}^3$, $a_{min} = -2 \, \text{m/s}^2$, $c_{min} = -4140 \, \text{N}$, $\tau = 0.1$
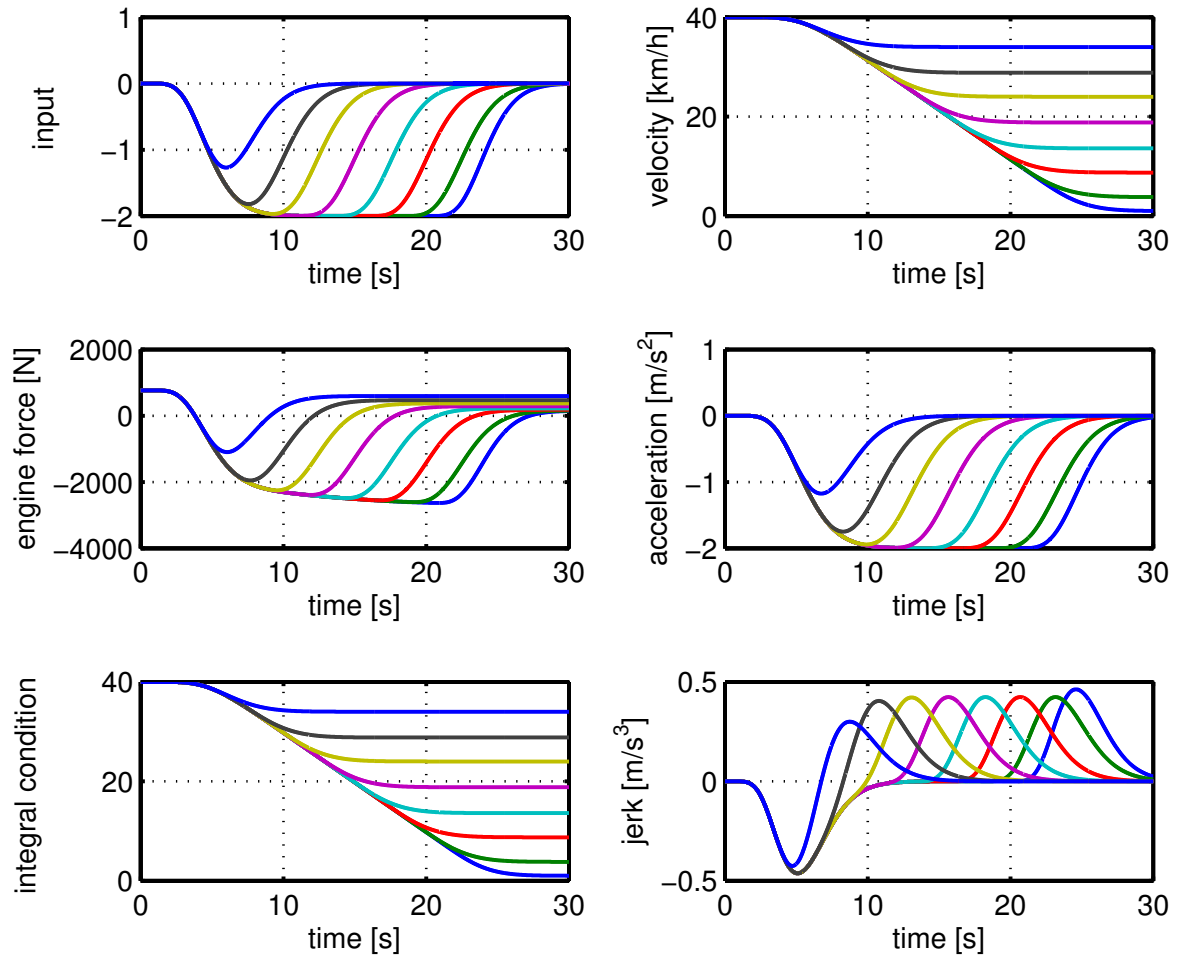
Figure 47: Minimum trajectories of 10. vehicle with $j_{min} = -5\,\text{m/s}^3$, $a_{min} = -2\,\text{m/s}^2$, $c_{min} = -4140\,\text{N}$, $\tau = 0.1$

Next, $c_{\min} = -11730\,\text{N}$ for all vehicles in the platoon. The simulation results are shown in Fig. 48, Fig. 49 and Fig. 50 for the chosen vehicle string. The generated input signal for each velocity change is shown in Fig. 48. As determined in the velocity plots, the vehicles reach different final velocities in different times. In all cases, the integral condition in (4.24) is fulfilled. Also, both the vehicle acceleration and jerk constraint is not violated since it is bounded by design according to Theorem 3. All follower vehicles do not violate the force constraint. In particular, the braking force stays well above the defined limit due to the imposed acceleration and jerk constraints.
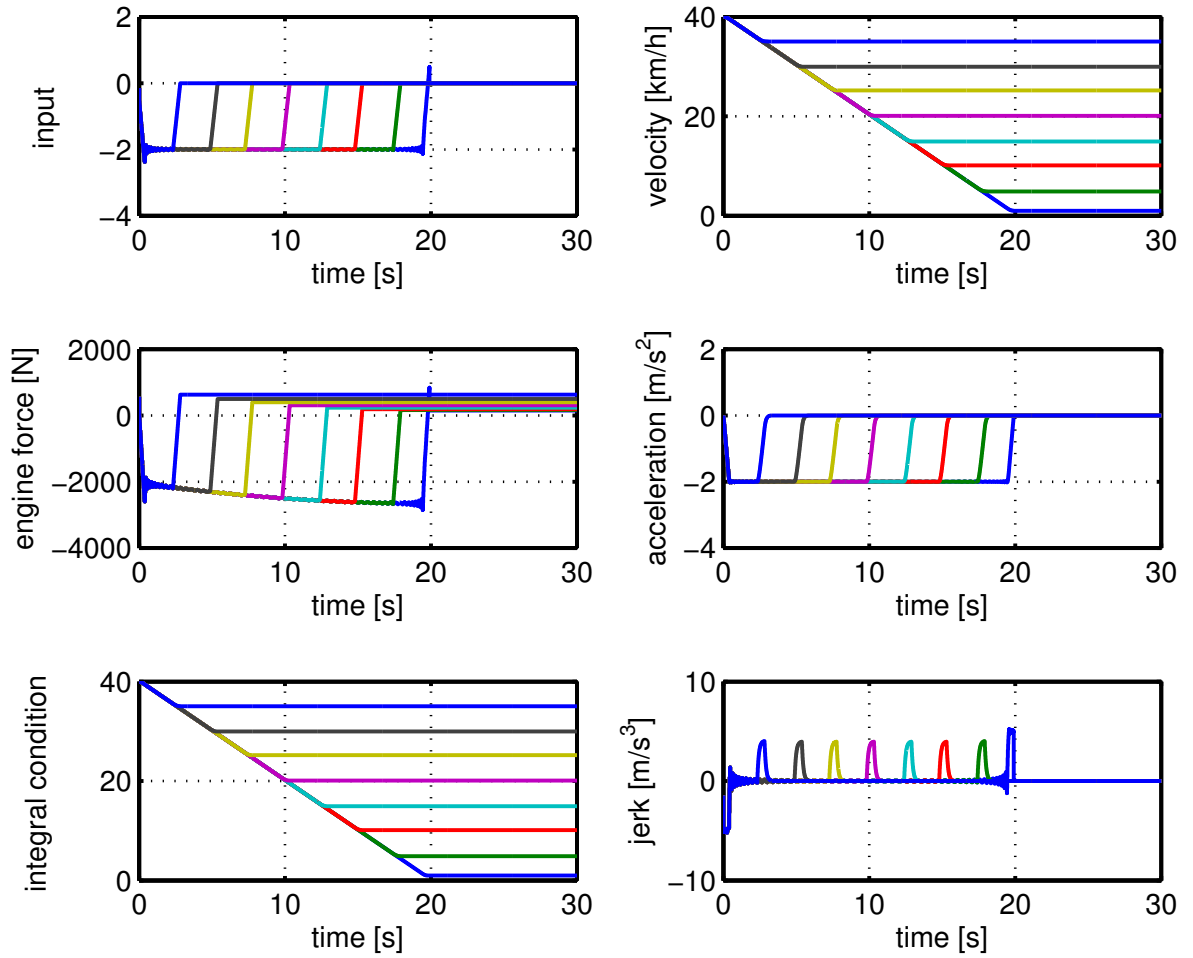
Figure 48: Minimum trajectories of leader vehicle with $j_{\min} = -5\,\text{m/s}^3$, $a_{\min} = -2\,\text{m/s}^2$, $c_{\min} = -11730\,\text{N}$, $\tau = 0.1$
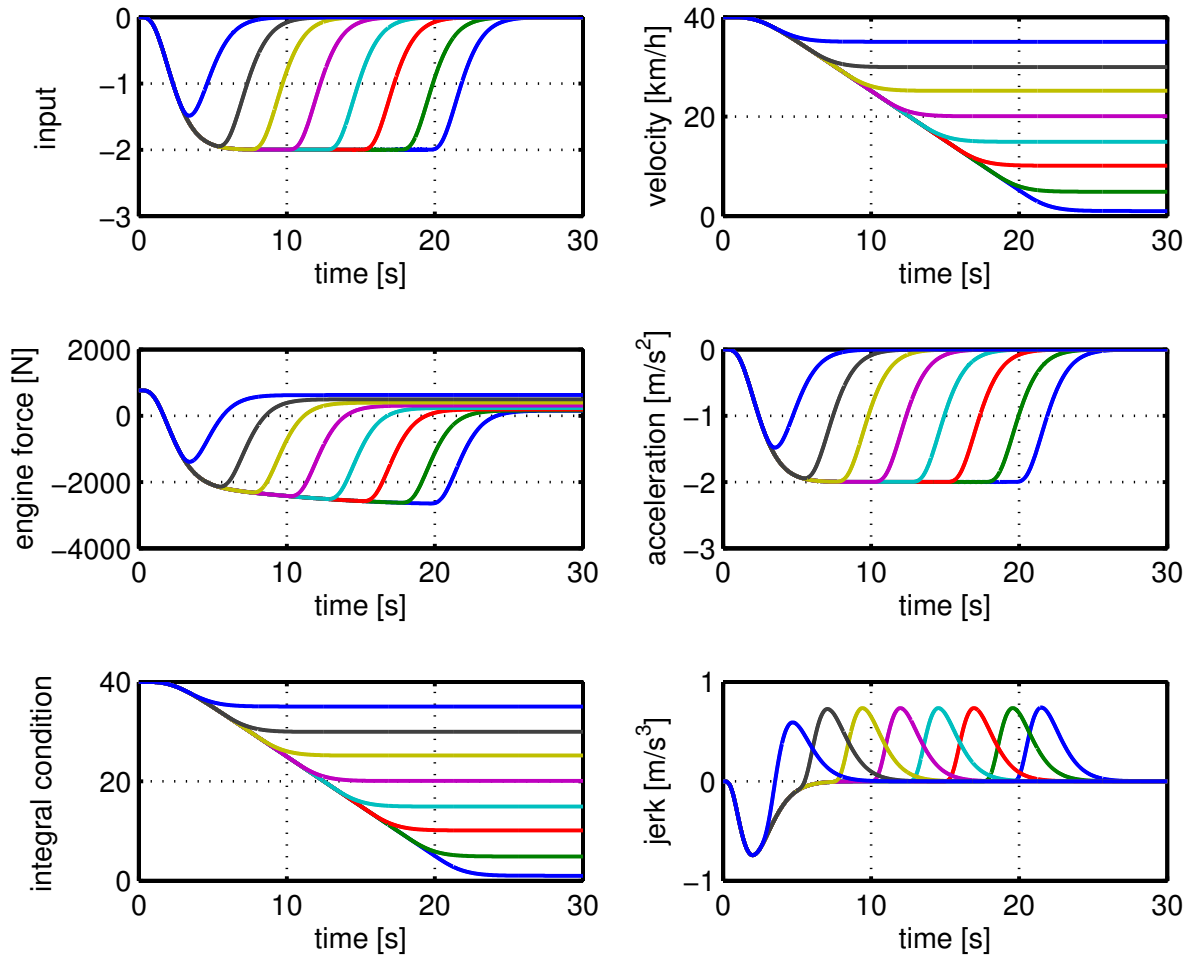
Figure 49: Minimum trajectories of 5. vehicle with $j_{\min} = -5\,\text{m/s}^3$, $a_{\min} = -2\,\text{m/s}^2$, $c_{\min} = -11730\,\text{N}$, $\tau = 0.1$
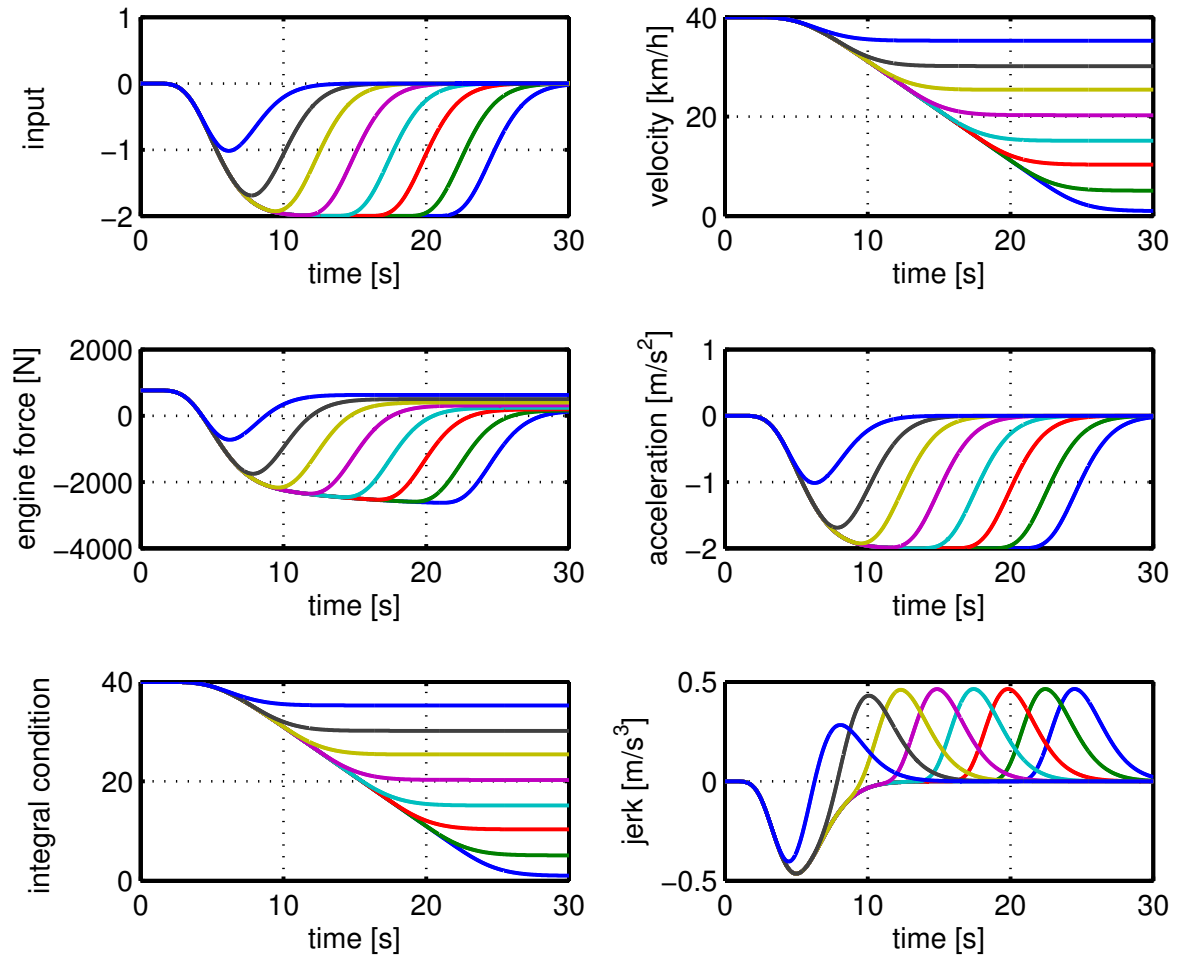
Figure 50: Minimum trajectories of 10. vehicle with $j_{min} = -5\,\text{m/s}^3$, $a_{min} = -2\,\text{m/s}^2$, $c_{min} = -11730\,\text{N}$, $\tau = 0.1$

In the last experiment in this section, the input signal $u_{0,min}$ is generated for $\tau = 0.8$ and $c_{min} = -11730\,\mathrm{N}$. The simulation results are shown in Fig. 51, Fig. 52 and Fig. 53. The generated input signal by optimal control is shown for different final velocities in Fig. 51. For smaller velocity differences, the braking force is applied to the vehicles for a shorter time. Moreover, $a_{min} \leq a_i$ is fulfilled such that the acceleration signal of all vehicles stays in the defined limits. Besides, the integral condition $v_i(0) + \int u_{i,min}(t)dt \geq 0$ is fulfilled by all vehicles. Eventually, the jerk signal plot of the vehicles shows that the jerk values are as well between the defined limits.
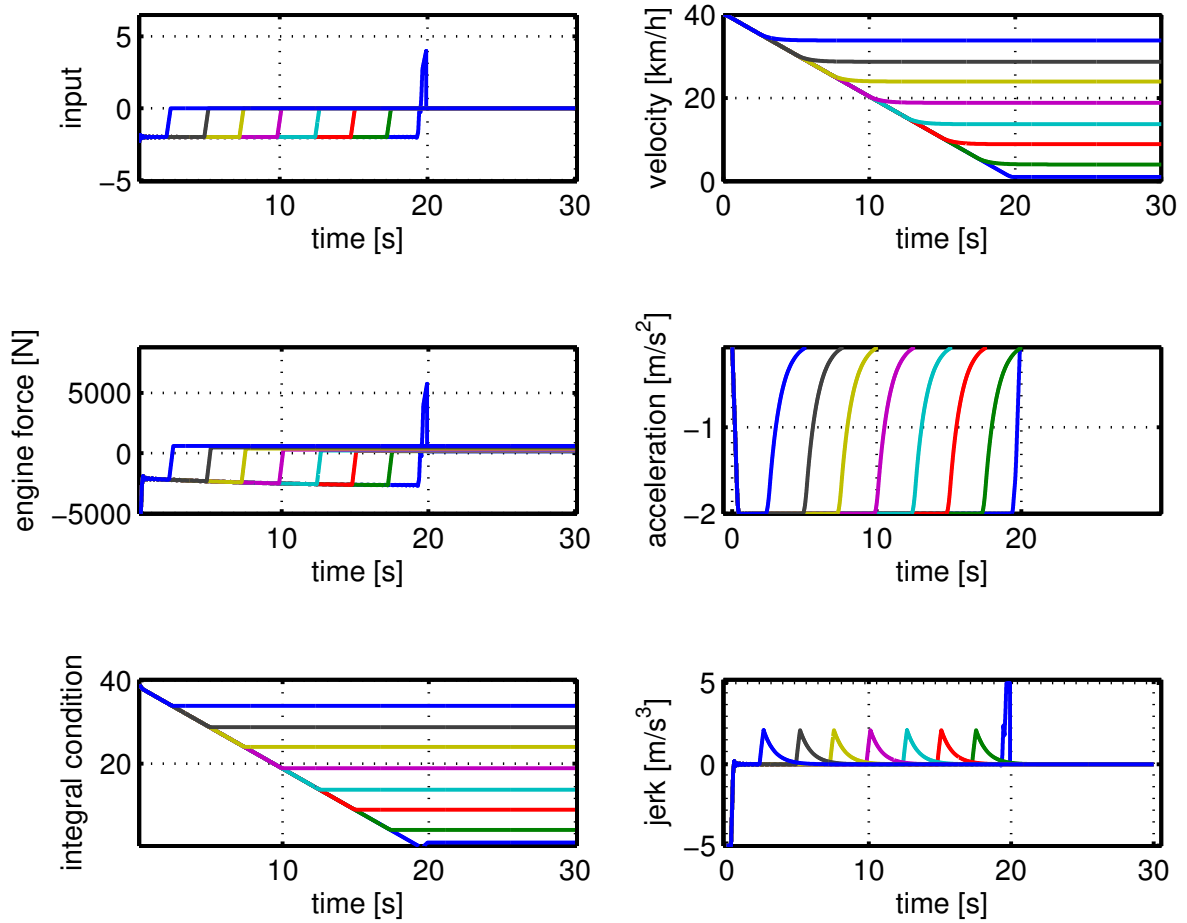
Figure 51: Minimum trajectories of leader vehicle with $j_{min} = -5\,\mathrm{m/s^3}$, $a_{min} = -2\,\mathrm{m/s^2}$, $c_{min} = -11730\,\mathrm{N}$, $\tau = 0.8$
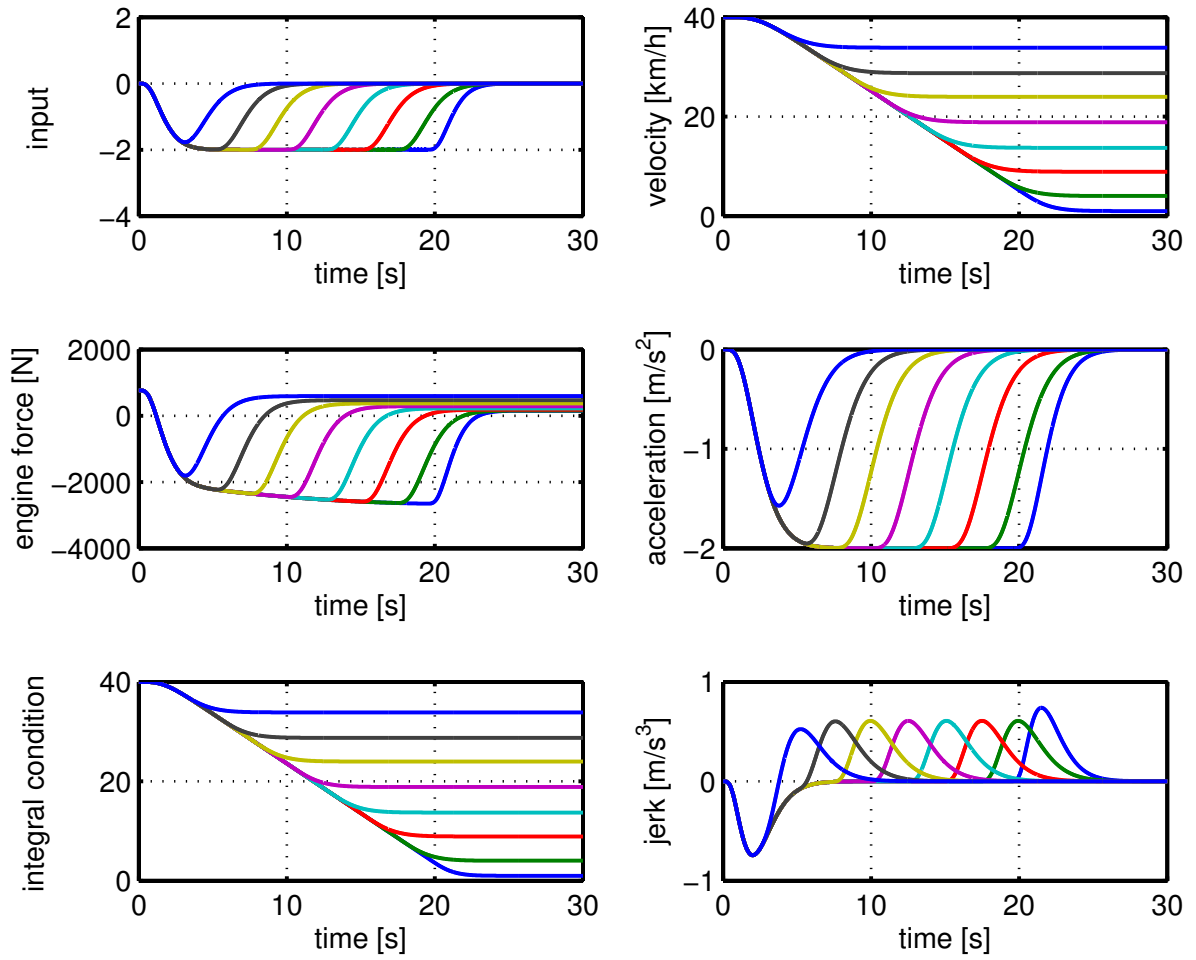
Figure 52: Minimum trajectories of 5. vehicle with $j_{min} = -5 \, \text{m/s}^3$, $a_{min} = -2 \, \text{m/s}^2$, $c_{min} = -11730 \, \text{N}$, $\tau = 0.8$
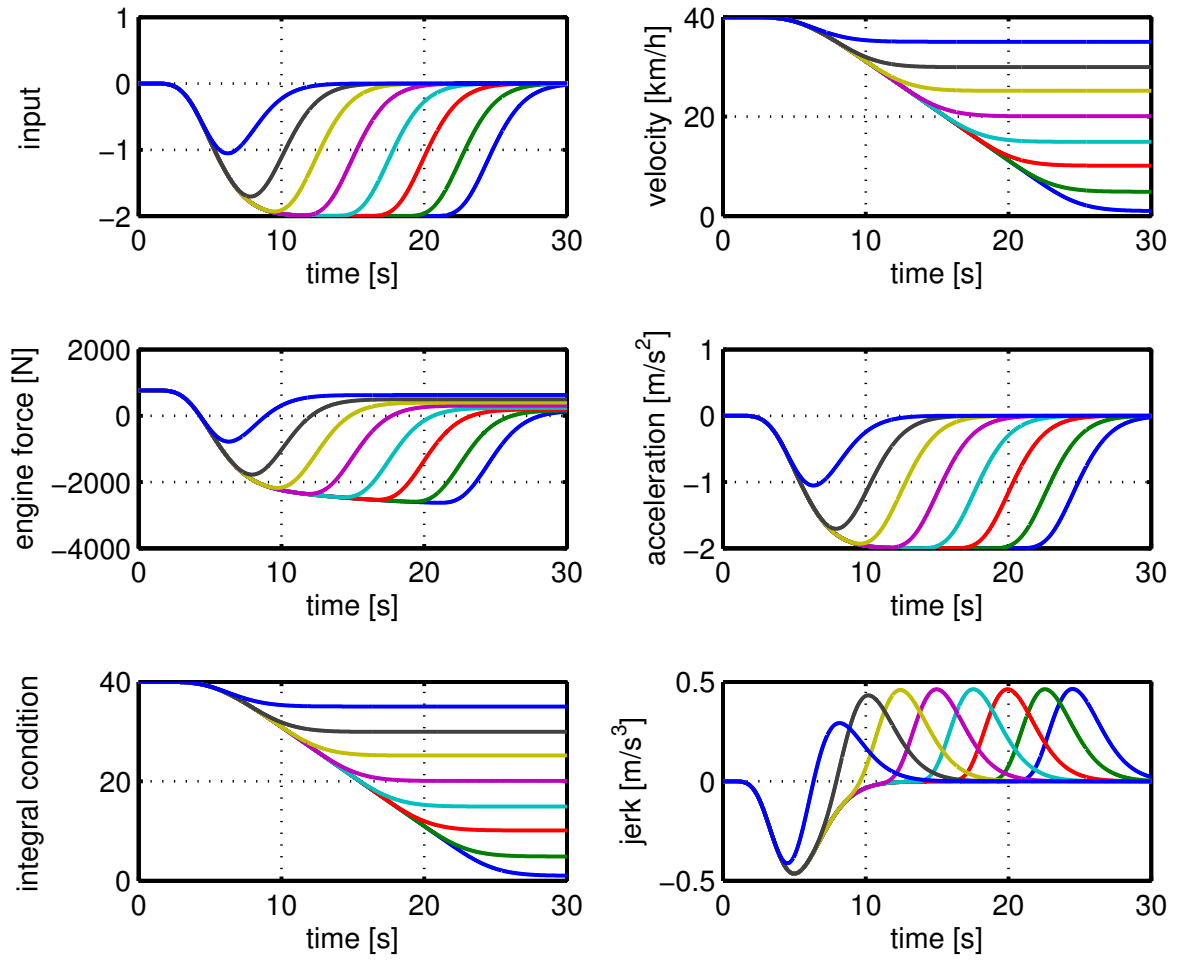
Figure 53: Minimum trajectories of 10. vehicle with $j_{min} = -5\,\text{m/s}^3$, $a_{min} = -2\,\text{m/s}^2$, $c_{min} = -11730\,\text{N}$, $\tau = 0.8$

4.8 Velocity Independent Conditions

The input signal generation in the previous section requires the solution of an optimal control problem for different initial velocities. The results in this section determine conditions under which optimal input trajectories can be directly computed without solving an optimal control problem.

4.8.1 General Condition for the Maximum Engine Force

A possible disadvantage of the results in Theorem 1,2 and 3 is that a different maximum input trajectory $u_{\max,v,i}(t)$ has to be computed for each equilibrium point with velocity v. We next present a condition on the input signal u_0 of the leader vehicle that does not depend on the initial velocity v.

Theorem 4. *Consider a vehicle string with a leader vehicle and N vehicles in the feedback loop in Fig. 10 and with the state space model in (4.6) and (4.7). Assume that K_{ff} and K_{fb} are designed such that $||\Gamma||_\infty \leq 1$ and $\gamma(t) \geq 0$ is fulfilled. Assume that the acceleration of the leader vehicle is bounded by $a_0(t) \leq a_{max}$ and the velocity of the leader vehicle is bounded by $0 \leq v_0(t) \leq v_{max}$. Then, it holds that*

$$c_i(t) \leq c_{max} \quad \text{for all} \quad i = 1, ..., N$$

if $u_0(t)$ is chosen such that for all $t \geq 0$

$$u_0(t) \leq u_{max} := \frac{c_{max} - d_m - 0.5\,\sigma A c_d v_{max}^2 - \tau\,\sigma A c_d v_{max} a_{max}}{m}. \tag{4.51}$$

Proof. We prove the assertion by using Theorem 3. Considering that $0 \leq v_0(t) \leq v_{\max}$ and $a_0(t) \leq a_{\max}$, it holds for all $i = 0, \dots, N$ that

$$0 \leq v_i(t) \leq v_{\max} \text{ and } a_i(t) \leq a_{\max}.$$

Likewise, it is true for all $i = 0, \dots, N$ that

$$u_i(t) \leq u_{\max}$$

Then, we compute

$$
\begin{aligned}
c_i(t) &= m u_i(t) + d_\mathrm{m} + 0.5\,\sigma A c_\mathrm{d}\, v_i(t)^2 + \tau\,\sigma A c_\mathrm{d}\, v_i(t)\, a_i(t) \\
&\le m u_\mathrm{max} + d_\mathrm{m} + 0.5\,\sigma A c_\mathrm{d}\, v_\mathrm{max}^2 + \tau\,\sigma A c_\mathrm{d}\, v_\mathrm{max}\, a_\mathrm{max} \\
&= m\,\frac{c_\mathrm{max} - d_\mathrm{m} - 0.5\,\sigma A c_\mathrm{d}\, v_\mathrm{max}^2 - \tau\,\sigma A c_\mathrm{d}\, v_\mathrm{max}\, a_\mathrm{max}}{m} + d_\mathrm{m} \\
&\quad + 0.5\,\sigma A c_\mathrm{d}\, v_\mathrm{max}^2 + \tau\,\sigma A c_\mathrm{d}\, v_\mathrm{max}\, a_\mathrm{max} \\
&= c_\mathrm{max}.
\end{aligned}
$$

This proves Theorem 4. $\qquad\square$

Theorem 4 only requires to determine u_max in (4.51). That is, there is no dependency on the initial velocity v and a re-computation of the bounding trajectory for each v is avoided. Furthermore, u_max only requires the value of the maximum acceleration a_max and the maximum velocity v_max. The maximum velocity is directly given by the maximum feasible travel velocity of vehicle strings. We next show two possible cases for directly determining a_max and the implication for the computation of u_max.

In the first case, we determine a_max without posing any restrictions.

Corollary 1. *Consider the setting in Theorem 4. Then, it holds that $a_{max} = u_{max}$ and u_{max} can be evaluated as*

$$
u_{max} = \frac{c_{max} - d_\mathrm{m} - 0.5\,\sigma A c_d\, v_{max}^2}{m + \tau\,\sigma A c_d\, v_{max}}. \tag{4.52}
$$

Proof. We first respect that

$$
\dot{a}_0(t) = -\frac{1}{\tau}\, a_0(t) + \frac{1}{\tau}\, u_0(t),
$$

which directly implies that $\max_t\{a_0(t)\} \le \max_t\{u_0(t)\} = u_\mathrm{max}$. That is, it holds that $a_\mathrm{max} = u_\mathrm{max}$ in (4.51). In order to determine u_max, it is hence only required to solve

$$
u_\mathrm{max} = \frac{c_\mathrm{max} - d_\mathrm{m} - 0.5\,\sigma A c_\mathrm{d}\, v_\mathrm{max}^2 - \tau\,\sigma A c_\mathrm{d}\, v_\mathrm{max}\, u_\mathrm{max}}{m}.
$$

The solution directly yields (4.52). $\qquad\square$

In the second case, we determine $u_{\min}$ in case of an acceleration constraint for driving comfort.

Corollary 2. *Consider the setting in Theorem 4. Assume that the acceleration of the leader vehicle is bounded by $a_0(t) \leq a_{max}$. Then, u_{max} can be directly evaluated as in (4.51).*

4.8.2 General Condition for the Minimum Engine Force

In analogy to the discussion in Section 4.4, the disadvantage of the result in Theorem 2 is the fact that a different minimum input trajectory $u_{\min,v,i}(t)$ has to be computed for each equilibrium point with velocity v. We next derive a condition on the input signal $u_0(t)$ of the leader vehicle that does not depend on the initial velocity v.

Theorem 5. *Consider a vehicle string with a leader vehicle and N vehicles in the feedback loop in Fig.10 and with the state space model in (4.6) and (4.7). Assume that K_{ff} and K_{fb} are designed such that $||\Gamma||_\infty \leq 1$ and $\gamma(t) \geq 0$ is fulfilled. Assume that the vehicle string starts from an initial velocity of $v_i(0) = v$ and the acceleration of the leader vehicle is bounded by $a_0(t) \geq a_{min}$. Then, it holds that*

$$c_i(t) \geq c_{min} \quad for\ all \quad i = 1,...,N$$

if $u_0(t)$ is chosen such that for all $t \geq 0$

$$u_0(t) \geq u_{min} := \frac{c_{min} - d_m + 0.5\,\sigma A c_d\,\tau^2 a_{min}^2}{m} \ and\ v_0(t) \geq 0. \tag{4.53}$$

Proof. We prove the assertion by induction on the vehicle index i. First consider the leader vehicle $i = 0$. We know by assumption that

$$u_0(t) \geq u_{\min}$$
$$a_0(t) \geq a_{\min}$$
$$v_0(t) \geq 0.$$

That is,

$$m u_0(t) \geq m u_{\min}$$
$$\tau \sigma A c_d v_0(t) a_0(t) \geq \tau \sigma A c_d v_0(t) a_{\min}.$$

Then, it follows that

$$c_0(t) = m u_0(t) + d_{\mathrm{m}} + \frac{\sigma A c_{\mathrm{d}}}{2} v_0^2(t) + \tau \sigma A c_{\mathrm{d}} v_0(t) a_0(t)$$

$$\geq m u_0(t) + d_{\mathrm{m}} + \frac{\sigma A c_{\mathrm{d}}}{2} v_0^2(t) + \tau \sigma A c_{\mathrm{d}} v_0(t) a_{\min} =: c_0(v_0).$$

We next consider $c_0(v_0)$ as a function of the velocity v_0 and determine its minimum by evaluating

$$\frac{\partial c_0(v_0)}{\partial v_0} = \sigma A c_{\mathrm{d}} v_0 + \tau \sigma A c_{\mathrm{d}} a_{\min} = 0$$

$$\Rightarrow v_0 = -\tau a_{\min} =: v_{\min}.$$

Substituting $v_{\min}$ in $c_0(v_0)$ and using $u_{\min}$ in (4.53), we obtain the minimum force of vehicle 0 as

$$c_0(v_{\min}) = m u_{\min} + d_{\mathrm{m}} - \frac{\tau^2 \sigma A c_{\mathrm{d}}}{2} a_{\min}^2$$

$$= c_{\min} - d_{\mathrm{m}} + \frac{\tau^2 \sigma A c_{\mathrm{d}}}{2} a_{\min}^2 + d_{\mathrm{m}} - \frac{\tau^2 \sigma A c_{\mathrm{d}}}{2} a_{\min}^2 = c_{\min}.$$

Since $c_0(v_{\min})$ is the minimum possible force of vehicle 0, it holds that

$$c_0(t) \geq c_{\min}.$$

In addition, we know that $u_0(t) \geq u_{\min}$ and $a_0(t) \geq a_{\min}$.

Now assume that $c_k(t) \geq c_{\min}$, $u_k(t) \geq u_{\min}$ and $a_k(t) \geq a_{\min}$ is valid for all vehicles $k \leq i$. For the induction step, it has to be shown that also $c_{i+1}(t) \geq c_{\min}$. To this end, we first apply Lemma 1 to obtain

$$u_{i+1}(t) \geq u_{\min}$$
$$a_{i+1}(t) \geq a_{\min}.$$

Then, we get

$$c_{i+1}(t) = m u_{i+1}(t) + d_{\mathrm{m}} + \frac{\sigma A c_{\mathrm{d}}}{m} v_{i+1}^2(t) + \sigma A c_{\mathrm{d}} v_{i+1}(t) a_{i+1}(t)$$

$$\geq m u_{\min} + d_{\mathrm{m}} + \frac{\sigma A c_{\mathrm{d}}}{m} v_{i+1}^2(t) + \sigma A c_{\mathrm{d}} v_{i+1}(t) a_{\min}(t) \geq c_0(v_{\min}) = c_{\min}.$$

This completes the proof of Theorem 5. $\qquad\square$

Theorem 5 only requires to determine $u_{\min}$ in (4.53), which does not depend on v. That is, no recomputation of the bounding trajectory is required for different initial velocities v. The computation of $u_{\min}$ only needs the value of the minimum acceleration $a_{\min}$. We next show two possible cases for directly determining $a_{\min}$ and the implication for the computation of $u_{\min}$.

In the first case, we determine $a_{\min}$ without any further restrictions.

Corollary 3. *Consider the setting in Theorem 5. Then, it holds that $a_{min} = u_{min}$ and u_{min} can be evaluated as*

$$u_{min} = \frac{1}{\sigma A c_d \tau^2}(m - \sqrt{m^2 - 2\sigma A c_d \tau^2 (c_{min} - d_m)}). \tag{4.54}$$

Proof. We first respect that

$$\dot{a}_0(t) = -\frac{1}{\tau} a_0(t) + \frac{1}{\tau} u_0(t),$$

which directly implies that $\min_t(a_0(t) \geq \min_t(u_0(t)) = u_{\min}$. That is, it holds that $a_{\min} = u_{\min}$ in (4.53). In order to determine $u_{\min}$ it is hence only required to solve

$$u_{\min} = \frac{c_{\min} - d_m + 0.5\,\sigma A c_d \tau^2 u_{\min}^2}{m}.$$

The solution yields

$$u_{\min} = \frac{1}{\sigma A c_d \tau^2}(m \pm \sqrt{m^2 - 2\sigma A c_d \tau^2 (c_{\min} - d_m)}).$$

Considering that $c_{\min} < 0$ and all other parameters are positive, the minimum input value is determined as in (4.54). $\square$

In the second case, we determine $u_{\min}$ for an acceleration constraint for driving comfort.

Corollary 4. *Consider the setting in Theorem 5. Assume that the acceleration of the leader vehicle is bounded by $a_0(t) \geq a_{min}$. Then, u_{min} can be directly evaluated as*

$$u_{min} = \frac{c_{min} - d_m + 0.5\,\sigma A c_d \tau^2 a_{min}^2}{m}. \tag{4.55}$$

Proof. The assertion directly follows from (4.53) in Theorem 5. □

4.8.3 Direct Trajectory Computation for Velocity Increases

In this section, we apply Theorem 4 and the related Corollary 1. That is, we assume that a maximum acceleration a_{max} and a maximum jerk j_{max} are given. The proposed input signal computation is based on the assumption that the maximum input signal u_{max} in Theorem 4 should be applied as long as possible without violating the constraints in order to perform a fast velocity change maneuver starting from velocity 0. That is, the basic acceleration trajectory for a speed-up maneuver has a shape as shown in Fig. 54. First, there is a phase where the acceleration increases starting from zero (equilibrium point at the initial velocity). Then, there is a phase where the acceleration decreases back to zero, when reaching the equilibrium point of the desired final velocity.
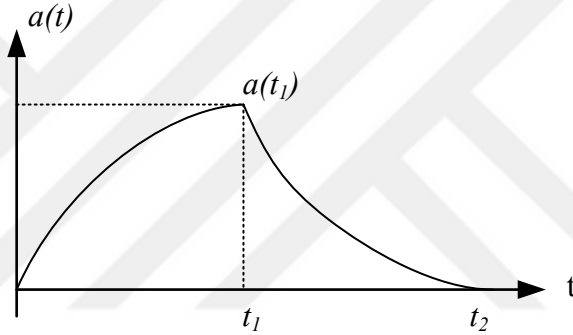
Figure 54: Acceleration signal for different input trajectories

By assumption, the initial acceleration is $a_0(0) = 0$. Using the equation

$$\dot{a}_0(t) = -\frac{1}{\tau} a_0(t) + \frac{1}{\tau} u_0(t), \tag{4.56}$$

from the plant model (τ is the drive-line time constant), it is readily observed that the initial jerk is given by $\dot{a}_0(0) = \frac{1}{\tau} u_0(0)$. Using the limits a_{max} and j_{max} and the computed u_{max}, six different cases are distinguished depending on the values of a_{max}, j_{max} and τ. We next explain these cases.

Different Cases for the Acceleration Increase

In this case, we assume that acceleration is increasing as indicated in Fig. 54. Then we have six possible different cases as shown in Fig. 55.
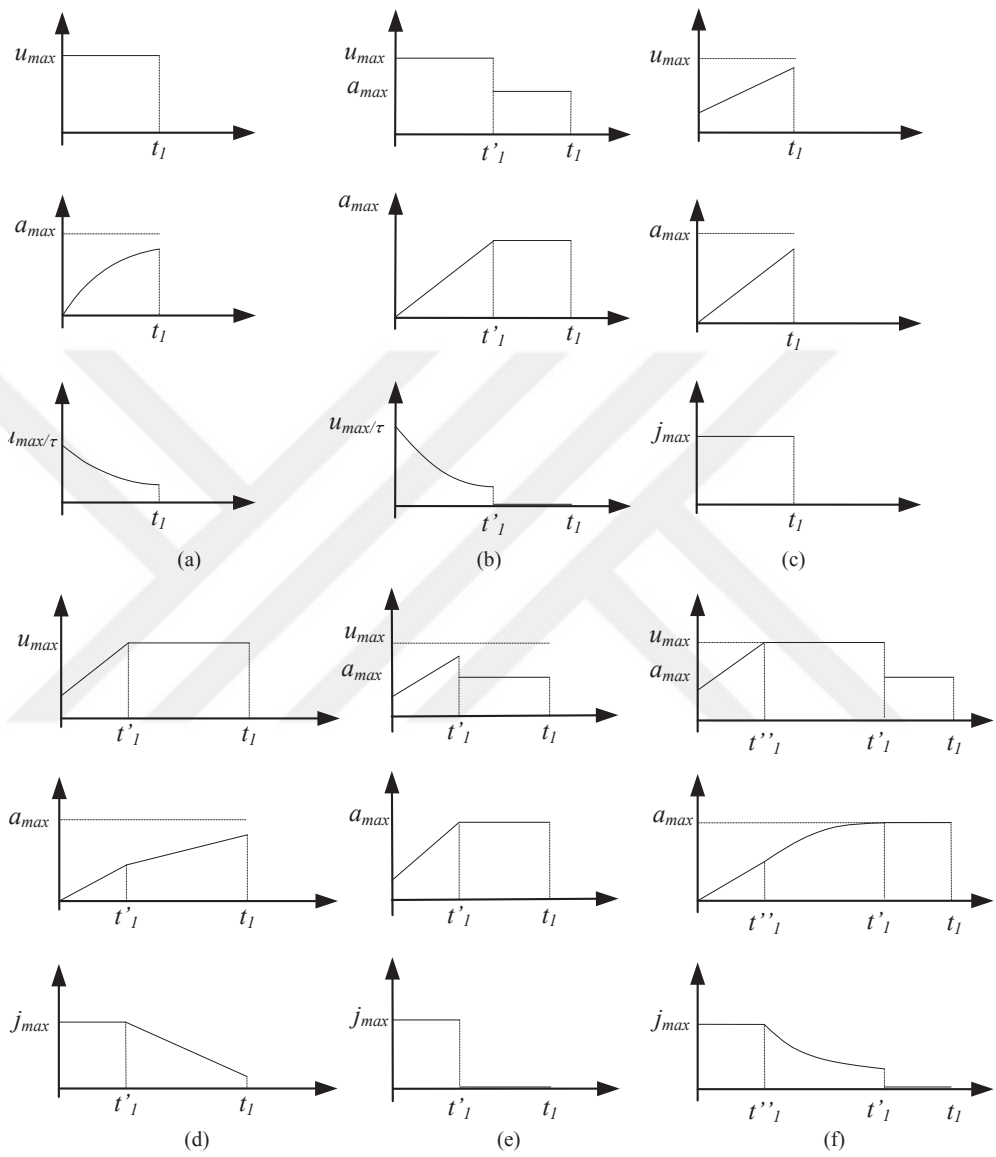
Figure 55: Different scenarios for the input signal computation when accelerating

Case I-a

Since $a_0(0) = 0$, it holds that $u_0(0) = \tau a_0(0)$. When applying the maximum jerk, this means that $u_0(0) = \tau j_{max}$. If $\tau j_{max} \geq u_{max}$, the maximum jerk cannot be applied at time 0. Instead, the fastest speed-up without violating any constraint is achieved when applying u_{max}. In that case, the acceleration and jerk behave according to (4.56) with $u_0(t) = u_{max}$. This scenario is shown in Fig. 55 (a), where the speed-up phase finishes at time t_1'.

Case I-b

This case starts analogous to case I-a due to $\tau j_{max} \geq u_{max}$. If $u_{max} > a_{max}$ and u_{max} is applied for a sufficiently long time, $a_0(t)$ reaches the acceleration limit at some time t_1'. After that, $u_0(t) = a_{max}$ in order to achieve the maximum acceleration $a_0(t) = a_{max}$ until t_1 as in Fig. 55 (c).

Case I-c

In this case, $u_{max} > \tau j_{max}$ such that the maximum jerk can be applied without violating the input constraint. That is, $a_0(t) = j_{max} t$ and hence

$$u_0(t) = (\tau + t) j_{max} \tag{4.57}$$

is used until the end of the speed-up phase at time t_1 as shown in Fig. 55 (b).

Case I-d

This case starts in the same way as case I-c. However, it happens that the maximum jerk is applied for a long time such that the input signal reaches the maximum allowable value of u_{max} at time t_1'. After that, u_{max} is applied in order to achieve the fastest possible speed-up without violating the input constraint $u_0(t) \leq u_{max}$. This scenarios is shown in Fig. 55 (d).

Case I-e

This case starts in the same way as case I-c. However, the maximum jerk is applied for a long time period such that the maximum acceleration a_{max} is reached at time t_1'. That is, the input signal is applied according to (4.58) until t_1'. After that, $u_0(t) = a_{max}$ is applied such that the speed-up with the maximum acceleration $a_0(t) = a_{max}$ occurs as indicated in Fig. 55 (e).

Case I-f

This case starts in the same way as case I-d. However, applying $u_0(t) = u_{max}$ for a long enough time, the acceleration limit a_{max} is reached at time t_1'. After that, $u_0(t) = a_{max}$ is applied such that the speed-up with the maximum acceleration $a_0(t) = a_{max}$ occurs as indicated in Fig. 55 (f).

2. Different cases when decelerates

In the second phase, the acceleration decreases to zero as in Fig.54. There are three possible cases for such maneuver as explained below.

Case D-a

In this case, we assume $u_{min} \geq \tau j_{min}$, such that u_{min} must be applied as seen in Fig. 56 (a). Applying u_{min}, $a_0(t)$ decreases until reaching zero at time t_1 in this case.

Case D-b

In this case, $u_{min} < \tau j_{min}$. That, is we apply the minium jerk initially such that $a_0(t) = j_{min} t$ and

$$u_0(t) = (\tau + t) j_{min} \tag{4.58}$$

$u_0(t)$ is applied to decrease $a_0(t)$ until the minimum input avlue u_{min} is reached at time t_1'. At the end, $u_0(t) = u_{min}$ is applied until the acceleration reaches zero at time t_1 as shown in Fig. 56 (b).

Case D-c

This case is analogous to case D-b. However, here the acceleration reaches the value zero before the minimum input value u_{min} is reached. That is, input signal is applied until t_1 as shown in Fig. 56 (c).

In the next subsections, we show an example for input trajectories. That is, we combine suitable cases described above then we analytically compute input trajectories.
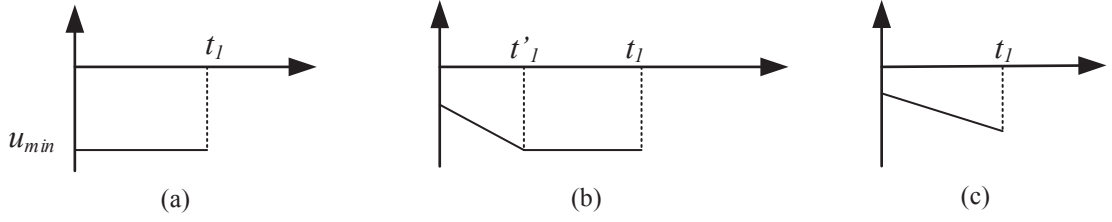
Figure 56: Different scenarios for the input signal computation when decelerating

1) Computation of different input trajectories for velocity increasing

For illustration, we next show several possible speed-up scenarios which combine possible cases for phase 1 (acceleration increase) and phase 2 (acceleration decrease) in Fig. 54. We first show the possible scenarios when using case I-a for phase 1 in Fig. 57 (a), (b), (c). The figure also shows the applied input signals and the corresponding acceleration signals.
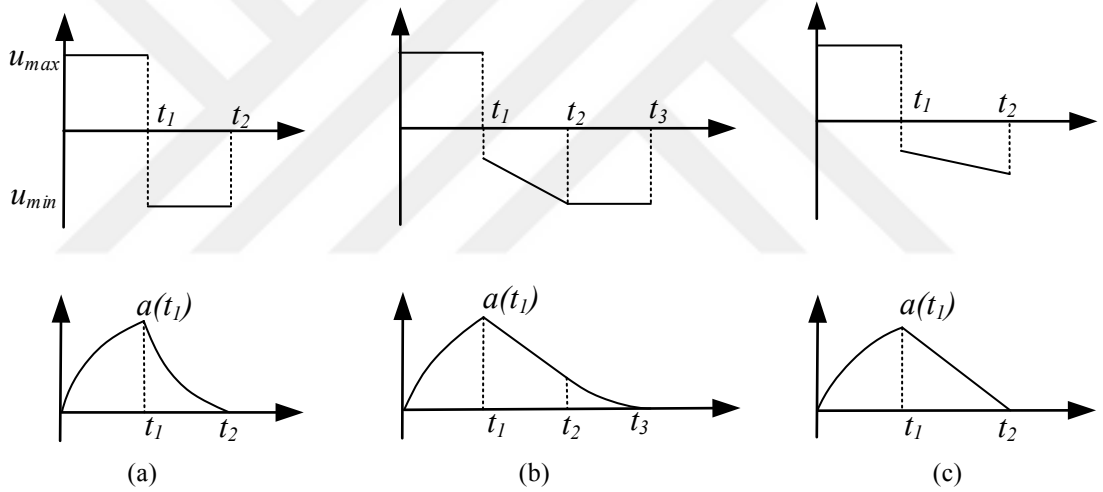
Figure 57: Input trajectory combinations with Case I-a when accelerating.

The trajectory computation for the shown scenarios is as follows.

First, consider Fig. 57 (a). In phase 1, we apply $u_0(t)$ until time t_1 as seen in Fig.57. It holds that $u_{\max} \leq \tau j_{\max}$. That is, initially, $u_0(t) = u_{\max}$ until time t_1. Using (4.56), the acceleration increases according to

$$a_0(t) = (1 - e^{-t/\tau}) u_{\max}$$

until $a_0(t_1)$ is reached. We emphasize that $a_0(t_1)$ never reaches the limit $a_{\max}$ in this

case.

Integrating $a_0(t)$, the velocity difference until t_1 is

$$\Delta v_0(t) = u_{\max}\left(t + \tau\left(1 - e^{-t/\tau}\right)\right).$$

Hence, a velocity increase of

$$\Delta v_1 = u_{\max}\left(t_1 + \tau\left(1 - e^{-t_1/\tau}\right)\right)$$

is achieved until time t_1. This time interval is analogous in all the combinations with phase 2.

Case I-a and D-a

Referring to Fig. 57 (a), we introduce the time differences

$$\Delta t_1 = t_1, \quad \Delta t_2 = t_2 - t_1$$

Between t_1 and t_2, $u_{\min}$ is applied such that the acceleration

$$a_0(t_2) = a(t_1) + (u_{\min} - a(t_1))(1 - e^{-\Delta t_2/\tau}) = 0$$

is obtained. The acceleration is decreased to zero in order to reach an equilibrium point with constant velocity. Then, time t_2 is computed in terms of t_1 as

$$\Delta t_2 = -\tau \ln(1 + a(t_1)/(u_{\min} - a(t_1)))$$

Integrating $a_0(t)$, the velocity difference is

$$\Delta v_0(t) = t\, a(t_1) + t\left(e^{-t/\tau} - 1\right)(a(t_1) - u_{\min})$$

The corresponding velocity increase is

$$\Delta v_2 = \Delta t_2\, a(t_1) + \Delta t_2\left(e^{-\Delta t_2/\tau} - 1\right)(a(t_1) - u_{\min})$$

Together, the velocity difference in terms of t_1 during the overall maneuver is

$$\begin{aligned}
\Delta v &= \Delta v_1 + \Delta v_2 \\
&= t_1\, u_{\max} + \tau\, u_{\max}\left(1 - e^{-t_1/\tau}\right) + \Delta t_2\, a(t_1) + \Delta t_2\left(e^{-t_1/\tau} - 1\right)(a(t_1) - u_{\min})
\end{aligned}$$

That is, assuming an initial velocity v and a final desired velocity $v + \Delta v$, Δt_1 can be computed using MATLAB. After computation of t_1, we can compute t_2.

As a result, the input signal for the velocity change according to combination of Case I-a and Case D-a is

$$u_0(t) = \begin{cases} u_{\max} & \text{if } t \le t_1 \\ u_{\min} & \text{if } t_1 \le t \le t_2 \\ 0 & \text{otherwise} \end{cases} \tag{4.59}$$

Case I-a and D-b

Referring to Fig. 57 (b), we introduce the time differences

$$\Delta t_1 = t_1, \quad \Delta t_2 = t_2 - t_1, \quad \Delta t_3 = t_3 - t_2.$$

Between t_1 and t_2, the input signal is $u_0(t) = a_0(t_1) + \tau j_{\min} + (t - t_1) j_{\min}$ and it holds that $u_0(t_2) = u_{\min}$. Then, Δt_2 is obtained as

$$a_0(t_1) + \tau j_{\min} + t j_{\min} = u_{\min} \Rightarrow \Delta t_2 = (u_{\min} - \tau j_{\min} - a_0(t_1)) / j_{\min}$$

The corresponding acceleration is

$$a_0(t) = a(t_1) + t j_{\min}$$

Integrating $a_0(t)$, the velocity difference is

$$\Delta v_0(t) = t\, a(t_1) + \Delta t^2\, j_{\min}/2$$

Hence, a velocity increase of

$$\Delta v_2 = \Delta t_2\, a(t_1) + \Delta t_2^2\, j_{\min}/2$$

is obtained until time t_2. In the last time interval, the acceleration is decreased to zero in order to reach the equilibrium point with constant velocity. $u_0(t) = u_{\min}$ until time t_3. It holds that

$$a_0(t) = a(t_2) + (u_{\min} - a(t_2))(1 - e^{-(t-t_2)/\tau})$$

The velocity difference is computed after integrating $a_0(t)$

$$\Delta v_3 = \Delta t_3 \, u_{\min} - \tau \, a(t_2) \, e^{-\Delta t_3/\tau} + \tau \, u_{\min} \, e^{-\Delta t_3/\tau}.$$

The time required for this maneuver is

$$a(t_2) + (u_{\min} - a(t_2)) \, (e^{-\Delta t_3/\tau} - 1) = 0 \Rightarrow \Delta t_3 = \tau \, \ln(a(t_2)/(u_{\min} - a(t_2)))$$

Together, the velocity difference during the overall maneuver is

$$
\begin{aligned}
\Delta v &= \Delta v_1 + \Delta v_2 + \Delta v_3 \\
&= u_{\max} \, (t_1 + \tau \, (1 - e^{-t_1/\tau})) + \Delta t_2 \, a(t_1) + \Delta t_2^2 \, j_{\min}/2 \\
&\quad + \Delta t_3 \, u_{\min} - \tau \, a(t_2) \, e^{-\Delta t_3/\tau} + \tau \, u_{\min} \, e^{-\Delta t_3/\tau}
\end{aligned}
$$

If Δv is written in terms of t_1, then MATLAB can compute Δt_1 assuming an initial velocity v and a final desired velocity $v + \Delta v$. After solving for t_1, we can compute t_2 and t_3.

As a result, the input signal for the velocity change for this case is

$$
u_0(t) = \begin{cases}
u_{\max} & \text{if } t \leq t_1 \\
a_0(t_1) + j_{\min} \, (\tau + t - t_1) & \text{if } t_1 \leq t \leq t_2 \\
u_{\min} & \text{if } t_2 \leq t \leq t_3 \\
0 & \text{otherwise}
\end{cases}
\tag{4.60}
$$

Case I-a and D-c

Referring to Fig.57 (c), we introduce the time differences

$$\Delta t_1 = t_1, \quad \Delta t_2 = t_2 - t_1.$$

Between t_1 and t_2, the input signal is $u_0(t) = a(t_1) + \tau \, j_{\min} + (t - t_1) \, j_{\min}$. The input signal at time t_2 does not reach its minimum value $u_{\min}$ but the acceleration reaches the value zero at that time.

Performing this maneuver with the possible minimum jerk $j_{\min}$, we compute

$$a_0(t) = a(t_1) + (t - t_1) \, j_{\min}$$

If we insert $u(t_2)$ in this equation, time require for this maneuver is computed as

$$\Delta t_2 \, j_{\min} + a(t_1) = 0 \Rightarrow \Delta t_2 = -a(t_1)/j_{\min}.$$

Integrating $a_0(t)$, the velocity difference is

$$\Delta v_2 = \Delta t_2 \, a(t_1) + \Delta t_2^2 \, j_{\min}/2.$$

The overall velocity difference is

$$\begin{aligned}
\Delta v &= \Delta v_1 + \Delta v_2 \\
&= u_{\max} \left(t_1 + \tau \left(1 - e^{-t_1/\tau} \right) \right) + \Delta t_2 \, a(t_1) + \Delta t_2^2 \, j_{\min}/2.
\end{aligned}$$

Δv is written in terms of t_1 using above equation. That is, MATLAB can compute t_1 assuming an initial velocity v and a final desired velocity $v + \Delta v$. After solving for t_1, we can compute t_2.

The resulting input signal for the velocity change for this case is

$$u_0(t) = \begin{cases} u_{\max} & \text{if } t \leq t_1 \\ a_0(t_1) + j_{\min} \left(\tau + t - t_1 \right) & \text{if } t_1 \leq t \leq t_2 \\ 0 & \text{otherwise} \end{cases} \tag{4.61}$$

We note that a similar computation can be carried out to explicitly determine the input signal for any velocity changes following the cases introduced above. The computation of all cases is not done in this thesis document due to the large overall number of $6 \cdot 3 = 18$ cases. All cases were implemented in Matlab. We further note that the occurrence of the different cases is not a choice but the validity of each case for certain velocity changes depends on the actual parameter values $j_{\max}, j_{\min}, a_{\max}, a_{\min}, u_{\max}, u_{\min}, \tau$ defined for the particular vehicle application.

4.8.4 Direct Trajectory Computation for Velocity Decreases

We note that an analogous analytical computation to Section 4.8.3 can be performed for input signals $u_0(t)$ that lead to a velocity decrease. In this case, different cases have to be distinguished based on the minimum values of acceleration and jerk $a_{\min}$ and $j_{\min}$. The explicit formulation of the input signal computation is actually the same as in the

case of a velocity increasing. The only difference is that, instead of using the maximum values $a_{\max}$, $j_{\max}$, $u_{\max}$ the minimum values of $a_{\min}$, $j_{\min}$, $u_{\min}$ have to be substituted in the respective equations. Because of this reason we do not repeat all the cases but refer to the explanations in the previous section. Next, we give an example to show how minimum input trajectories are computed.

We consider a slow-down maneuver, where phase 1 (decreased acceleration) corresponds to case I-B in Fig. 55 (replacing $a_{\max}$ by a negative $a_{\min}$ and $u_{\max}$ by a negative $u_{\min}$). That is, the acceleration decreases until time t_1. After time t_1, we apply the input trajectories corresponding to the cases D-a, D-b, D-c to increase $a_0(t)$ back to zero (here, the minimum values $j_{\min}$, $a_{\min}$, $u_{\min}$ are replaced by the maximum values $j_{\max}$, $a_{\max}$, $u_{\max}$, respectively). The obtained trajectories are displayed in Fig. 58.
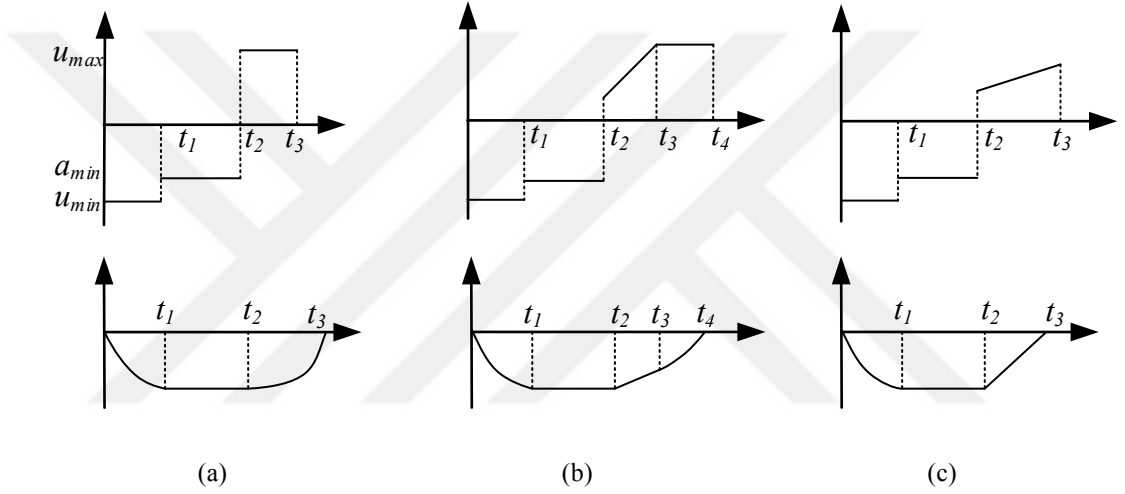
Figure 58: Input trajectory combinations with Case 2d when decelerating

At first, $u_0(t) = u_{\min}$ is applied until time t_1. Using (4.56), the acceleration decreases with

$$a_0(t) = (1 - e^{-t/\tau}) u_{\min}$$

until it reaches $a_{\min}$. Then t_1 is computed as

$$(1 - e^{-t/\tau}) u_{\min} = a_{\min} \Rightarrow t_1 = -\tau \ln(1 - a_{\min}/u_{\min})$$

Integrating $a_0(t)$, the velocity difference is

$$\Delta v_0(t) = u_{\min} (t + \tau (1 - e^{-t/\tau}))$$

Hence, a velocity decrease of

$$\Delta v_1 = u_{\min}\left(t_1 + \tau\left(1 - e^{-t_1/\tau}\right)\right)$$

is achieved until time t_1. Between t_1 and t_2, $u_0(t) = a_{\min}$ is applied such that a constant acceleration $a_0(t) = a_{\min}$ is obtained. The corresponding velocity decrease is

$$\Delta v_2 = a_{\min}\Delta t_2$$

This time interval computation for phase 1 (decreased acceleration) is the same for the next computations to increase $a_0(t)$ back to zero.

Combination with Case D-a

Referring to Fig. 58 (a), we introduce the time differences

$$\Delta t_1 = t_1, \quad \Delta t_2 = t_2 - t_1, \quad \Delta t_3 = t_3 - t_2$$

Until time t_2, the computations are explained above. Between t_2 and t_3, $u_0(t) = u_{\max}$ is applied such that the acceleration is

$$a_0(t) = a_{\min} + (u_{\max} - a_{\min})(1 - e^{-(t-t_2)/\tau}) = 0$$

The acceleration is increased to zero in order to reach an equilibrium point with constant velocity. Then, the time required for this maneuver is

$$\Delta t_3 = -\tau\ln(u_{\max}/(u_{\max} - a_{\min}))$$

and the corresponding velocity difference is

$$\Delta v_3 = \Delta t_3\,u_{\max} - \tau\,u_{\max}\,e^{-\Delta t_3/\tau} + \tau\,a_{\min}\,e^{-\Delta t_3/\tau}$$

That is, the overall velocity difference for the maneuver evaluates to

$$\begin{aligned}
\Delta v &= \Delta v_1 + \Delta v_2 + \Delta v_3 \\
&= u_{\min}\,t_1 + u_{\min}\,\tau\left(1 - e^{-t_1/\tau}\right) + a_{\min}\Delta t_2 + \Delta t_3\,u_{\max} - \tau\,u_{\max}\,e^{-\Delta t_3/\tau} + \tau\,a_{\min}\,e^{-\Delta t_3/\tau}
\end{aligned}$$

Since we know the values of t_1 and t_3, t_2 can be directly computed using the initial velocity v and final desired velocity $v + \Delta v$.

94

The resulting input signal for this case is

$$
u_0(t) = \begin{cases}
u_{\min} & \text{if } t \leq t_1 \\
a_{\min} & \text{if } t_1 \leq t \leq t_2 \\
u_{\max} & \text{if } t_2 \leq t \leq t_3 \\
0 & \text{otherwise}
\end{cases} \tag{4.62}
$$

Combination with Case D-b

Referring to Fig. 58 (b), we introduce the time differences

$$
\Delta t_1 = t_1, \quad \Delta t_2 = t_2 - t_1, \quad \Delta t_3 = t_3 - t_2, \quad \Delta t_4 = t_4 - t_3.
$$

Between t_2 and t_3, $u_0(t) = a_{\min} + \tau j_{\max} + (t - t_2) j_{\max}$ is applied using the maximum jerk $j_{\max}$. The acceleration is increasing according to

$$
a_0(t) = a_{\min} + (t - t_2) j_{\max}.
$$

The time required for this maneuver is $\Delta t_3 = -a_{\min} / j_{\max}$. Then, the velocity difference is

$$
\Delta v_3 = \Delta t_3 a_{\min} + \Delta t_3^2 j_{\max} / 2
$$

After time t_3, $u_0(t) = u_{\max}$ is applied and the acceleration is computed from

$$
a_0(t) = a(t_3) + u_{\max} \left(e^{-(t-t_3)/\tau} - 1 \right) - a(t_3)\left(e^{-(t-t_3)/\tau} - 1 \right) = 0
$$

Since $a(t_3) = a_{\min} + \Delta t_3 j_{\max}$, the time required for this time interval is

$$
\Delta t_4 = -\tau \ln(a(t_3)/(u_{\max} - a(t_3)))
$$

The velocity difference is computed after integrating $a_0(t)$

$$
\Delta v_4 = \Delta t_4 u_{\max} - \tau a(t_3) e^{-\Delta t_4/\tau} + \tau u_{\max} e^{-\Delta t_4 \tau}.
$$

That is, the overall velocity difference is

$$
\begin{aligned}
\Delta v &= \Delta v_1 + \Delta v_2 + \Delta v_3 + \Delta v_4 \\
&= u_{\min} t_1 + u_{\min} \tau (1 - e^{-t_1/\tau})) + a_{\min} \Delta t_2 + \Delta t_3 a_{\min} \\
&\quad + \Delta t_3 a_{\min} + \Delta t_3^2 j_{\max}/2 + \Delta t_4 u_{\max} - \tau a(t_3) e^{-\Delta t_4/\tau} + \tau u_{\max} e^{-\Delta t_4 \tau}.
\end{aligned}
$$

Since we know the values of t_1, t_3 and t_4, using the initial velocity v and final desired velocity $v + \Delta v$, t_2 can be computed easily.

The resulting input signal for this case is

$$u_0(t) = \begin{cases} u_{\min} & \text{if } t \leq t_1 \\ a_{\min} & \text{if } t_1 \leq t \leq t_2 \\ a_{\min} + j_{\max}(\tau + t - t_2) & \text{if } t_2 \leq t \leq t_3 \\ u_{\max} & \text{if } t_3 \leq t \leq t_4 \\ 0 & \text{otherwise} \end{cases} \tag{4.63}$$

Combination with Case D-c

Referring to Fig. 58 (c), we introduce the time differences

$$\Delta t_1 = t_1, \quad \Delta t_2 = t_2 - t_1, \quad \Delta t_3 = t_3 - t_2.$$

Between t_2 and t_3, $u_0(t) = a_{\min} + \tau j_{\max} + (t - t_2) j_{\max}$ is applied. The acceleration is increasing according to

$$a_0(t) = a_{\min} + (t - t_2) j_{\max}$$

and the time required for this maneuver is $\Delta t_3 = -a_{\min}/j_{\max}$. Then, the velocity difference is

$$\Delta v_3 = \Delta t_3 a_{\min} + \Delta t_3^2 j_{\max}/2$$

Together, the overall velocity difference is

$$\begin{aligned} \Delta v &= \Delta v_1 + \Delta v_2 + \Delta v_3 \\ &= u_{\min} t_1 + u_{\min} \tau (1 - e^{-t_1/\tau}) + a_{\min} \Delta t_2 + \Delta t_3 a_{\min} + \Delta t_3^2 j_{\max}/2. \end{aligned}$$

After the computed variables t_1 and t_3 are inserted in the equation for Δv, t_2 can be computed depending on Δv.

The resulting input signal for this case is

$$u_0(t) = \begin{cases} u_{\min} & \text{if } t \leq t_1 \\ a_{min} & \text{if } t_1 \leq t \leq t_2 \\ a_{\min} + j_{\max}(\tau + t - t_2) & \text{if } t_2 \leq t \leq t_3 \\ 0 & \text{otherwise} \end{cases} \tag{4.64}$$

Again, we only show the computation for a single case of phase 1 for illustration. We note that the computation for the other cases is analogous and was implemented in Matlab in the scope of the thesis.

4.8.5 Discussion

In summary, this section assumes that bounds a_{max}, a_{min} for the acceleration and j_{max}, j_{min} for the jerk are given in order to ensure the driving comfort. In addition, it is possible to compute maximum values u_{max} (Corollary 1 and 2) and minimum values u_{min} (Corollary 3 and 4) for the input signal. Using these bounds, the previous discussion shows that it is possible to analytically compute input trajectories for speed-up (Section 4.8.3) and slow-down (Section 4.8.4) maneuvers for any given velocity change Δv. Using these input trajectories for the leader vehicle, it is guaranteed by Theorem 5 and 6 that the engine/braking force of none of the vehicles in a vehicle string saturates. In addition, it follows from Theorem 3 that none of the vehicles in a string violates the acceleration and jerk constraints. The proposed computation is particularly advantageous in practical applications. Different from the computations in Section 4.3 and 4.4, where an optimal control problem needs to be solved, the computations in this section can be performed analytically.

4.9 Simulation Results for Computed Input Signal - Theorem 4

We next show examples for the computation of the input signal for speed-up maneuvers. In the simulations, we consider velocity changes from an initial velocity 0 m/s to different final velocities $v = 5, 10, 15, 20, 25, 30, 35, 40$ m/s. The same vehicle parameters as in Table 2 are used with different values of τ. Also, $j_{max} \leq 5$ m/s^3, $a_{max} \leq 2$ m/s^2 are set for the simulations.

$c_{max} = 2470$ N and $\tau = 0.1$ are set for the simulations in Fig. 59 to Fig. 61. The leader vehicle simulation result is shown in Fig. 59. According to Theorem 4, $u_{max} = 1.5$ is determined when the final velocity is $v_i = 5$ m/s. The results obtained for the following vehicles in Fig. 60, Fig. 61 confirm that no violation occurs in the input signal. In addition, it can be seen that all vehicles reach their desired final velocity, whereby the time interval for the maneuver increases with the velocity difference. The engine force of all vehicles stays below the given maximum force value. In this case, it is interesting to observe that the acceleration never reaches its maximum allowable value

of $a_{max} = 2\,m/s^2$ in Fig. 59 to Fig. 61. This is due to the fact that $u_{max} < a_{max}$ in this example. The last plot of the figures also confirms that the constraints on the jerk are met by all vehicles in the string. It is concluded that computed input signal in Fig. 59 is an example of Case I-a and D-a.

Figure 59: Different velocity changes: Trajectories of the leader vehicle with $j_{max} = 5\,m/s^3$, $a_{max} = 2\,m/s^2$, $c_{max} = 2470\,N$, $\tau = 0.1$

Figure 60: Different velocity changes: Trajectories of the 5. vehicle with $j_{max} = 5 \, \text{m/s}^3$, $a_{max} = 2 \, \text{m/s}^2$, $c_{max} = 2470 \, \text{N}$, $\tau = 0.1$

Figure 61: Different velocity changes: Trajectories of the 10. vehicle with $j_{max} = 5\,\mathrm{m/s^3}$, $a_{max} = 2\,\mathrm{m/s^2}$, $c_{max} = 2470\,\mathrm{N}$, $\tau = 0.1$

In the next simulation example, $c_{max} = 6140$ N and $\tau = 0.1$ are set in Fig. 62 to Fig. 64[61]. The leader vehicle input signal indicates that $u_{max} = 2.1 > a_{max}$ is determined when the final velocity is $v_i = 5$ m/s in Fig. 62. Acceptable results are also obtained by the following vehicles input signal plot as shown in Fig. 63 and Fig. 64. As expected, the vehicles reach the final velocity values in different time intervals as can be seen in the velocity plots of the figures. Again, the force constraint is met for all vehicles. The constraints on acceleration and jerk are met by all vehicles as in Fig. 63 to Fig. 65. It is pointed out that computed input signal in Fig. 62 is an example of Case I-e and D-c.
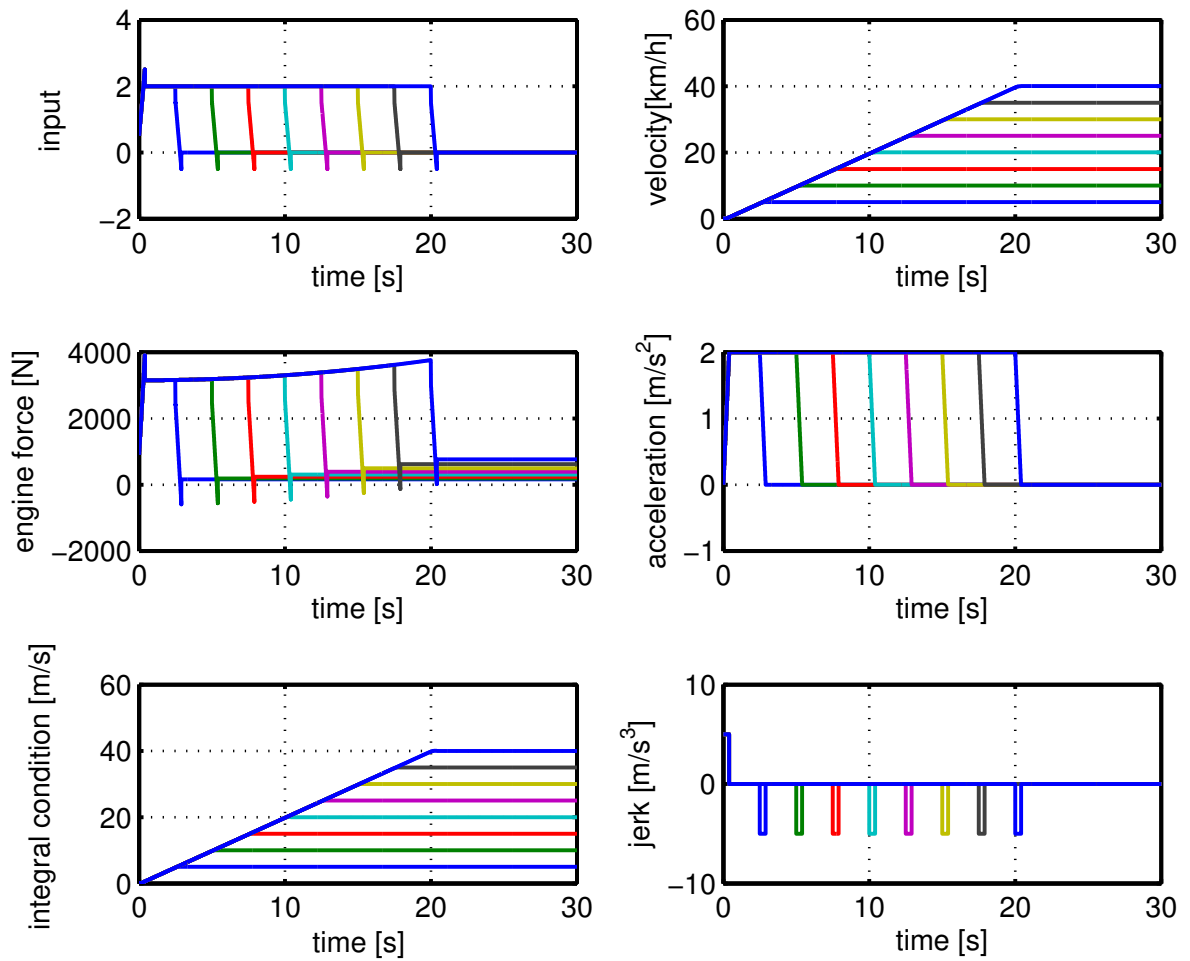
Figure 62: Different velocity changes: Trajectories of the leader vehicle with $j_{max} = 5$ m/s^3, $a_{max} = 2$ m/s^2, $c_{max} = 6395$ N, $\tau = 0.1$
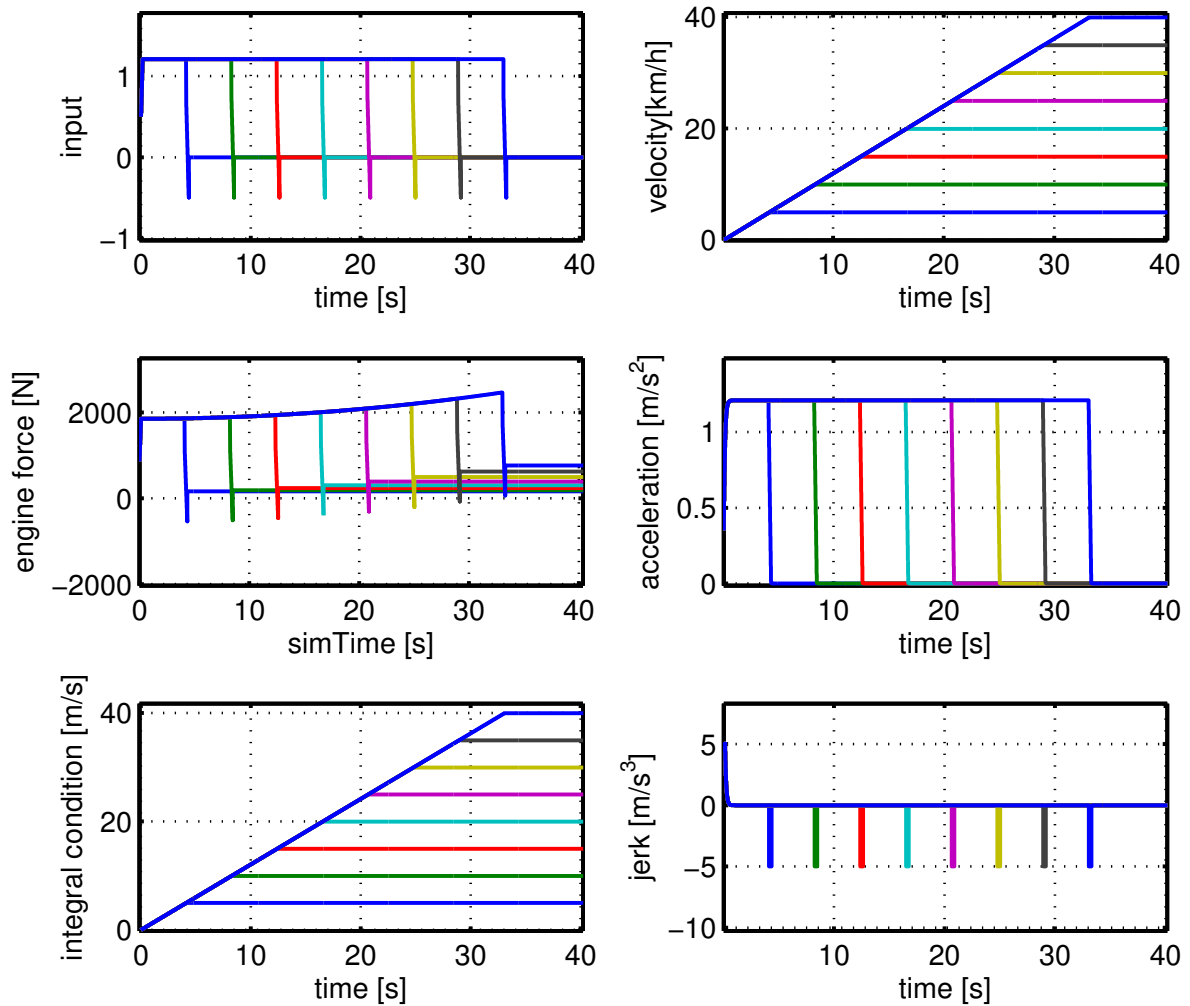
Figure 63: Different velocity changes: Trajectories of the 5. vehicle with $j_{max} = 5\,\text{m/s}^3$, $a_{max} = 2\,\text{m/s}^2$, $c_{max} = 6395\,\text{N}$, $\tau = 0.1$

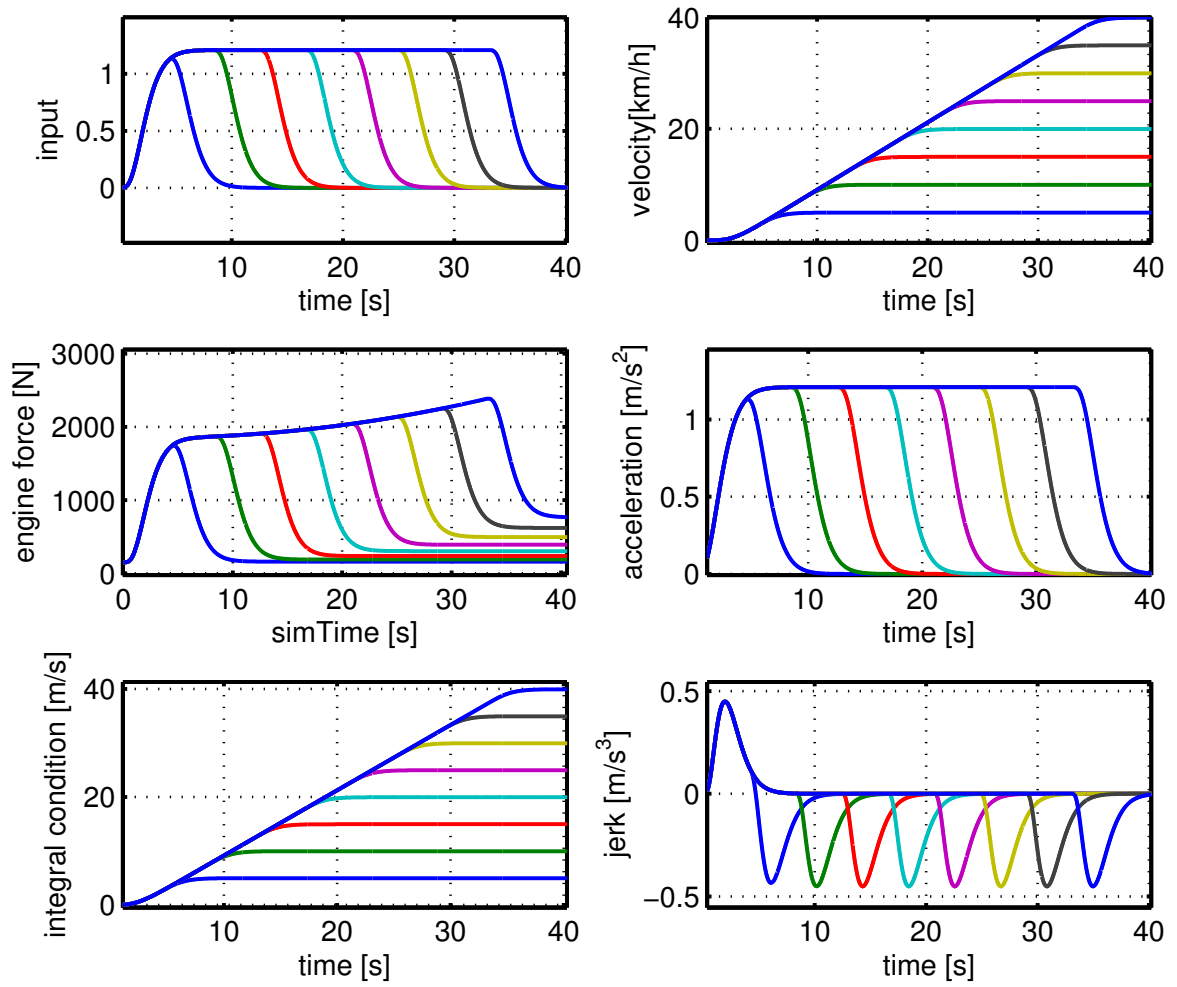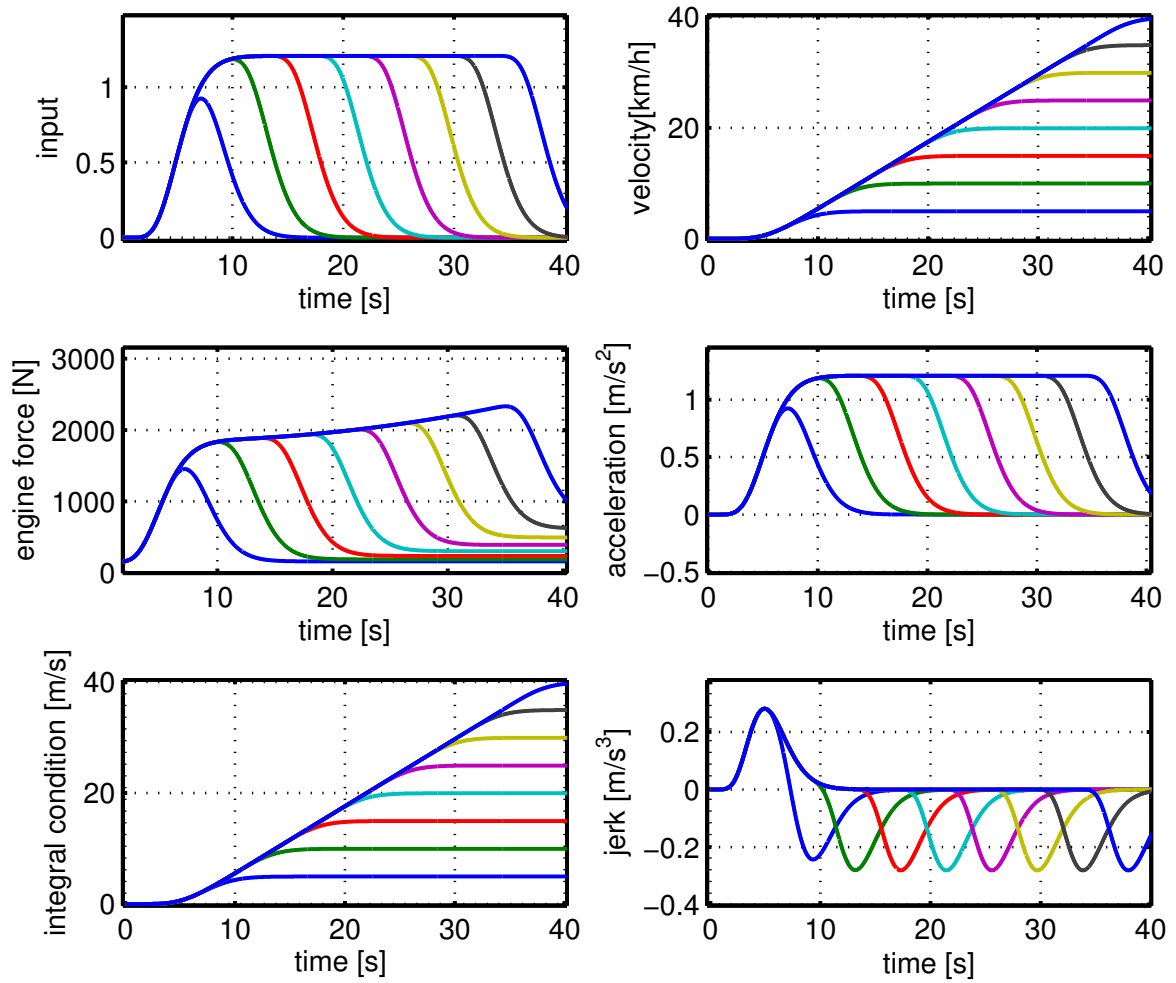**Figure 64:** Different velocity changes: Trajectories of the 10. vehicle with $j_{max} = 5\,\text{m/s}^3$, $a_{max} = 2\,\text{m/s}^2$, $c_{max} = 6395\,\text{N}$, $\tau = 0.1$

In the last simulation for the maximum input signal trajectory u_{max}, we set $c_{max} = 6140$ N and $\tau = 0.8$ in Fig. 65 to Fig. 67. The leader vehicle simulation result is shown in Fig. 59. Referring to the stated parameters, $u_{max} = 4.8 > a_{max}$ is determined as shown in the leader vehicle plot in Fig. 65. Also, the computed vehicle input signal fulfill Theorem 4. Secondly, the velocity plots indicate that different final velocities have an effect on the engine force. In any case, the engine force does not saturate. Finally, acceleration and jerk constraints are also met by all vehicles. It is seen that the computed input signal in Fig. 65 is an example of Case I-b and D-c.

Figure 65: Different velocity changes: Trajectories of the leader vehicle with $j_{max} = 5\,\text{m/s}^3$, $a_{max} = 2\,\text{m/s}^2$, $c_{max} = 6395\,\text{N}$, $\tau = 0.8$
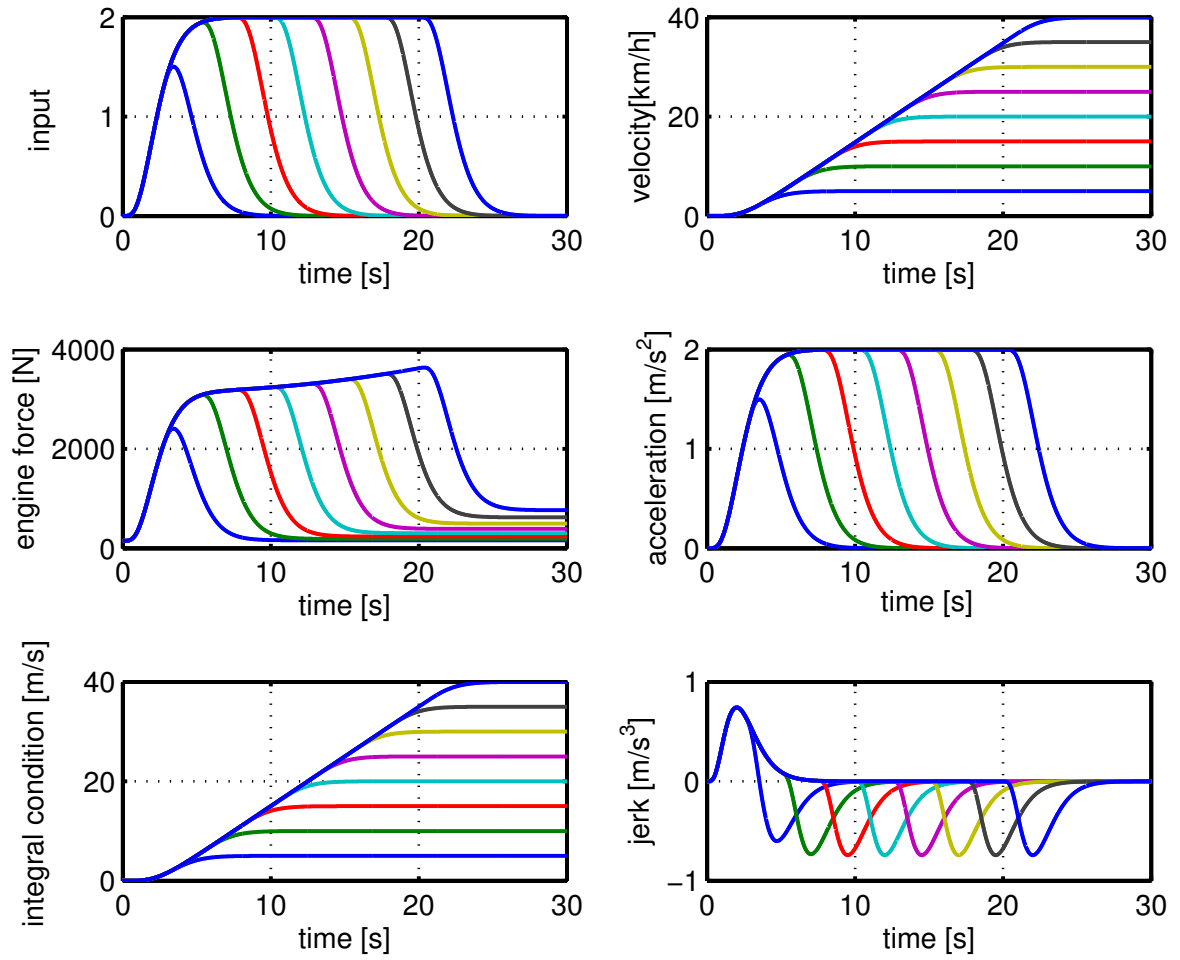
Figure 66: Different velocity changes: Trajectories of the 5. vehicle with $j_{\max} = 5 \, \text{m/s}^3$, $a_{\max} = 2 \, \text{m/s}^2$, $c_{\max} = 6395 \, \text{N}$, $\tau = 0.8$
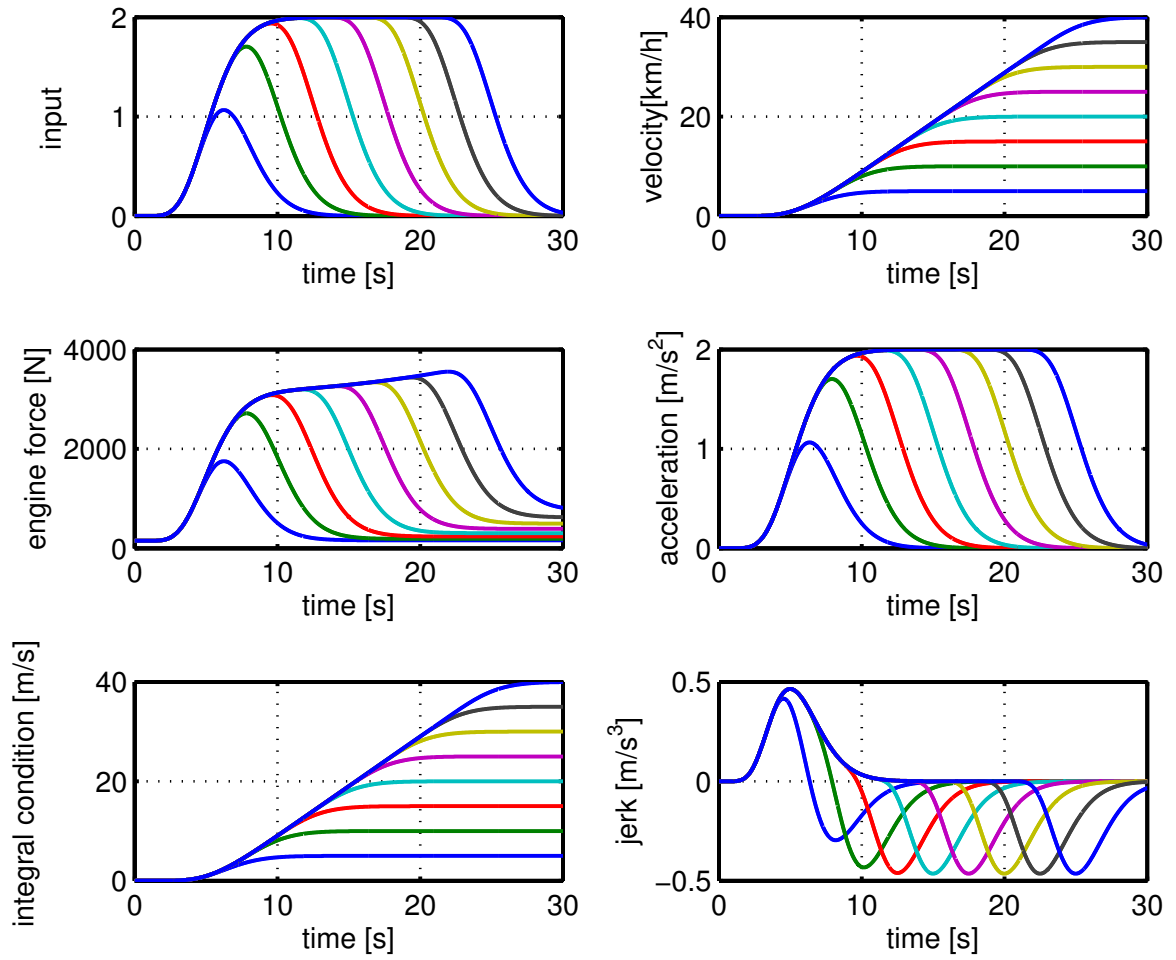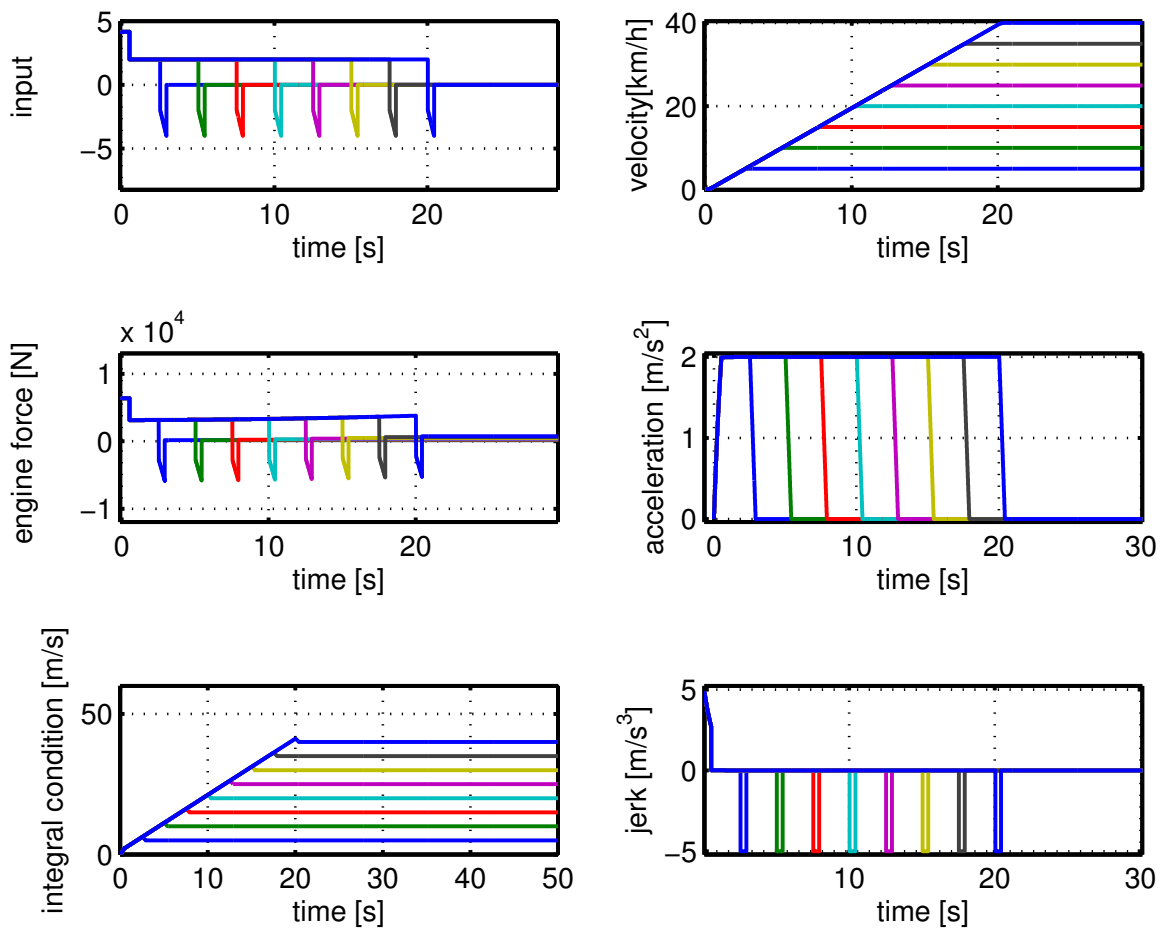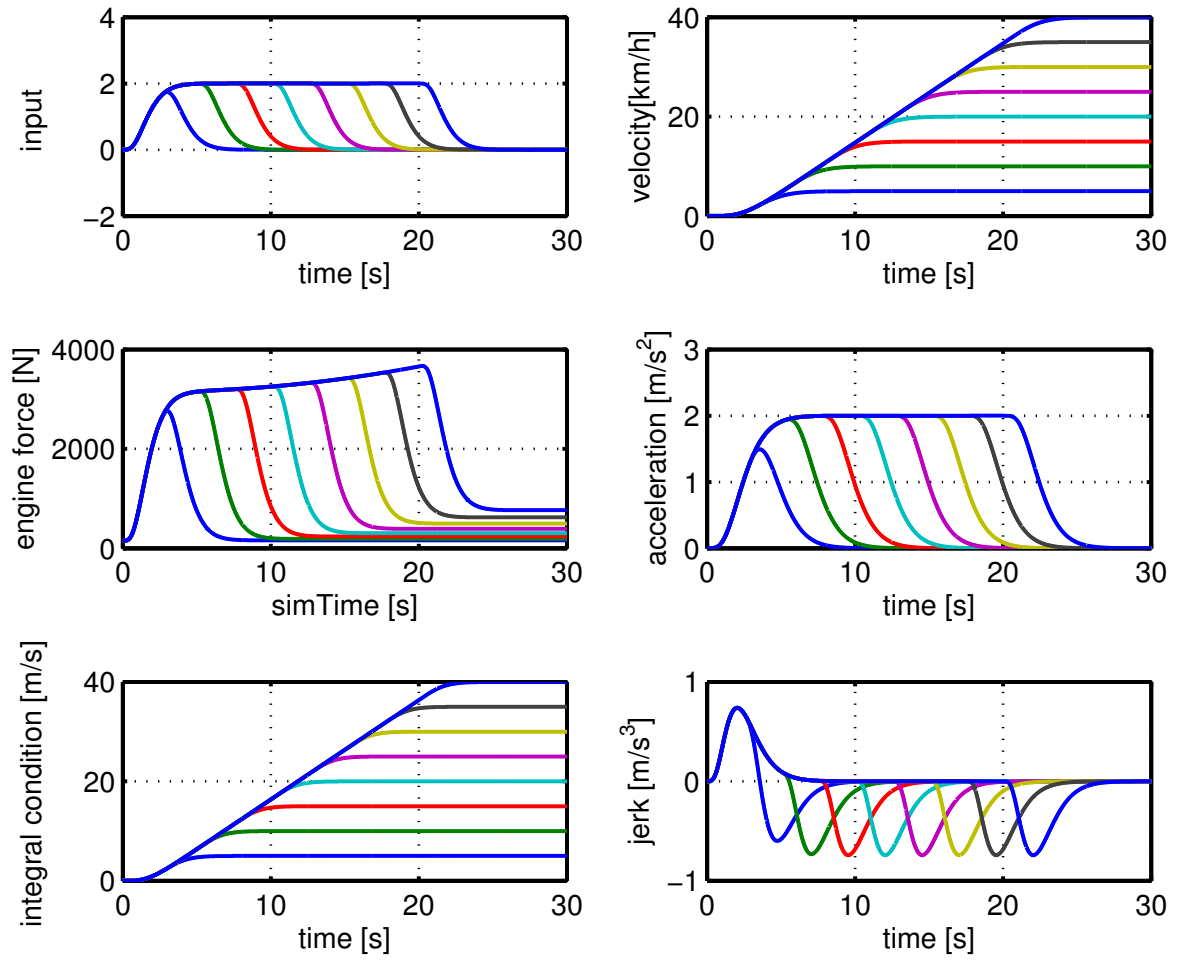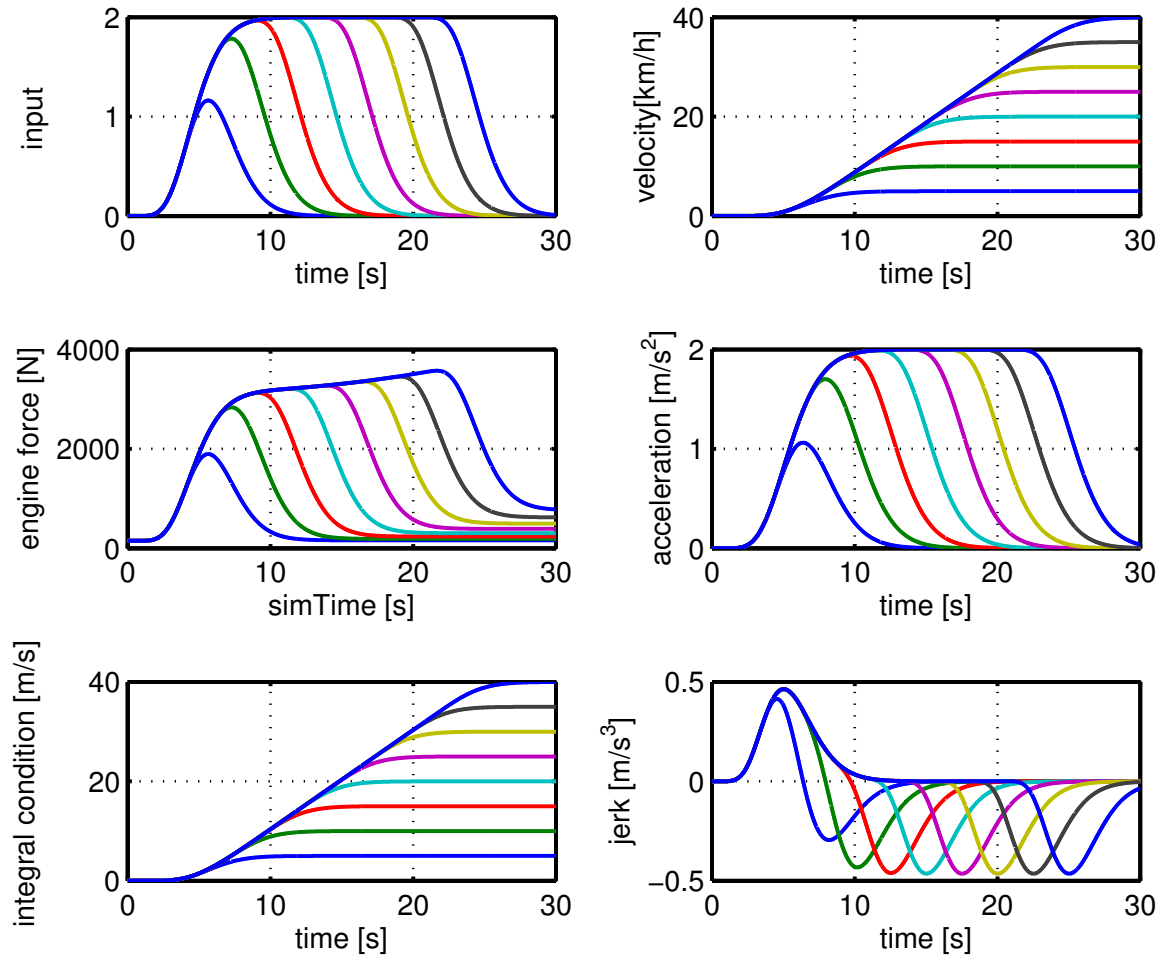
Figure 67: Different velocity changes: Trajectories of the 10. vehicle with $j_{max} = 5\,\mathrm{m/s^3}$, $a_{max} = 2\,\mathrm{m/s^2}$, $c_{max} = 6395\,\mathrm{N}$, $\tau = 0.8$

4.10 Simulation Results for Computed Input Signal - Theorem 5

The minimum input trajectory u_{max} is computed according to Theorem 5 for slow-down maneuvers. The initial velocity of the vehicles is $v_i = 40$ m/s and different final velocity values are chosen for the computation. Also, $j_{min} = -5$ m/s^3, $a_{min} = -2$ m/s^2 and the values in Table 1 are used in the simulation.

The first simulation is implemented with $c_{min} = -4140$ N for $\mu = 0.3$ and $\tau = 0.1$ parameters. The computation of the input signal with different final velocities is presented in Fig. 68. The signals of the other vehicles are shown in Fig. 69 and Fig. 70. It is confirmed that the condition $u_{min} \leq u_{i,min}$ is ensured for each selected vehicle in the simulation. Since the engine force signal is bounded by -4140 N, the selected vehicles stay in the defined limits as seen in the figures. For different velocity differences, the engine force is applied to the vehicles in different times. To illustrate, if the velocity difference is 40 m/s as in velocity plot of the Fig. 68, then the engine force is applied for about 20 seconds. On the other hand, if the velocity difference is 20 m/s, then the engine force is applied for around 10 seconds. The subsequent plots denote the acceleration signal of the selected vehicles. As stated in Theorem 3, the acceleration constraint holds for all vehicles. The last plots display the jerk signal of the vehicles. The constraint -5 m/s$^3 \leq j_i \leq 5$ m/s^3 is not violated as can be seen in Fig. 68, Fig. 69 and Fig. 70. It is shown that the computed input signal in Fig. 68 is an example of Case I-e and D-c.

Figure 68: Different velocity changes: Trajectories of the leader vehicle with $j_{\min} = -5\,\mathrm{m/s^3}$, $a_{\min} = -2\,\mathrm{m/s^2}$, $c_{\min} = -4140\,\mathrm{N}$, $\tau = 0.1$

Figure 69: Different velocity changes: Trajectories of the 5. vehicle with $j_{min} = -5\,\mathrm{m/s^3}$, $a_{min} = -2\,\mathrm{m/s^2}$, $c_{min} = -4140\,\mathrm{N}$, $\tau = 0.1$

Figure 70: Different velocity changes: Trajectories of the 10. vehicle with $j_{\min} = -5\,\mathrm{m/s^3}$, $a_{\min} = -2\,\mathrm{m/s^2}$, $c_{\min} = -4140\,\mathrm{N}$, $\tau = 0.1$

For the following simulation the minimum brake force is changed to $c_{\min} = -11730\,\text{N}$. The computed input signal is represented in Fig. 71. For example, if the velocity difference is 40 m/s, the input signal is computed as shown with the blue line in Fig. 71. It starts from a constant value and then decreases up to -2.1. After, it increases to 2 until 20 seconds and eventually it jumps to a positive value. The computed input signal is applied to the leader vehicle for different final velocity values as shown in Fig. 72 and Fig. 73. It is verified that the input signal always fulfills the inequality $u_{\min} \leq u_{i,\min}$ for each vehicle i in the platoon. As emphasized in Theorem 6, the acceleration signal is bounded even if we set different final velocity values. The last figure of the plots indicate the jerk signal where is also bounded for each vehicles. It is concluded that the computed input signal in Fig. 71 is an example of Case I-e and D-c.

Figure 71: Different velocity changes: Trajectories of the leader vehicle with $j_{min} = -5\,\text{m/s}^3$, $a_{min} = -2\,\text{m/s}^2$, $c_{min} = -11730\,\text{N}$, $\tau = 0.1$
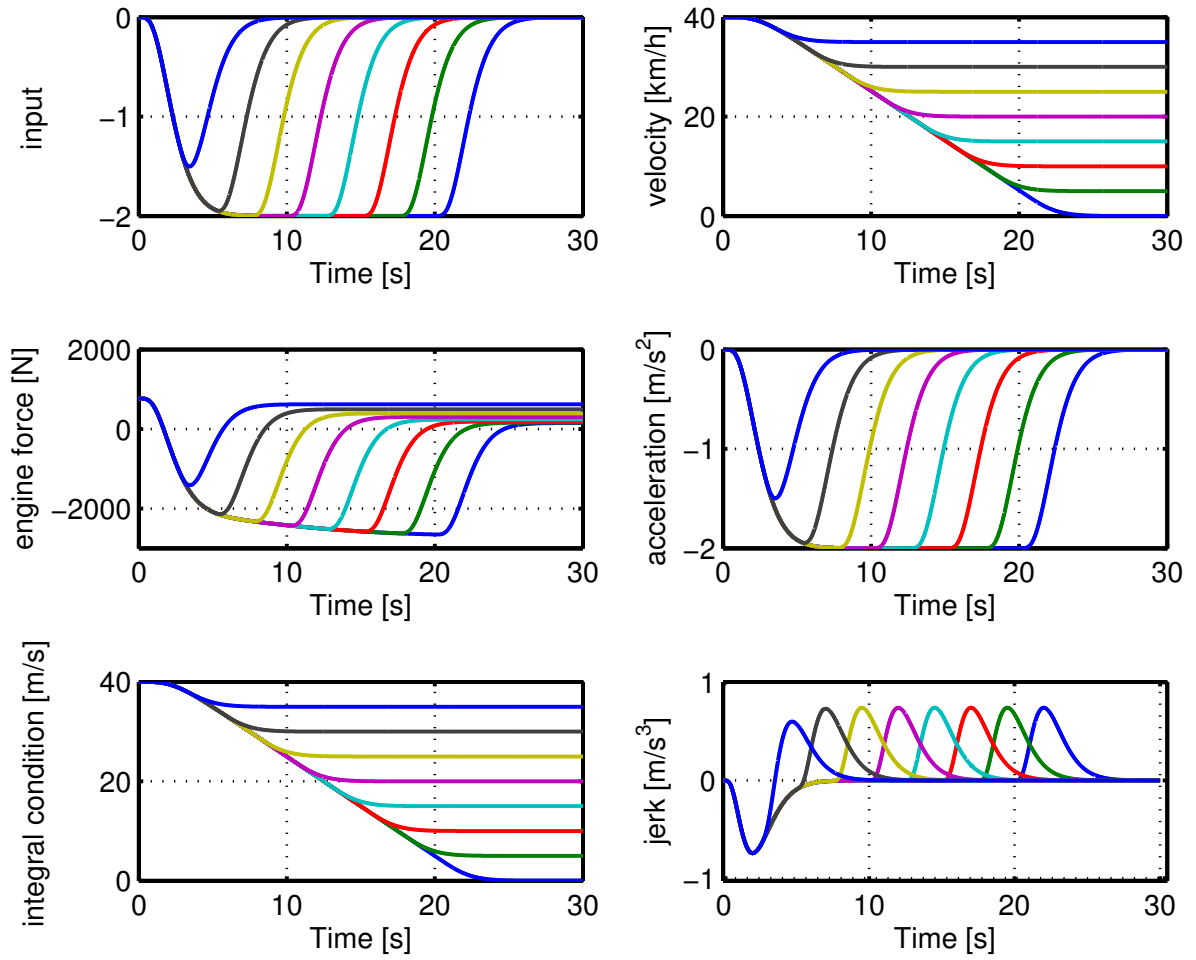
Figure 72: Different velocity changes: Trajectories of the 5. with $j_{\min} = -5\,\mathrm{m/s^3}$, $a_{\min} = -2\,\mathrm{m/s^2}$, $c_{\min} = -11730\,\mathrm{N}$, $\tau = 0.1$
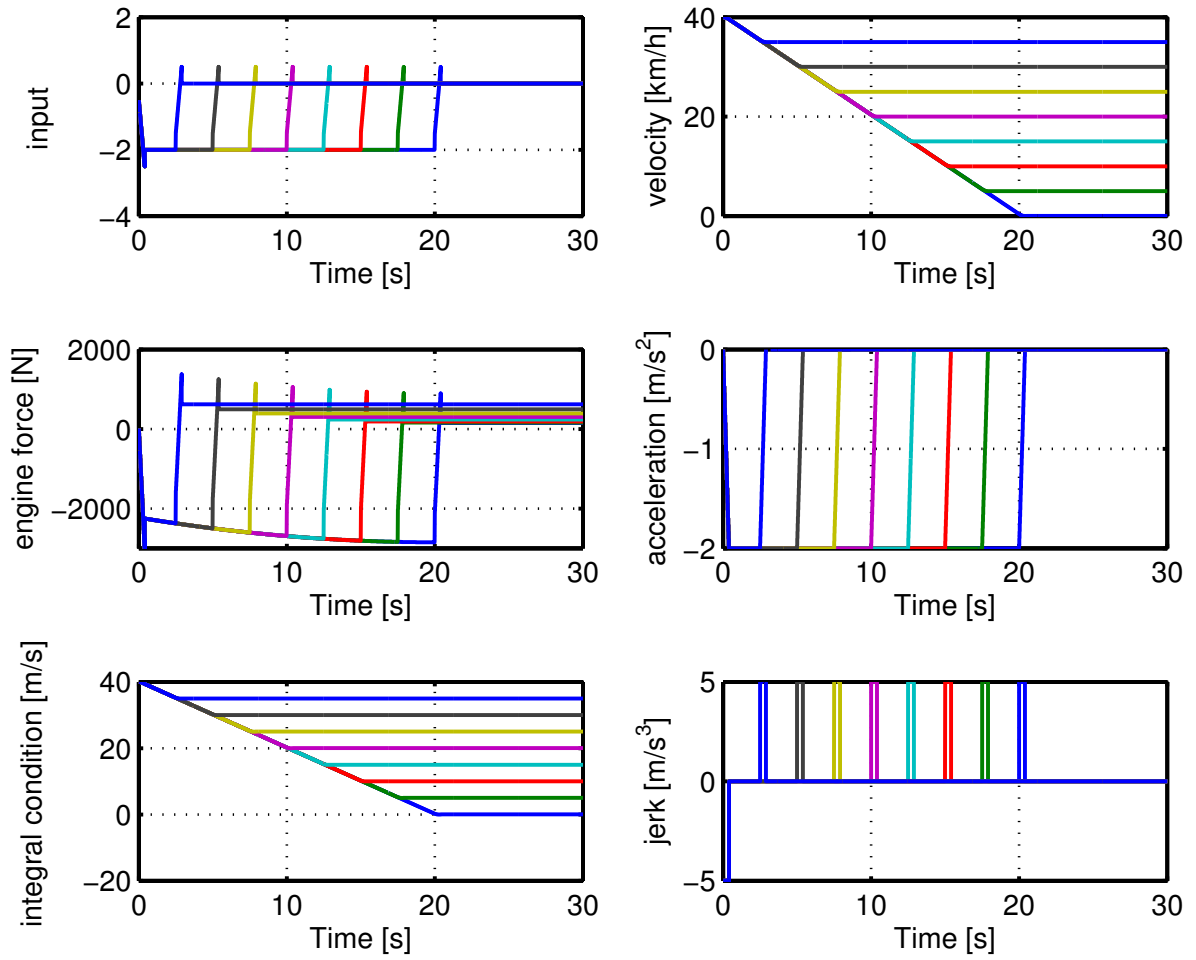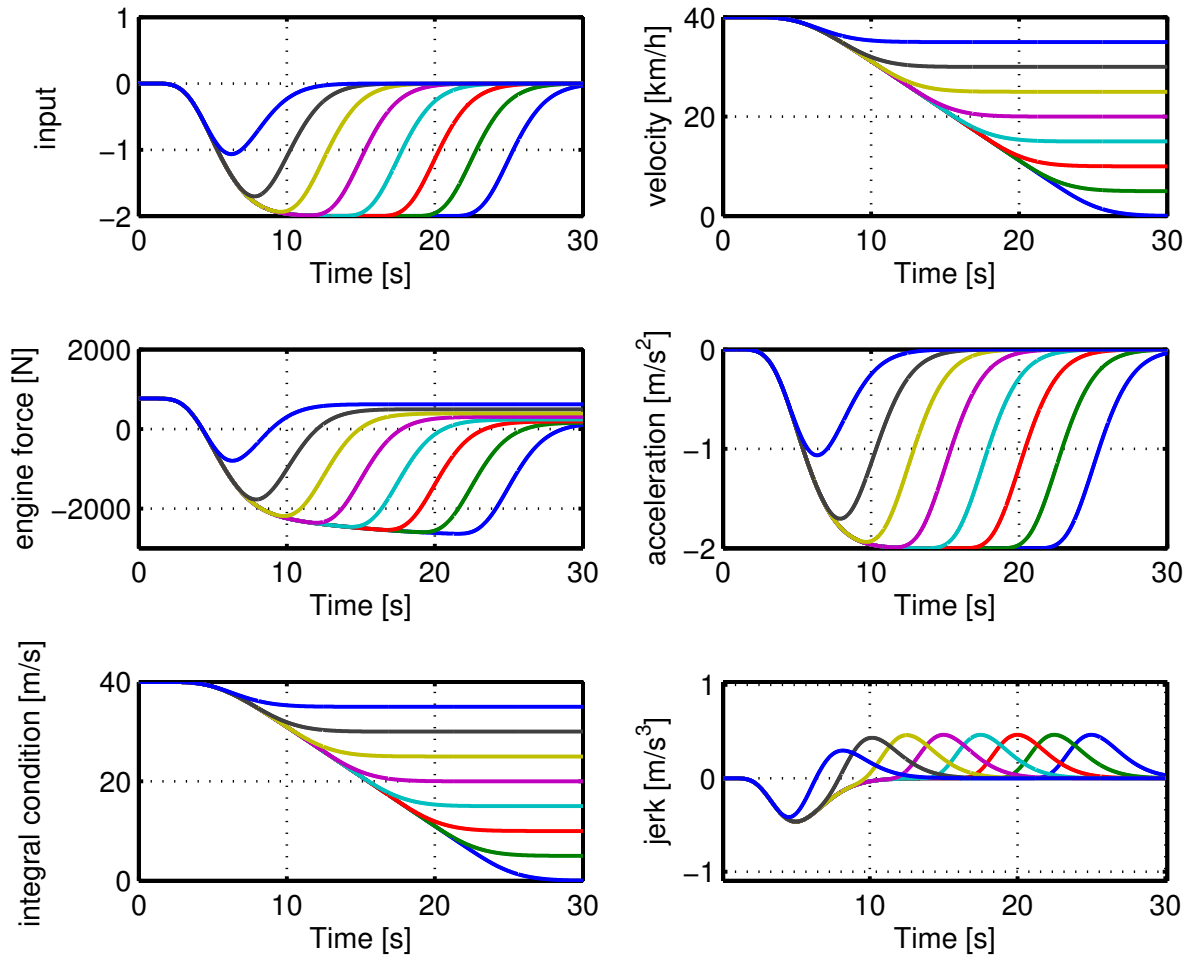
Figure 73: Different velocity changes: Trajectories of the 10. vehicle with $j_{min} = -5\,\text{m/s}^3$, $a_{min} = -2\,\text{m/s}^2$, $c_{min} = -11730\,\text{N}$, $\tau = 0.1$

The final simulation is implemented with $c_{min} = -11730\,\text{N}$ and $\tau = 0.8$. The computed input signal is indicated in Fig. 74. After applying this input signal to the leader vehicle, the input signal of the other vehicles is plotted as shown in Fig. 75 and Fig. 76. It can be seen that the minimum input bound is not violated as required by Theorem 6. Acceleration and jerk constraint are also met by each vehicle in the string. It is observed that the computed input signal is an example of Case I-e and D-c.
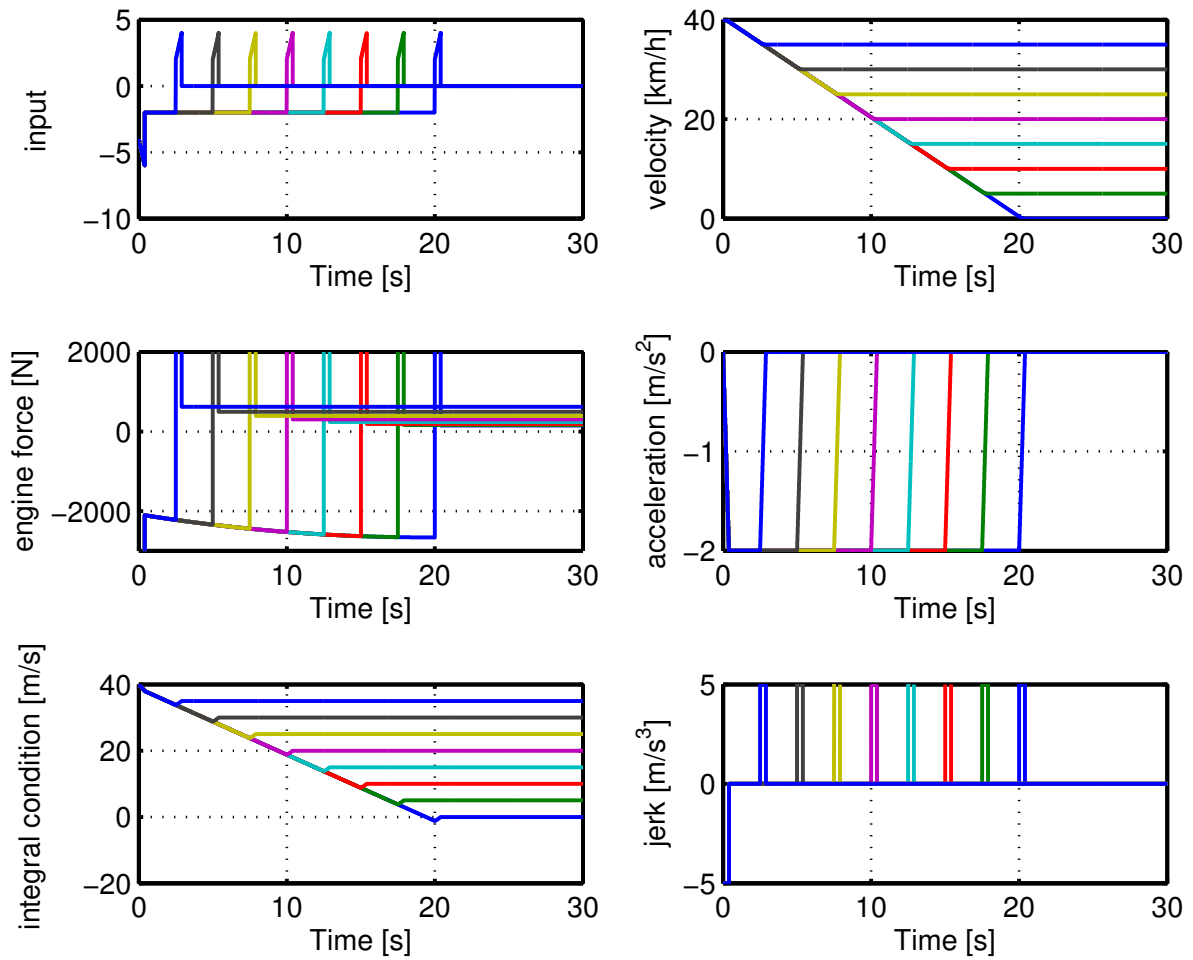
Figure 74: Different velocity changes: Trajectories of the leader vehicle with $j_{min} = -5\,\text{m/s}^3$, $a_{min} = -2\,\text{m/s}^2$, $c_{min} = -11730\,\text{N}$, $\tau = 0.8$
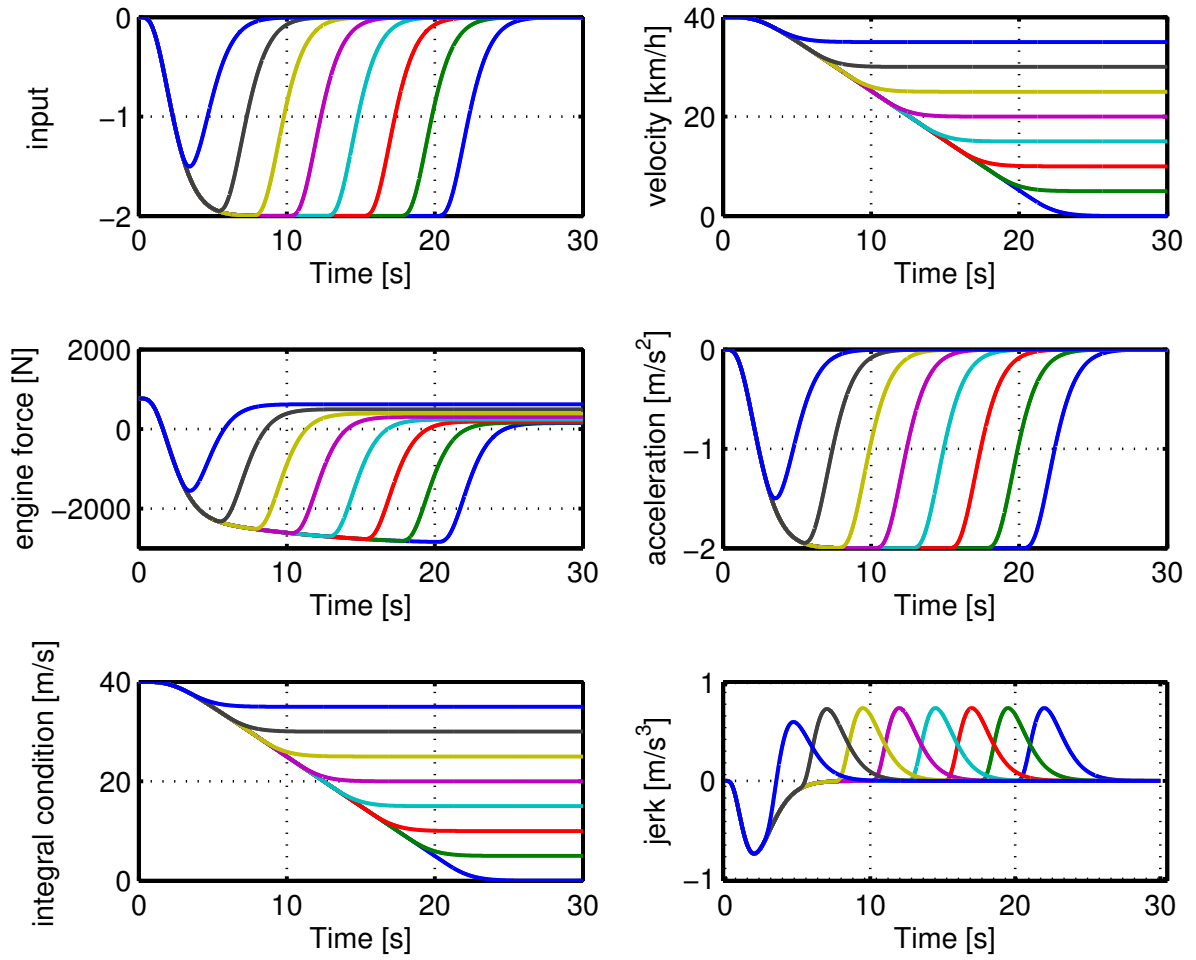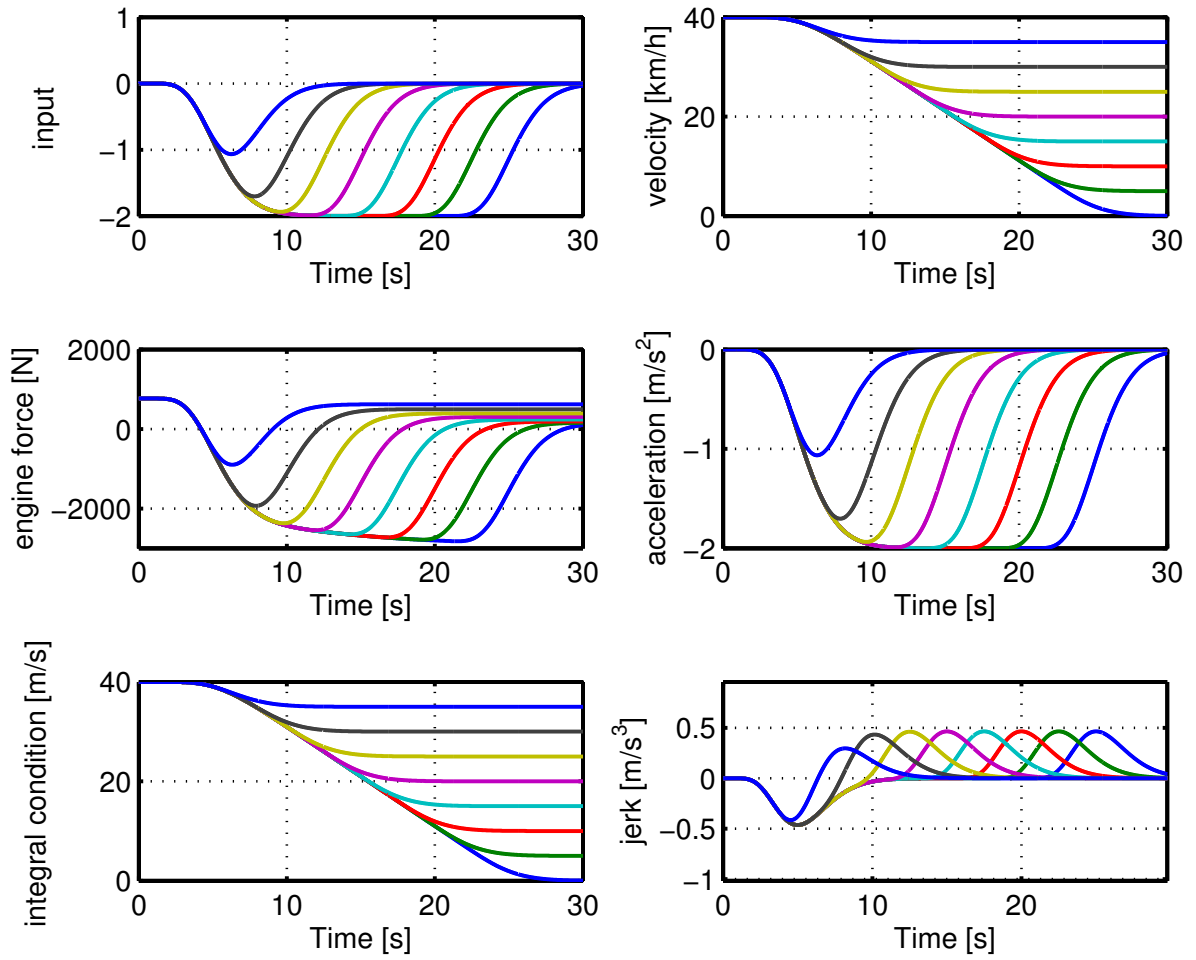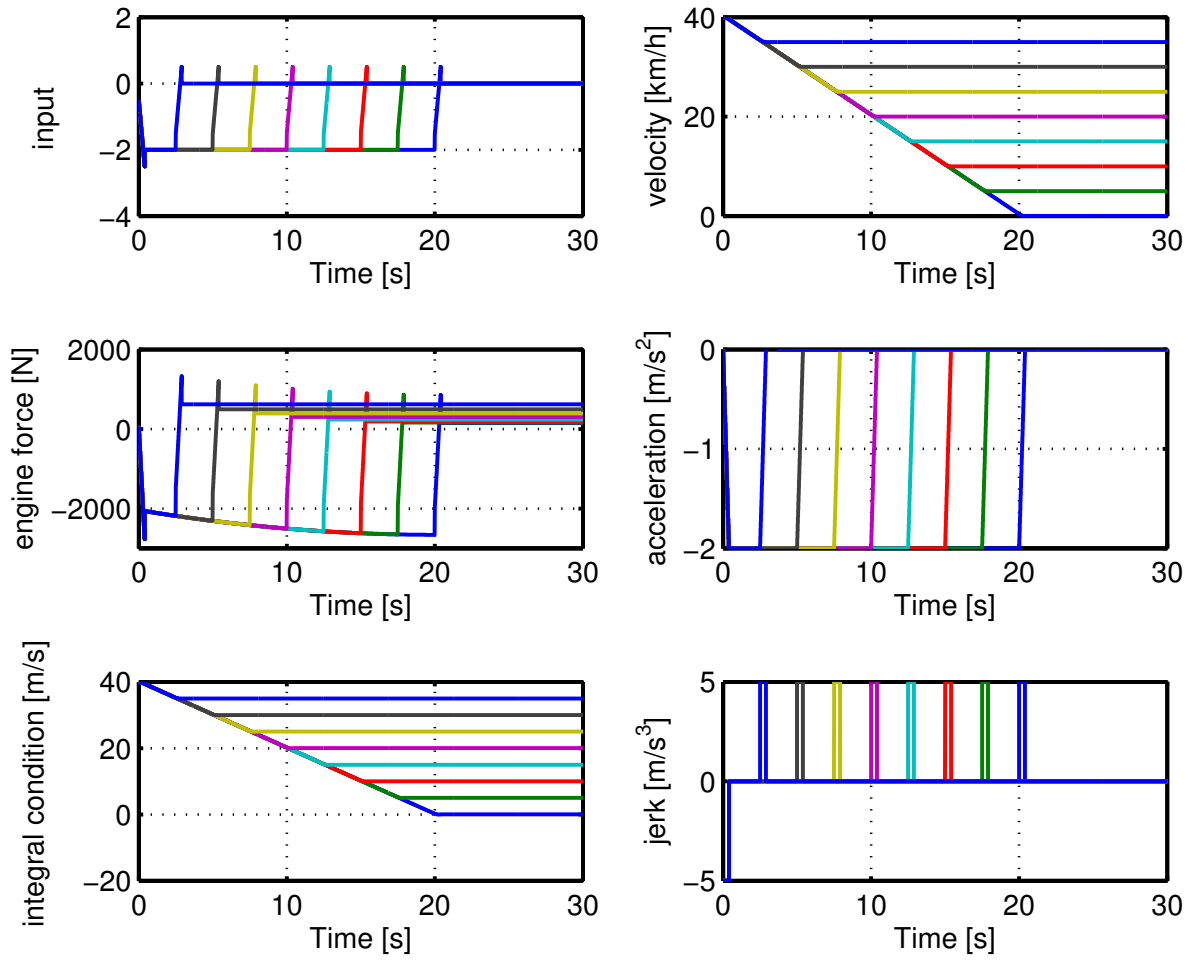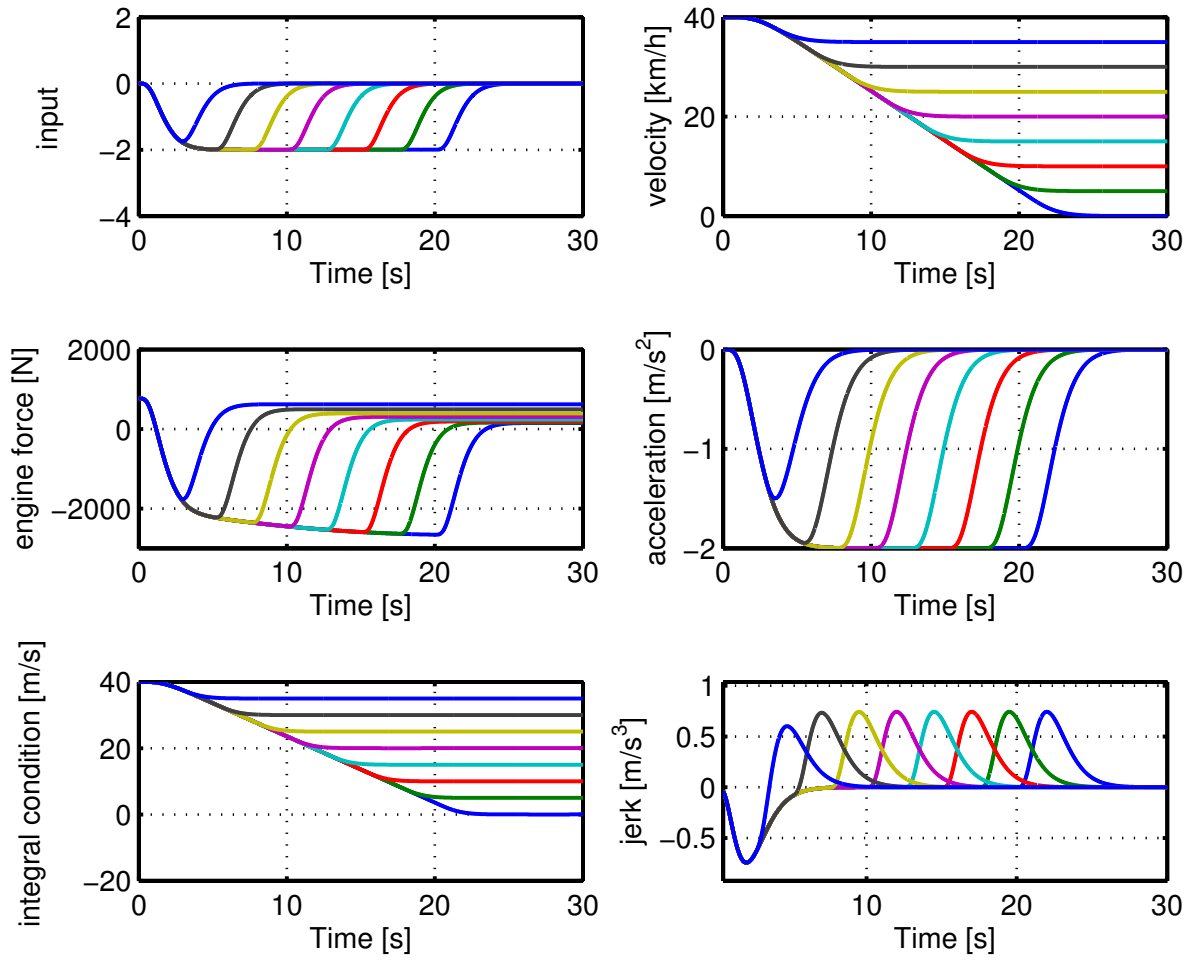
Figure 75: Different velocity changes: Trajectories of the 5. vehicle with $j_{min} = -5\,\mathrm{m/s^3}$, $a_{min} = -2\,\mathrm{m/s^2}$, $c_{min} = -11730\,\mathrm{N}$, $\tau = 0.8$
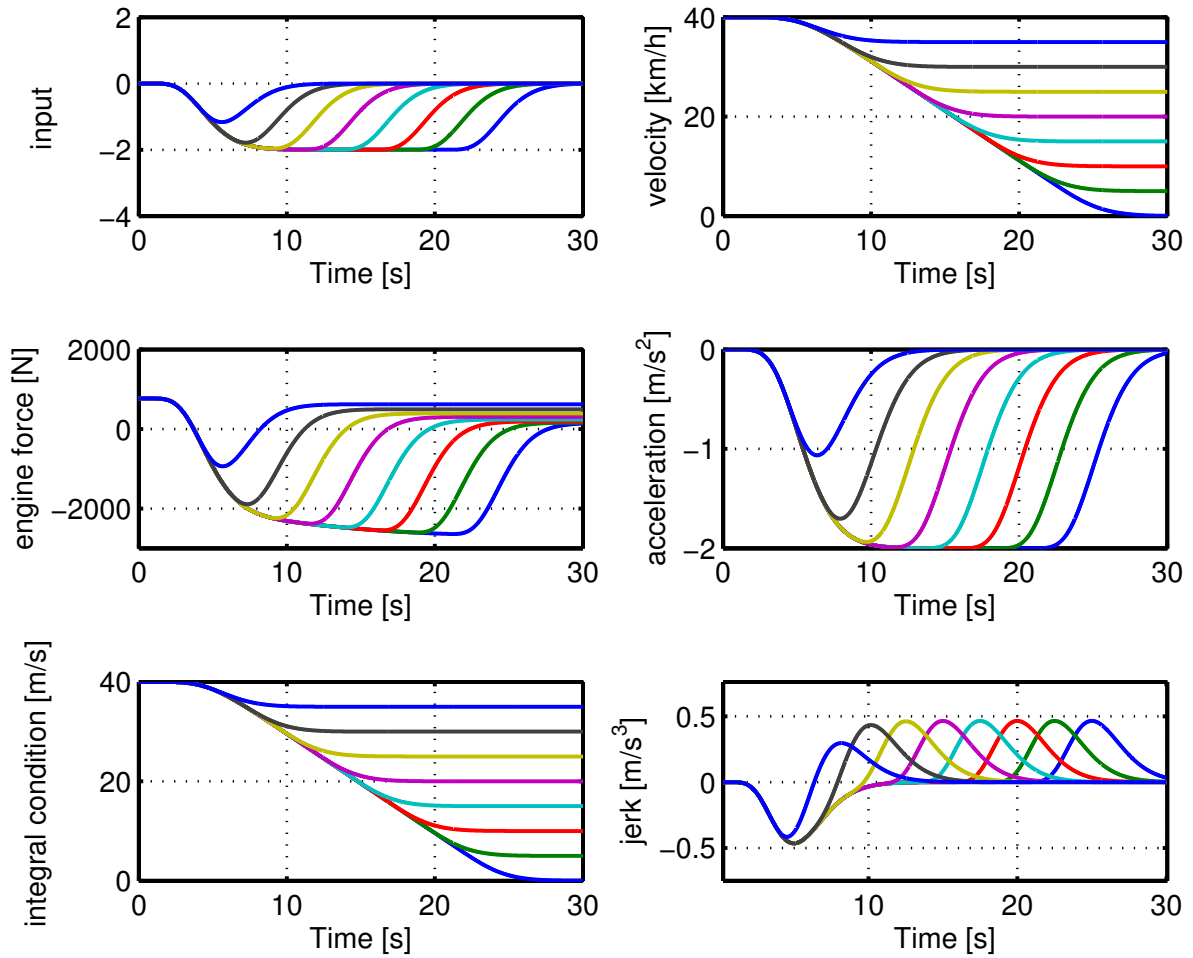
Figure 76: Different velocity changes: Trajectories of the 10. with $j_{\min} = -5\,\text{m/s}^3$, $a_{\min} = -2\,\text{m/s}^2$, $c_{\min} = -11730\,\text{N}$, $\tau = 0.8$

4.11 Maneuver Times

Section 4.3, 4.4 and Section 4.8 propose different conditions for input signals that ensure preserving string stability under engine force saturation. Hereby, the example signals for the simulations in Section 4.6 and 4.7 are computed using time-optimal control with a constraint on acceleration, jerk and the engine force. On the other hand, the signals in Section 4.9 and 4.10 are computed for an absolute bound on the vehicle input signal. In this section, the completion times of maneuvers are compared for the different simulation scenarios. The results are summarized in Table 3. Here, Theorem 1 (velocity-dependent) and Theorem 4 (velocity-independent) correspond to speed-up

maneuvers and Theorem 2 (velocity-dependent) and Theorem 5 (velocity-independent) correspond to slow-down maneuvers.

Table 3: Maneuver completion times in seconds.

Δv	5	10	15	20	25	30	35	40
$\tau = 0.1, c_{\max} = 2470, c_{\min} = -4140$								
Theorem 1	3.379	6.436	9.545	12.734	16.037	19.496	23.163	27.109
Theorem 4	4.354	8.488	12.623	16.757	20.892	25.027	29.161	33.296
Theorem 2	2.300	4.800	7.299	9.799	12.297	14.800	17.297	19.800
Theorem 5	2.900	5.400	7.900	10.400	12.900	15.400	17.900	20.400
$\tau = 0.1. c_{\max} = 6395. c_{\min} = -11730$								
Theorem 1	2.900	5.400	7.899	10.400	12.900	15.399	17.899	20.400
Theorem 4	2.900	5.400	7.900	10.400	12.900	15.400	17.900	20.400
Theorem 2	2.300	4.800	7.299	9.799	12.297	14.800	17.297	19.800
Theorem 5	2.900	5.400	7.900	10.400	12.900	15.400	17.900	20.400
$\tau = 0.8. c_{\max} = 6395. c_{\min} = -11730$								
Theorem 1	2.920	5.420	7.920	10.420	12.920	15.419	17.919	20.424
Theorem 4	2.931	5.431	7.931	10.431	12.931	15.431	17.931	20.431
Theorem 2	2.300	4.800	7.299	9.799	12.298	14.800	17.297	19.800
Theorem 5	2.900	5.400	7.900	10.400	12.900	15.400	17.900	20.400

It is readily observed that the maneuver times for the velocity-independent computation are always slightly larger than the respective maneuver times of the velocity-dependent case. The reason is that we compute trajectories for the velocity-dependent case in Section 4.6 and 4.7 using time-optimal control. Considering that it is not suitable to compute the trajectories according to Theorem 1 and 2 using optimal control in real-time, slower trajectories are expected in practice. In any case, it can be seen that the trajectories according to Theorem 4 and 5 are only considerably slower than the related trajectories for Theorem 1 and 2 in the case of a small engine force. This case corresponds to driving on wet asphalt with a low friction coefficient. In such scenario, time-optimal maneuvers are not of high importance anyway.

In summary, this comparison further clarifies that the input signal according to Theorem 4 and 5 are most suitable for velocity changes of vehicle string without violating the engine force constraint. These signals allow fast maneuvers and can be computed in real-time.

CHAPTER 5

CONCLUSION AND FUTURE WORK

Cooperative adaptive cruise control (CACC) is a recent technology that enables vehicle following in the form of vehicle strings at small inter-vehicle spacings. Here, the fulfillment of string stability when using CACC is essential in order to ensure driving comfort and driving safety. String stability guarantees that fluctuations and disturbances are attenuated along a vehicle string.

In the literature, string stability is commonly studied based on a linear vehicle model. That is, string stability can be confirmed as long as the linear model is valid. However, in case of nonlinear behavior, for example because of force saturation, string stability can no longer be ensured. In this thesis, we study the case where the vehicles are modeled as nonlinear systems including air drag and friction forces. In this model, the input signal is the potentially limited engine force. After applying feedback linearization, it is shown that the resulting linear system is suitable for the string stable CACC design as long as the engine force of all vehicles stays within its bounds.

Based on this model, the main focus of the thesis is finding conditions under which the engine force of none of the vehicles in a string saturates. To this end, it is observed that the signals of all vehicles in a string depend on the input signal of the leader vehicle. That is, it is only required to determine conditions on the input signal of the leader vehicle of a string. As the first contribution of the thesis, we formulate a reach-ability problem under state constraints in order to verify if the engine force of any vehicle saturates. Such problem can generally be solved by the level set method as a computational tool. It is shown that this reach-ability analysis is indeed solvable when considering the leader vehicle alone with two system states. Nevertheless, already a string with two vehicles leads to a state space model with 6 states that is too large for using the level set method. In summary, although it is possible to theoretically formulate the studied problem as a reach-ability analysis, its computational solution is not practical. As a remedy, a direct analysis of the nonlinear model is carried out.

The main contribution of the thesis is to determine different sufficient conditions on the input signal of the leader vehicle to preserve string stability for velocity change maneuvers even in the case of actuator saturation. First, a set of velocity-dependent conditions is developed. Here, it is required to determine a maximum (minimum) input trajectory for each possible initial velocity. Such input trajectories can for example be determined offline using optimal control. Knowing these maximum (minimum) input trajectories, it holds that any input signal below the maximum input trajectory/above the minimum input trajectory avoids saturation of the engine force. That is, suitable input trajectories for any desired velocity change can be computed in real-time based on the maximum/minimum trajectories. Second, a set of velocity-independent conditions is derived. Using an absolute maximum (minimum) value for the input signal, optimal trajectories for any velocity change can be computed analytically, whereby it is ensured that the engine force does not saturate. From the practical perspective, the second set of conditions is highly beneficial since it can be evaluated in real-time. It only has to be noted that the maneuver times of the second method are slightly longer than the corresponding maneuvers of the first method. The obtained results are illustrated by extensive simulation experiments.

The current formulation is for the case of homogeneous vehicle strings, where each vehicle has the same dynamic properties. Future work will extend the obtained results to the case of heterogeneous vehicle strings.

REFERENCES

[1] **Baskar L.D., De Schutter B., Hellendoorn J., Papp Z., (2011),***"Traffic Control and Intelligent Vehicle Highway; Systems: A Survey"*, IET Intell. Transp. Syst., Vol. 5, Iss. 1, P.P.38–52.

[2] **Mashrur A. Chowdhury, Adel Wadid Sadek, (2003),** *"Fundamentals of Intelligent Transportation Systems Planning",* 2003, ARTECH HOUSE, INC. P.P.1-7/35-55.

[3] **Robayet Nasim, Andreas Kassler, (2012),** *"Distributed Architectures for Intelligent Transport Systems: A Survey",* 2012 IEEE Second Symposium on Network Cloud Computing and Application.

[4] **Petros A. Ioannou (ed), (1997),** *"Automated Highway Systems",* Springer-Verlag US.

[5] **Astrid Linder, Albert Kircher, Anna Vadeby, Sara Nygardhs, (2007),** *"Intelligent Transport Systems (ITS) in Passenger Cars and Methods for Assessment of Traffic Safety Impact",* VTI, report 604A.

[6] **Bin Ran, Peter J. Jin, David Boyce, Tony Z. Qiu, Yang Cheng, (2013),** *"Cooperative Adaptive Cruise Control, Design and Experiments Transportation Research: Impact of Intelligent Transportation System Technologies on Next-Generation Transportation Modeling",* Taylor and Francis Group, LLC.

[7] **Gerrit J. L. Naus, RenÃⓒ P. A. Vugts, Jeroen Ploeg, Marinus (RenÃⓒ) J. G. van de Molengraft, and Maarten Steinbuch, (2010),** *"String-Stable CACC Design and Experimental Validation: A Frequency-Domain Approach",* IEEE Transactions on Vehicular Technology, Vol. 59, No. 9.

[8] **Fernandes P., Nunes U., (2012),** *"Platooning With IVC-Enabled Autonomous Vehicles: Strategies to Mitigate Communication Delays, Improve Safety and Traffic Flow",* Intelligent Transportation Systems, IEEE Transactions on , Vol. 13, No. 1, P.P.91-106.

[9] **Jeroen Ploeg, Dipan P. Shukla, Nathan van de Wouw, and Henk Nijmeijer, (2014),** *"Controller Synthesis for String Stability of Vehicle Platoons",* IEEE Transactions on Intelligent Transportation Systems, Vol. 15, No. 2.

[10] **Oncu S., Ploeg J., van de Wouw N., Nijmeijer H., (2014),** *"Cooperative Adaptive Cruise Control: Network-Aware Analysis of String Stability",* Intelligent Transportation Systems, IEEE Transactions on , Vol. 15, No. 4, P.P.1527-1537.

[11] **Kianfar R., Ali M., Falcone P., Fredriksson J., (2014),** *"Combined Longitudinal and Lateral Control Design for String Stable Vehicle Platooning within a Designated Lane",* Intelligent Transportation Systems (ITSC), 2014 IEEE 17th International Conference on, P.P.1003-1008, 8-11.

[12] **G. Marsden, M. McDonald, M. Brackstone, (2001),** *"Towards an Understanding of Adaptive Cruise Control",* Transportation Research Part C. 9, P.P.33-51.

[13] **Vahidi A., Eskandarian A., (2003),** *"Research Advances in Intelligent Collision Avoidance and Adaptive Cruise Control",* Intelligent Transportation Systems, IEEE Transactions on , Vol.4, No.3, P.P.143-153.

[14] **Kesting A., Treiber M., Schnhof M., Helbing D., (2008),** *"Adaptive Cruise Control Design for Active Congestion Avoidance",* Transportation Research Part C 16,P.P.668–683.

[15] **Vicente Milanés, Steven E. Shladover, (2014),** *"Modeling Cooperative and Autonomous Adaptive Cruise Control Dynamic Responses Using Experimental Data",* Transportation Research Part C. 48, P.P.285–300.

[16] **B. S. Kerner, (2009),** *"Introduction to Modern Traffic Flow Theory and Control: The Long Road to Three-Phase Traffic Theory"*, Springer, Berlin, New York.

[17] **Naus G.J. L., Vugts R. P. A., Ploeg J., van de Molengraft M. J. G., Steinbuch M., (2010)**, *"String-Stable CACC Design and Experimental Validation: A Frequency-Domain Approach"*, IEEE Transactions on Vehicular Technology, vol. 59, no. 9, pp. 4268 - 4279.

[18] **Ploeg J., Shukla D.P., van de Wouw N., Nijmeijer H., (2014)**, *" Controller Synthesis for String Stability of Vehicle Platoons"*, IEEE Transactions On Vehicular Technology, vol. 15, no. 2.

[19] **Oncu, S., Ploeg, J., van de Wouw N., Nijmeijer H., (2014)**, *"Cooperative Adaptive Cruise Control: Network-Aware Analysis of String Stability"*, Intelligent Transportation Systems, IEEE Transactions on, vol.15, no.4, pp. 1527-1537.

[20] **Kianfar R., Ali M., Falcone P., Fredriksson J., (2014)**, *"Combined longitudinal and lateral control design for string stable vehicle platooning within a designated lane"*, Intelligent Transportation Systems (ITSC), IEEE 17th International Conference on, pp.1003 – 1008.

[21] **Kerner B.S., (2009)**, *"Introduction to Modern Traffic Flow Theory and Control: The Long Road to Three-Phase Traffic Theory"*, IEEE Transactions on, Springer, Berlin, New York.

[22] **Milanes V., Shladover S.E., (2014)**, *"Modeling cooperative and autonomous adaptive cruise control dynamic responses using experimental data"*, Transportation Research : Part C, vol. 48, pp. 285–300.

[23] **Dunbar W. B., Caveney D. S., (2012)**, *" Distributed Receding Horizon Control of Vehicle Platoons: Stability and String Stability"*, IEEE Transactions On Automatic Control, vol. 57, no. 3.

[24] **Kamal M.A.S., Imura J., Hayakawa T., Ohata A., Aihara K., (2014)**, *"Smart Driving of a Vehicle Using Model Predictive Control for Improving Traffic Flow"* IEEE Transactions on Intelligent Transportation Systems, vol. 15, no. 2.

[25] **Davis L. C., (2014)**, *"Nonlinear dynamics of autonomous vehicles with limits on acceleration"*, Physica A : Statistical Mechanics and its Applications, vol. 405, pp. 128-139.

[26] **Bingol H.,Cankaya E.,Schmidt K.W. (2014)**, *"Eyleyici Doyumu Altinda Dizi Kararli Kooperatif Otomatik Seyir Kontrolu"*, Pamukkale Univ. Muh. Bilim Dergisi, vol. 22, pp. 636-642.

[27] **Christopher Nowakowski, Steven E. Shladover, Delphine Cody, Fanping Bu, Jessica O'Connell, John Spring, Susan Dickey, David Nelson, (2011)**, *"Cooperative Adaptive Cruise Control: Testing Drivers Choices of Following Distances",* California PATH Research Report, UCB-ITS-PRR-2011-01.

[28] **Dey K. C. ,Yan L., Wang X.,Wang Y.,Shen H., Chowdhury M., Yu L., Qiu C., Soundararaj V., (2016),** *"A review of communication, driver characteristics, and controls aspects of cooperative adaptive cruise control (CACCC)"*, IEEE Transactions on Intelligent Transportation Systems, vol. 17, no. 2, pp. 491–509.

[29] **Swaroop D., Hedrick J. K., (1996),** *"String stability of interconnected systems"*, in IEEE Transactions on Automatic Control, vol. 41, no. 3, pp. 349-357.

[30] **Eyre J., Yanakiev D., Kanellakopoulos I., (1998)**, *"A Simplified Framework for String Stability Analysis of Automated Vehicles"*, Vehicle System Dynamics, International Journal of Vehicle Mechanics and Mobility, 30:5, pp. 375-405.

[31] **Fernandes P., Nunes U., (2012),** *"Platooning With IVC-Enabled Autonomous Vehicles: Strategies to Mitigate Communication Delays, Improve Safety and Traffic Flow"*, Intelligent Transportation Systems, IEEE Transactions on, vol.13, no.1, pp. 91-106.

[32] **Wang C., Nijmeijer H., (2015),** *"String Stable Heterogeneous Vehicle Platoon Using Cooperative Adaptive Cruise Control"*, IEEE 18th International Conference on Intelligent Transportation Systems, Las Palmas, pp. 1977–1982.

[33] **Ploeg J., van de Wouw N., Nijmeijer H., (2014)**, *"Lp String Stability of Cascaded Systems: Application to Vehicle Platooning"*, IEEE Transactions On Control Systems Technology, vol. 22, no. 2.

[34] **Sheikholeslam S., Desoer, C. A., (1993)**, *"Longitudinal control of a platoon of vehicles with no communication of lead vehicle information: a system level study"*, Vehicular Technology, IEEE Transactions on, vol. 42, no. 4, pp. 546–554.

[35] **Liang C.Y., Peng H., (1999)**, *"Optimal Adaptive Cruise Control with Guaranteed String Stability"*, Vehicle System Dynamics, vol. 32, no. 4-5, pp. 313–330.

[36] **Guo G., Yue W., (2011),** *"Hierarchical platoon control with heterogeneous information feedback"*, IET Control Theory & Applications, vol. 5, no. 15, pp. 1766–1781.

[37] **Ghasemi A., Kazemi R., Azadi S., (2013),** *"Stable Decentralized Control of a Platoon of Vehicles With Heterogeneous Information Feedback"*, in IEEE Transactions on Vehicular Technology, vol. 62, no. 9, pp. 4299–4308.

[38] **Yonggui L., Huanli G., Bugong X., Guiyun L., Hui C., (2015)**, *"Autonomous coordinated control of a platoon of vehicles with multiple disturbances"*, IET Control Theory & Applications, vol. 8, no. 18, pp. 2325-2335.

[39] **Guo G., Yue W., (2014)**, *"Sampled-Data Cooperative Adaptive Cruise Control of Vehicles With Sensor Failures"*, Intelligent Transportation Systems, IEEE Transactions on , vol.15, no.6, pp. 2404–2418.

[40] **Ghasemi A., Rouhi S., (2015)**, *"A safe stable directional vehicular platoon"*, Proc IMechE Part D: J Automobile Engineering, vol. 229, no. 8, pp. 1083–1093.

[41] **Mannering F.L., Kilareski W. P., Washburn S.S., (2005)**, *"Principles of Highway Engineering and Traffic Analysis"*, Third Edition.

[42] **Soner H.M, (1986)**, *"Optimal Control with State-space Constraint"*, Siam Journal on Control and Optimization, vol. 24, no. 3.

[43] **Kurzhanski A. B., Mitchell I. M., Varaiya P. (2006)**, *"Optimization Techniques for State-Constrained Control and Obstacle Problems"*, Journal of Optimization Theory and Applications, vol. 128, no. 3, pp. 499-521.

[44] **Bokanowski O., Forcadel N., Zidani H., (2010)**, *"Reach-ability and Minimal Times for State Constrained Nonlinear Problems without Any Controllability Assumption"*, SIAM J. Control Optim., vol. 48, no. 7, pp. 4292–4316.

[45] **Mitchell I., Bayen A.M., Tomlin C.J, (2011)**, *"Validating a Hamilton-Jacobi Approximation to Hybrid System Reachable Sets"*, Hybrid Systems: Computation and Control, vol. 2034, pp. 418-432.

[46] **Holzinger M. J., Scheeres D. J., (2011)**, *"Reach-ability set subspace computation for nonlinear systems using sampling methods"*, 50th IEEE Conference on Decision and Control and European Control Conference, Orlando, FL, USA, pp. 7317-7324.

[47] **Margellos K., Lygeros J., (2011)**, *"Hamilton-Jacobi Formulation for Reach-Avoid Differential Games"*, IEEE Transactions on Automatic Control, vol. 56, no. 8, pp. 1849-1861.

[48] **Margellos K., Lygeros J., (2013)**, *"Viable set computation for hybrid systems"*, Nonlinear Analysis: Hybrid Systems, vol. 10, pp. 45-62.

[49] **Mitchell I.A., (2008)**, *"The Flexible, Extensible and Efficient Toolbox of Level Set Methods"*, Journal of Scientific Computing, vol. 35, no. 2-3, pp. 300-329.

[50] **Hoberock L.,L.,(1977)**, *"A survey of longitudinal acceleration comfort studies in ground transportation vehicles"*, J. Dyn. Sys., Meas., Control, vol. 99, no. 2, pp.76-84.

[51] **Wu Z.,Liu Y. and Pan G.,(2009)**, *"A smart car control model for brake comfort based on car following"*, EEE Transactions on Intelligent Transportation Systems, vol. 10, no. 1, pp. 42-46.

[52] **Dovgan E., Tusar T., Javorski M. and Filipic B.,(2012)**, *"Discovering comfortable driving strategies using simulation-based multiobjective optimization"*, Informatica, vol. 36, no. 3, pp. 319-326.

[53] **Matsuzaki R., Kamai K., and Seki R.,(2015)**, *"Intelligent tires for identifying coefficient of friction of tire/road contact surfaces using three-axis accelerometer"*, Smart Materials and Structures, vol. 24, no. 2, p. 025010.

[54] **Nandi A. K., Chakraborty D., and Vaz W., (2015)**, *"Design of a comfortable optimal driving strategy for electric vehicles using multi-objective optimization"*, Journal of Power Sources, vol. 283, pp. 1-18.

[55] **Gillespie T. D., (1992)**, *"Fundamentals of Vehicle Dynamics"*, Society of Automotive Engineers Inc, [Online]. Available: http://gen.lib.rus.ec/book/index.php?md5=2F2BD161400D361E2B3A03767931A15D

[56] **Peng H., and Hu J.S., (1996)**, *"Traction/braking force distribution for optimal longitudinal motion during curve following"*, Vehicle System Dynamics, vol. 26, no. 4, pp. 301-320.

[57] **Ming Q., (1997)**, *"Sliding mode controller design for abs system"*, Master's thesis, Virginia Polytechnic Institute and State University.

<p style="text-align:center">**CURRICCULUM VITAE**</p>

PERSONAL INFORMATION

Surname, Name: `Bingöl, Hilal`

Nationality: `Turkey`

Date and Place of Birth: `1988, Ankara`

Marital Status: `Single`

Phone: `+90 505 614 22 02`

Email: `hilalbngl@gmail.com`

<p style="text-align:center">**EDUCATION**</p>

Degree	Institution	Year
MS	Çankaya University, Electronic and Communication Eng.	2017
B.Sc.	Çankaya University, Electronics and Communication Engineering.	2014
High School	Aydınlıkevler Y.D.A High School	2006

FOREIGN LANGUAGES

`Turkish, English`

HOBBIES

`Archaeology, Traveling, Reading`